Pinhole Interference in Three-Dimensional Fuzzy Space

by

Dario Trinchero

Thesis presented in partial fulfilment of the requirements for the degree of Master of Science (Physics) in the Faculty of Science at Stellenbosch University

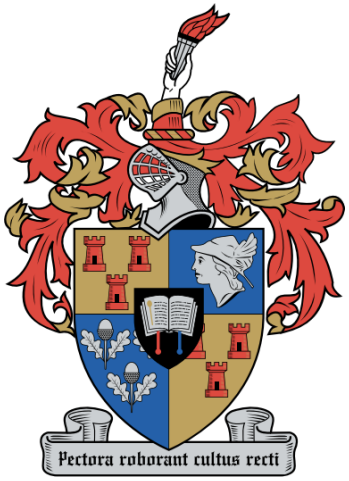

Supervisor: Prof. F. G. Scholtz

December 2022

Declaration

By submitting this thesis electronically, I declare that the entirety of the work contained therein is my own, original work, that I am the sole author thereof (save to the extent explicitly otherwise stated), that reproduction and publication thereof by Stellenbosch University will not infringe any third party rights and that I have not previously in its entirety or in part submitted it for obtaining any qualification.

Date: December 2022

Abstract

We investigate a quantum-to-classical transition which arises naturally within the *fuzzy sphere* formalism for three-dimensional non-commutative quantum mechanics. We focus on treating a two-pinhole interference configuration within this formalism, as it provides an illustrative toy model for which this transition is readily observed and quantified. Specifically, we demonstrate a suppression of the quantum interference effects for objects passing through the pinholes with sufficiently-high energies or numbers of constituent particles.

Our work extends a similar treatment of the double slit experiment, presented in [32], within the two-dimensional Moyal plane, only it addresses two key shortcomings that arise in that context. These are, firstly that the interference pattern in the Moyal plane lacks the expected reflection symmetry present in the pinhole setup, and secondly that the quantum-to-classical transition manifested in the Moyal plane occurs only at unrealistically high velocities and/or particle numbers. Both of these issues are solved in the fuzzy sphere framework.

Opsomming

Ons ondersoek 'n kwantum-na-klassieke oorgang wat natuurlik ontstaan binne die *wasige sfeer*-formalisme vir drie-dimensionele nie-kommutatiewe kwantummeganika. Ons fokus op 'n twee-speldgat interferensie eksperiment binne hierdie formalisme, aangesien dit 'n illustratiewe opstelling verskaf waarvoor hierdie oorgang geredelik waargeneem en gekwantifiseer kan word. Spesifiek demonstreer ons 'n onderdrukking van kwantum interferensie vir voorwerpe wat deur die twee speldgate beweeg met voldoende hoë energieë of aantal samestellende deeltjies.

Ons werk bou voort op 'n soortgelyke analise van die dubbelspleet-eksperiment, uitgevoer in [32], binne die twee-dimensionele Moyal-vlak. Dit spreek egter twee sleuteltekortkominge wat in daardie konteks ontstaan aan. Eerstens, vertoon die interferensiepatroon in die Moyal-vlak nie die verwagte refleksie-simmetrie nie, maar dit is wel in die speldgat-opstelling teenwoordig, en tweedens vind die kwantum-na-klassieke oorgang in die Moyal-vlak plaas by onrealisties hoë snelhede en/of deeltjie getalle. Albei hierdie kwessies word in die wasige sfeer-raamwerk opgelos.

Acknowledgements

Primarily I am grateful to my supervisor, Prof. Frederik Scholtz, who closely guided this research at every step along the way; my silly questions were always patiently received, and feedback on my work never failed to be encouraging, even when it was critical. I always left meetings with high morale and a clear direction. Prof. Scholtz was always also pivotal in organising the Stellenbosch University Faculty of Science Postgraduate Research Conference at which I presented this work, and also helped with filing many a funding progress report, sometimes on short notice.

I am also extremely grateful to Dr Bruce Bartlett who, aside from having always acted as a mentor and role model, provided many insightful mathematical comments and questions which guided my attention at several points throughout this investigation, and ultimately deepened my understanding of the subject matter. Bruce also on numerous occasions put considerable effort into writing recommendation letters for my funding applications, and otherwise helping organise my future studies.

This research was funded in part by a grant from the Harry Crossley Foundation, and in part by an award from the Skye Foundation. Many thanks are extended to both of these organisations without whom this research would not have been possible.

Finally, I would be remiss to not acknowledge my family and my partner, Bianca (with whom I shared the experience of completing a Masters degree), all of whom have been extremely supportive throughout the two-year journey.

Dedications

This thesis is dedicated to my grandfather,
who has always been my biggest fan,
and who would have rejoiced in my completion of it.

Contents

List of Figures

List of Tables

Nomenclature

Lie groups and algebras

$\mathrm{SU}(n)$	Special unitary Lie group
$\mathfrak{su}(n)$	Special unitary Lie algebra
ad	Adjoint (algebra) representation
Ad	Adjoint (group) representation

Fuzzy space

$\mathcal{H}_\mathrm{c}$	Configuration space, a.k.a. fuzzy space or Fock space
$\lvert\psi\rangle$	Generic configuration in $\mathcal{H}_\mathrm{c}$
$\lvert\boldsymbol{z}\rangle$	Coherent state, where $\boldsymbol{z} \in \mathbb{C}^2$ is a complex vector
$\hat{x}$	Operator acting on $\mathcal{H}_\mathrm{c}$ (lower case)
$\mathbf{1}_\mathrm{c}$	Identity operator on $\mathcal{H}_\mathrm{c}$
a_μ	Annihilation operator on Fock space, $\mathcal{H}_\mathrm{c}$
$\mathscr{B}_2(\mathcal{H}_\mathrm{c})$	Space of Hilbert-Schmidt operators on $\mathcal{H}_\mathrm{c}$

Quantum state space

$\mathcal{H}_\mathrm{q}$	Quantum state space; subspace of $\mathscr{B}_2(\mathcal{H}_\mathrm{c})$ generated by coordinate operators
$\lvert\psi)$	Quantum state in $\mathcal{H}_\mathrm{q}$
$\hat{X}$	Quantum observable acting on $\mathcal{H}_\mathrm{q}$ (upper case)
$\mathbf{1}_\mathrm{q}$	Identity operator on $\mathcal{H}_\mathrm{q}$
$\psi(\boldsymbol{z})$	Position representation of state $\lvert\psi)$, with position encoded in $\boldsymbol{z} \in \mathbb{C}$
$\star$	Voros product

Physical constants

$\hbar$	Planck constant	[J s]

λ	Non-commutative parameter	[m]
k_B	Boltzmann constant	[$\mathrm{J\,K^{-1}}$]

Subscripts and superscripts

ph	Physical — identifies elements of $\mathscr{B}_2(\mathcal{H}_\mathrm{c})$ as also being in $\mathcal{H}_\mathrm{q}$
(n)	nth — pertaining to the nth particle in a collection
tot	Total — pertaining to the entirety of a collection of particles

Other standard notation

δ_{ij}	Kronecker delta symbol
ϵ_{ijk}	Levi-Civita symbol
σ^i	Pauli matrix ($i \in \{1,2,3\}$); one component of the vector $\boldsymbol{\sigma}$
$T_k(x)$	Touchard polynomial

Other non-standard notation

R	Dimensionless radius, defined r/λ
κ	Dimensionless wavenumber, defined λk
$\mathbb{N}$	Natural numbers, which we take to include 0
d^4z	Shorthand for integral measure $d\,\mathrm{Re}(z_1)d\,\mathrm{Im}(z_1)d\,\mathrm{Re}(z_2)d\,\mathrm{Im}(z_2)$

Chapter 1

Introduction

1.1 Background

Non-commutative quantum mechanics (NCQM) sets ordinary quantum mechanics within a spacetime with non-commutative geometry. In practice, this simply means that we impose a non-trivial commutator $[\hat{x}_i, \hat{x}_j]$ of coordinate operators. Aside from this, the constructions are those of ordinary quantum mechanics — states are elements of a Hilbert space like any other, and observables are Hermitian operators on that Hilbert space. However, this description threatens to over-simplify; the non-commutativity does still have many important implications on the structure of space at short length scales which translate into unique attributes of NCQM when compared to ordinary quantum mechanics. In particular, non-commutativity imposes a minimum length scale, characterised by the so-called "non-commutative parameter". This minimum scale requires us to rethink the construction of position eigenstates, position measurements, and wavefunctions; it ultimately requires replacing of the very notion of a point in space with a "fuzzy" counterpart.

The idea of a non-commutative model of spacetime is not new. Snyder proposed such a quantised spacetime as far back as 1947 [43], in an attempt to regularise field theories. This idea would later be superseded by renormalisation, but other motivations for considering such models soon arose in its place. Specifically, arguments presented by Doplicher *et al.* [17] emphasise the need for a description of spacetime with nontrivial behaviour at short length scales, and they propose non-commutative spacetime as a primary candidate. Subsequent work by Seiberg *et al* [40], as well as Alekseev *et al* [4], demonstrated how field theories on non-commutative space arise as certain simple limits of string theories[1] — popular contenders for a quantum theory of gravity. Together, these works constitute a compelling argument that non-commutative spacetime may play some role in a consistent formulation of quantum mechanics and gravity.

These advances generated considerable interest in the field in recent years, in particular leading to formulations of both quantum mechanics [38, 6] and quantum field theory [18] on non-commutative spaces. Several classical problems from ordinary quantum mechanics were translated into this framework and reexamined, including the spectrum of the spherical well [12], and general scattering theory in three dimensions [27].

[1] Indeed, in the case of [4], the non-commutative space arising as a limit is the "*fuzzy sphere*", which is the space we adopt for our formalism.

The geometry of non-commutative spaces has also been the topic of much recent work in pure mathematics. Most notably, work by Alain Connes [13] was able to generalise the well-known Gelfand duality between commutative C*-algebras and locally-compact Hausdorff spaces to the case of a non-commutative C*-algebra. Loosely speaking, a non-commutative space can then be viewed as the formal dual of a non-commutative C*-algebra; these spaces are equipped with generalised notions of various geometrical constructs, such as distance measures, exterior derivatives, and so on. We do not require the full machinery of these constructions for our investigation, but the interested reader should note that the fuzzy space we define in the next chapter is analysed within the framework of Connes in [16].

1.2 Motivation & problem statement

Despite all of the motivation for NCQM discussed above, the primary motivation for this particular investigation has little to do with the potential relevance of NCQM to a quantum theory of gravity. Instead, we are motivated primarily by recent results suggesting that NCQM may also play a pivotal role in understanding another large open problem in modern physics, namely the *measurement problem*. In essence, this problem is concerned with the nature of a system's transition from quantum to classical behaviour. Historically, it has been largely treated as distinct from the problem of the unification of quantum mechanics with gravity; yet, there is reason to believe that the two problems may be related — for instance, arguments by Penrose [31] suggest that gravity may play a role in state reduction. The connection to NCQM in particular comes in the form of a recent investigation by Pittaway and Scholtz [32], which demonstrated that a continuous quantum-to-classical transition arises naturally within the non-commutative 2D plane (the "Moyal plane") formalism of NCQM.

Of particular relevance to this thesis is the section of [32] in which double-slit interference is treated within the non-commutative plane. Here it was found that the presence of non-commutativity modifies the standard interference pattern in a remarkable way — the quantum effects are suppressed for objects passing through the slits with sufficiently-high momenta or numbers of constituent particles. This is one manifestation of the remarkable quantum-to-classical transition to which we alluded; it suggests that the structure of space at the smallest length scales can play a direct role in the suppression of quantum effects at larger length scales.

It is natural to wonder whether a similar quantum-to-classical transition arises in other formalisms of NCQM, in particular in higher dimensions. Showing as much would firstly confirm once and for all that the non-commutative geometry is indeed the crucial ingredient for obtaining such an emergent transition. But even if we expect this to be the case, we may still wonder whether there might be any significant differences in the mechanisms behind this transition as manifested in different formalisms of NCQM. For instance, we may ask whether the strength of the quantum suppression will, in other NCQM formalisms, scale as a function of the same system parameters, and if so, whether the suppression will always become apparent at similar values of these parameters.

As a matter of fact, the two-dimensional interference calculation of [32] also comes with a number of caveats. Firstly, the commutation relations for the Moyal plane break rotational symmetry (we discuss the reason for this in section 2.1.1), and as such the final interference pattern fails to be symmetric under reflection about its centre. Secondly, and more crucially, if one supposes that the quantum-to-classical transition should occur at non-relativistic velocities, for a number of protons on the order of Avogadro's number, one derives the requirement that the non-commutative parameter be many orders of magni-

tude larger than the Planck length — much larger than expected. Conversely, fixing the non-commutative parameter at its expected order of magnitude sees quantum suppression occurring only for velocities far exceeding the speed of light. As such, when it comes to the question of whether the quantum-to-classical transition manifests at similar values of the system parameters in every framework of NCQM, it is clear that we at least have reason to hope for the contrary.

For all of the reasons above, it bears repeating the analysis in a three-dimensional (after all, we live in three-dimensional space) framework of NCQM; in particular one for which the commutation relations preserve rotational symmetry. This is our primary objective for this investigation: to compute and interpret the interference pattern for a double-pinhole interference setup in the three-dimensional fuzzy space formalism of NCQM (where rotational symmetry is indeed respected). Our expectation is that the reflection-asymmetry in the interference pattern will be absent in three dimensions, and also that the quantum effects will be more strongly suppressed than in two dimensions; that is, we expect to be able to observe interference suppression at realistic length scales and non-relativistic speeds. A positive result here would therefore constitute the first experimentally falsifiable macroscopic predictions of the short length scale structure of space.

It is worth stressing that, as in the two-dimensional investigation of [32], the reason for considering the double-pinhole setup in particular is merely that it serves as an excellent toy model with which to analyse the aforementioned expected quantum-to-classical transition. It is uniquely well-suited to this purpose for two reasons: firstly, it is a simple enough system for the calculation to be tractable (albeit slightly more algebraically technical in fuzzy space than in the Moyal plane), and secondly, it is easy to identify and quantify the effect of a quantum-to-classical transition for an interference setup, since such a transition manifests simply as a suppression of the interference detected at the screen. Perhaps a third advantage of investigating a particular (and particularly simple) experiment is that our results are thereby made more feasibly directly testable — indeed, experiments have already been conducted which are conceptually similar to the setup we describe, and it is not inconceivable that very similar experiments could probe the effect we predict. There are however still some challenges when it comes to comparing the outcomes of such experiments with our predictions — we discuss this matter towards the end of section 4.5.

1.3 Structural outline

The remainder of this thesis is structured as follows. In chapter 2 we review the formalism of fuzzy space NCQM, and derive several (known) results upon which we depend in later calculations. In chapter 3, we review the plane- and spherical wave solutions to the non-commutative free-particle Schrödinger equation. Chapter 4 contains our main calculation and analysis. We calculate the interference pattern for a double-pinhole interference setup, first in ordinary commutative quantum mechanics and subsequently in the fuzzy space NCQM formalism. We verify that the non-commutative result reduces to the commutative one in the appropriate "commutative limit", and subsequently discuss the physical implications of the result — most notably, the conditions under which the interference suppression becomes significant. Next, we explore how our result scales with multiple particles. Once we account for many particles, we are able to demonstrate that our setup exhibits a quantum-to-classical transition already at realistic energies and length scales. Finally, we make contact with existing experimental work, and outline a few prospects for the future experimental realisation of our pinhole setup. In chapter 5, we summarise our findings and present a few concluding remarks. There are also two appendices to which we delegate some of the more technical aspects of the main calculation.

The main findings of this thesis have been submitted for publication. A preprint of the relevant paper is available on the arXiv [47].

Chapter 2

Formalism

In this chapter we outline the fuzzy space formalism for NCQM, in particular discussing the non-commutative analogues to each of those constructions in quantum mechanics that ordinarily rely on the existence of position eigenstates (such as position measurement, wavefunctions, etc). We try to motivate each of our definitions, of fuzzy space and subsequently quantum states and observables, as natural analogues of their usual commutative counterparts.

This chapter constitutes literature review — the three-dimensional fuzzy space formalism is well-established in existing literature [12, 37, 27, 20], and its development shares some similarities with that of the two-dimensional Moyal plane formalism [38, 32]. That said, we add a great deal of detail in the form of motivation and derivations. Also, some of our conventions (such as the definition of our POVM in section 2.2, or our choices of state normalisation) differ in places from each of the respective sources, so it is still worth being thorough in our presentation.

2.1 Non-commutative quantum mechanics

A sensible modern development [41] of commutative quantum (wave) mechanics may begin with the following steps (though perhaps not in as many words):

1. Define a *configuration space*, $\mathcal{H}_{\mathrm{c}}$, typically $\mathcal{H}_{\mathrm{c}} \coloneqq \mathbb{R}^3$, elements of which represent points in space.

2. Define quantum states as elements of a Hilbert space, $\mathcal{H}_{\mathrm{q}}$, typically $\mathcal{H}_{\mathrm{q}} \coloneqq \mathcal{L}^2(\mathbb{R}^3)$, which comprises square-integrable (wave)functions over the configuration space.

3. Define the (abstract) Heisenberg algebra, $\mathfrak{h}$, by the commutation relations

$$\begin{aligned}[x_i, p_j] &= i\hbar\delta_{ij}, \\ [x_i, x_j] &= [p_i, p_j] = 0.\end{aligned}$$

   These are the commutation relations that we eventually want our quantised position and momentum components to satisfy. These commutation relations (among many others in quantum mechanics) are derived systematically from analogous equations in classical mechanics. To be precise, we have applied the *quantisation prescription*

$\{\cdot,\cdot\} \to \frac{1}{i\hbar}[\cdot,\cdot]$. to the Poisson brackets (see 2.7.4 in [41], for instance),

$$\{x_i, p_j\} = \delta_{ij},$$
$$\{x_i, x_j\} = \{p_i, p_j\} = 0,$$

from classical mechanics.

4. Realise the desired commutation relations by selecting a (unitary) representation of $\mathfrak{h}$ in terms of operators $\hat{x}_i$ and $\hat{p}_j$ (called *observables*) on $\mathcal{H}_{\mathrm{q}}$.

   In this case, the Stone-von Neumann theorem (see chapter 14 of [21], for instance) ensures the uniqueness up to unitary equivalence of this representation, the standard choice for which is the Schrödinger representation,

$$\hat{x}_i\psi(\mathbf{x}) \coloneqq x_i\psi(\mathbf{x}), \quad \hat{p}_i\psi(\mathbf{x}) \coloneqq -i\hbar\frac{\partial}{\partial x_i}\psi(\mathbf{x}).$$

5. From this point, we can define other observables in terms of $\hat{x}_i$ and $\hat{p}_j$ (ignoring observables that pertain to internal degrees of freedom such as spin), all of which are self-adjoint operators acting on the Hilbert space of quantum states.

Of course, this is not a complete development — it omits mention of measurement, mixed states, dynamics, and so on. Moreover, the above description places special emphasis on *position* over other observables (indeed, wavefunctions are functions of position specifically). In fact, this construction, often called the "coordinate representation" or "Schrödinger representation", is but a special case of a more representation-agnostic approach (followed in [7], for instance) which begins instead by taking a completely abstract Hilbert space as the space of quantum states. For a general quantum state $|\psi\rangle$ in this abstract Hilbert space, we can recover the wave mechanics picture (the coordinate representation) by defining the corresponding wavefunction $\psi(\boldsymbol{x})$ as the inner product

$$\psi(\boldsymbol{x}) \coloneqq \langle \boldsymbol{x}|\psi\rangle\,, \tag{2.1.1}$$

where the states $|\boldsymbol{x}\rangle$ are the eigenstates of the position operators, $\hat{x}_i\,|\boldsymbol{x}\rangle = x_i\,|\boldsymbol{x}\rangle$. In this coordinate representation, the completeness relation,

$$\int d\boldsymbol{x}\,|\boldsymbol{x}\rangle\langle\boldsymbol{x}| = \mathbf{1}, \tag{2.1.2}$$

ensures square-integrability of the wavefunctions, since

$$\langle\psi|\psi\rangle = \int d\boldsymbol{x}\,\langle\psi|\boldsymbol{x}\rangle\,\langle\boldsymbol{x}|\psi\rangle = \int d\boldsymbol{x}\,\bar{\psi}(\boldsymbol{x})\,\psi(\boldsymbol{x}) < \infty. \tag{2.1.3}$$

We will see that our approach to formulating NCQM, which closely follows the constructions in [38] and [37], proceeds along very similar lines to the above — we similarly establish a configuration space, then a quantum state Hilbert space, and finally observables. Moreover, with the defining feature of NCQM being the non-commutativity of the coordinate operators, we will prefer a more concrete construction, like the first one discussed above, which explicitly places special emphasis on *position* and uses it to derive other observables where possible. That said, our development of NCQM will also differ from the above commutative approach in a few important ways:

1. The quantum state space we define will not contain wavefunctions in the usual sense of square-integrable complex-valued functions on configuration space. Indeed, the usual conception of wavefunctions as per (2.1.1) presents some difficulty in the non-commutative context, owing to the lack of position eigenstates. That said, we discuss the appropriate non-commutative analogues of such wavefunctions in section 2.2.3.

2. We will use spherical coordinates throughout; indeed, our non-commutative configuration space $\mathcal{H}_c$ (called "fuzzy space") already encodes positions in a radially-symmetric manner. This presents difficulty in working with momentum operators. In fact, even in ordinary commutative quantum mechanics, the momentum operators fail to be Hermitian when expressed in spherical coordinates.

   This is easily shown: simply write the (wave-mechanics) momentum operator $\hat{\boldsymbol{p}} = -i\hbar\boldsymbol{\nabla}$ in spherical coordinates,

   $$\hat{\boldsymbol{p}} = -i\hbar\left[\frac{\partial}{\partial r}\hat{\boldsymbol{r}} + \frac{1}{r}\frac{\partial}{\partial\theta}\hat{\boldsymbol{\theta}} + \frac{1}{r\sin\theta}\frac{\partial}{\partial\phi}\hat{\boldsymbol{\phi}}\right],$$

   and consider its matrix element with respect to two $l = 0$ states (*i.e.* states whose wavefunctions depend only on r), say $|\psi\rangle$ and $|\varphi\rangle$,

   $$\begin{aligned}\langle\psi|\hat{\boldsymbol{p}}\varphi\rangle &= \hat{\boldsymbol{r}}\int d\Omega\int_0^\infty dr\, r^2\,\bar{\psi}(r)\left[-i\hbar\frac{\partial}{\partial r}\right]\varphi(r)\\ &= -\hat{\boldsymbol{r}}\int d\Omega\int_0^\infty dr\,\left(\frac{\partial}{\partial r}\left[r^2\,\bar{\psi}(r)\right]\right)(-i\hbar)\,\varphi(r)\\ &= \hat{\boldsymbol{r}}\int d\Omega\int_0^\infty dr\, r^2\,\left(i\hbar\left[\frac{2}{r}+\frac{\partial}{\partial r}\right]\bar{\psi}(r)\right)\varphi(r)\\ &\neq \langle\hat{\boldsymbol{p}}\psi|\varphi\rangle\end{aligned}$$

   where on the second line, we integrated by parts (assuming the boundary term to vanish at infinity). We thus identify the Hermitian conjugate of $\hat{\boldsymbol{p}}$, written in the coordinate representation, as $-i\hbar\left[2/r + \partial/\partial r\right]$, meaning $\hat{\boldsymbol{p}}$ is not Hermitian in spherical coordinates.

   As a result of this complication, we avoid writing down the momentum operators entirely, focusing instead on *angular momentum* operators. This changes the algebra of observables we will seek to represent. Additional observables should all still be derivable from the base observables, only now these base observables will be position and angular momentum.

3. We will start by choosing the appropriate coordinate commutation relations (this being the defining feature of NCQM), corresponding roughly to step 3 of the above procedure, and only thereafter retroactively select appropriate configuration and state spaces (corresponding to steps 1 and 2).

2.1.1 Fuzzy space

As mentioned above, our starting point is a choice of non-trivial commutation relations for the coordinate operators. The simplest non-trivial choice would be requiring the operators to satisfy the Heisenberg-Moyal [20] commutation relations,

$$[\hat{x}_i, \hat{x}_j] = i\theta_{ij}, \tag{2.1.4}$$

that is, having the coordinates commute up to some constant tensor, θ_{ij}. This tensor must be skew-symmetric, since the left-hand side of (2.1.4) accrues a minus sign on exchange of

i and j; the inclusion of a factor of i then makes the right-hand-side Hermitian. While this choice is sufficient in two dimensions [38], the three-dimensional case requires more complicated commutation relations in order for rotational symmetry to be preserved. Indeed, we can easily see that (2.1.4) breaks rotational symmetry in any odd number of dimensions, say $2n+1$. By virtue of its skew-symmetry, the matrix θ must have a vanishing eigenvalue as its determinant vanishes:

$$\det\theta = \det\left(\theta^T\right) = \det(-\theta) = (-1)^{2n+1}\det\theta = -\det\theta;$$

but then the associated eigenvector will define a preferred commutative direction [12], which is what breaks rotational symmetry. While some problems, like the Aharonov-Bohm effect [8, 9] or indeed the Hydrogen atom [3, 11, 10] can nonetheless still be formulated and examined in 3D using these symmetry-breaking commutation relations, they are usually undesirable. For instance, as a direct consequence of their violation of rotational symmetry, these commutation relations give rise to problematic thermodynamic behaviour, including the failure of entropy to be extensive, and the absence of incompressibility for fermion gasses [28].

A more appealing viable alternative, which we adopt here, is the *fuzzy sphere* algebra [12, 37, 27, 20], defined by the commutation relations

$$[\hat{x}_i, \hat{x}_j] = 2i\lambda\epsilon_{ijk}\hat{x}_k, \tag{2.1.5}$$

where λ is a constant with dimensions of length, called the *non-commutative parameter*. As an abstract Lie algebra, the coordinate algebra is clearly isomorphic to $\mathfrak{su}(2)$ via the isomorphism $\hat{x}_i \mapsto \lambda\sigma^i$ (where the σ^i are the usual Pauli matrices).

We wish to realise this algebra in terms of coordinate operators acting on some concrete space. This amounts to a choice of Lie algebra representation. Although we eventually want our coordinate *observables* to be represented on the *quantum state space*, we will first imagine the coordinates as operators $\hat{x}_i$ on *configuration space*. The motivation for this will soon become apparent; in essence, we will define the quantum states in terms of these coordinate operators in a manner which will subsequently allow us to "lift" each operator $\hat{x}_i$ to a corresponding observable $\hat{X}_i$ acting on quantum states.

For the sake of concreteness, we adopt the Jordan-Schwinger representation (the reason for this particular choice will shortly become apparent), where $\mathfrak{su}(2)$ elements act on the two-boson-mode Fock space,

$$\mathcal{F} \coloneqq \operatorname{span}\left\{ |n_1, n_2\rangle \equiv \frac{(a_1^\dagger)^{n_1}(a_2^\dagger)^{n_2}}{\sqrt{n_1!n_2!}}|0\rangle \;\middle|\; n_1, n_2 \in \mathbb{N} \right\},$$

via the Lie algebra homomorphism sending each matrix $X \in \mathfrak{su}(2)$ to the bilinear operator $a_\mu^\dagger X_{\mu\nu} a_\nu$ acting on $\mathcal{F}$ (this homomorphism is called the "Jordan map" [39]). Here $a_\mu^\dagger$ and a_μ (for $\mu = 1, 2$) are the standard creation and annihilation operators respectively, and $|0\rangle \equiv |0,0\rangle \in \mathcal{F}$ is the vacuum state of the Fock space. In particular, if we consider our coordinates as $\mathfrak{su}(2)$ matrices, using the Lie algebra isomorphism $\hat{x}_i \mapsto \lambda\sigma^i$, they are represented under the Jordan map as the operators

$$\hat{x}_i = \lambda a_\mu^\dagger \sigma^i_{\mu\nu} a_\nu. \tag{2.1.6}$$

As an $\mathfrak{su}(2)$-representation, $\mathcal{F}$ is reducible, decomposing as usual into a direct sum of irreps,

$$\mathcal{F} = \bigoplus_{n\in\mathbb{N}} \mathcal{F}_n, \quad \text{where} \quad \mathcal{F}_n \coloneqq \operatorname{span}\left\{ |n_1, n_2\rangle \in \mathcal{F} \mid n_1 + n_2 = n \right\}. \tag{2.1.7}$$

Of course, since SU(2) is simply-connected, its (irreducible) representations are in a one-to-one correspondence with those of $\mathfrak{su}(2)$, and so each $\mathcal{F}_n$ can just as well be considered as a (indeed, up to isomorphism, the *unique*) $(n+1)$-dimensional SU(2) irrep [22].

Each irrep $\mathcal{F}_n$ is indexed by (indeed, an eigenspace of) the $\mathfrak{su}(2)$ Casimir operator, $\hat{r}^2 = \hat{x}_i\hat{x}_i$, which can be rewritten in terms of the boson number operator, $\hat{n} = a^\dagger_\mu a_\mu$, according to

$$\begin{aligned}
\hat{r}^2 &= \lambda^2(a^\dagger_\alpha \sigma^i_{\alpha\beta} a_\beta)(a^\dagger_\mu \sigma^i_{\mu\nu} a_\nu) \\
&= \lambda^2 a^\dagger_\alpha a_\beta a^\dagger_\mu a_\nu (2\delta_{\alpha\nu}\delta_{\beta\mu} - \delta_{\alpha\beta}\delta_{\mu\nu}) \\
&= \lambda^2(2a^\dagger_\alpha a_\beta a^\dagger_\beta a_\alpha - a^\dagger_\alpha a_\alpha a^\dagger_\mu a_\mu) \\
&= \lambda^2(2a^\dagger_\alpha a_\beta(a_\alpha a^\dagger_\beta - [a_\alpha, a^\dagger_\beta]) - \hat{n}^2) \\
&= \lambda^2(2a^\dagger_\alpha a_\alpha(a_\beta a^\dagger_\beta - 1) - \hat{n}^2) \\
&= \lambda^2(2\hat{n}(\hat{n} + [a_\beta, a^\dagger_\beta] - 1) - \hat{n}^2) \\
&= \lambda^2 \hat{n}(\hat{n} + 2).
\end{aligned}$$

In the above, we have invoked the completeness relation for the Pauli matrices,

$$\boldsymbol{\sigma}_{\alpha\beta} \cdot \boldsymbol{\sigma}_{\mu\nu} = 2\delta_{\alpha\nu}\delta_{\beta\mu} - \delta_{\alpha\beta}\delta_{\mu\nu}, \tag{2.1.8}$$

along with the standard commutation relations for creation and annihilation operators,

$$\begin{aligned}
[a_\mu, a^\dagger_\nu] &= \delta_{\mu\nu} \\
[a_\mu, a_\nu] &= 0 = [a^\dagger_\mu, a^\dagger_\nu].
\end{aligned} \tag{2.1.9}$$

It is convenient to consider the square root (to leading order in λ) of the Casimir operator as a measure of *radius*, given by

$$\hat{r} = \lambda(\hat{n} + 1), \tag{2.1.10}$$

which has the required dimensions of length. With this identification, we note that $\mathcal{F}$ contains every unique $\mathfrak{su}(2)$-irrep, and hence each quantised radius, exactly once. This motivates our choice of the Jordan-Schwinger representation: we can think of $\mathcal{F}$ as representing a construction of 3D space out of a collection of concentric spherical shells — one for each quantised radius.

We take the Fock space $\mathcal{F}$, called *fuzzy space*, as our *configuration space*, $\mathcal{H}_c$. We write its general element as a ket, $|\psi\rangle$, in standard Dirac notation, consistent with the notation used above. We stress two conceptual points pertaining to $\mathcal{H}_c$. The first likely goes without saying: though we have referred to $\mathcal{H}_c$ as a "two-boson-mode Fock space", and will occasionally reference related quantities such as boson number, creation operators, and so on, we should remember that the states in $\mathcal{H}_c$ do not count actual bosons in our system — the Fock space is merely a convenient concrete choice of vector space on which to represent our coordinates. Secondly, when describing the development of commutative quantum mechanics at the beginning of this chapter, we described elements of the configuration space as representing "points in space". Above, we conceptualised $\mathcal{H}_c$ as a sort of construction of 3D space out of concentric shells, but at the moment it is still unclear *which* elements of $\mathcal{H}_c$ precisely should stand in for individual points in space. These will turn out to be the *coherent states*, $\boldsymbol{z}$, but we will defer a thorough discussion of them to section 2.2.1.

2.1.2 Quantum state space

Our *quantum state (Hilbert) space*, $\mathcal{H}_{\mathrm{q}}$, is defined as the operator algebra acting on $\mathcal{H}_{\mathrm{c}}$ generated by the coordinates. We denote its elements with the notation $|\psi)$ to distinguish them from those of $\mathcal{H}_{\mathrm{c}}$. The inner product on $\mathcal{H}_{\mathrm{q}}$ is chosen to be the *weighted* Hilbert-Schmidt inner product[1]

$$(\psi|\phi) \coloneqq 4\pi\lambda^2 \operatorname{Tr}_{\mathrm{c}}\left(\psi^\dagger \hat{r}\phi\right) = 4\pi\lambda^3 \operatorname{Tr}_{\mathrm{c}}\left(\psi^\dagger(\hat{n}+1)\phi\right), \tag{2.1.11}$$

where the trace $\operatorname{Tr}_{\mathrm{c}}$ is performed over configuration space $\mathcal{H}_{\mathrm{c}}$. Using this inner product, we can characterise $\mathcal{H}_{\mathrm{q}}$ as the space of Hilbert-Schmidt operators on $\mathcal{H}_{\mathrm{c}}$ which commute with the Casimir operator [37] (as each of the coordinates generating $\mathcal{H}_{\mathrm{q}}$ commutes with $\hat{r}^2$), and express it in the form

$$\mathcal{H}_{\mathrm{q}} = \left\{ \psi \equiv \sum_{m_i,n_i} C^{m_1,m_2}_{n_1,n_2} (a_1^\dagger)^{m_1}(a_2^\dagger)^{m_2} a_1^{n_1} a_2^{n_2} \;\middle|\; \|\psi\| < \infty, \quad m_1+m_2 = n_1+n_2 \right\}, \tag{2.1.12}$$

where $\|\psi\| \coloneqq (\psi|\psi)$ uses the inner product of (2.1.11). In the above, the condition $m_1 + m_2 = n_1 + n_2$ ensures commutation with $\hat{r}^2$.

We will sometimes consider operators in the larger space, $\mathscr{B}_2(\mathcal{H}_{\mathrm{c}}) \supset \mathcal{H}_{\mathrm{q}}$, consisting of *all* Hilbert-Schmidt operators (not only those commuting with the Casimir) acting on $\mathcal{H}_{\mathrm{c}}$ (with the same inner product as on $\mathcal{H}_{\mathrm{q}}$). It can be shown [14] that $\mathscr{B}_2(\mathcal{H}_{\mathrm{c}})$ is also a Hilbert space with respect to the same inner product as defined in (2.1.11). Moreover, we have an isometric isomorphism (see section 2.6 of [23]),

$$\mathscr{B}_2(\mathcal{H}_{\mathrm{c}}) \cong \mathcal{H}_{\mathrm{c}} \otimes \mathcal{H}_{\mathrm{c}}^*, \tag{2.1.13}$$

where $\otimes$ denotes the *Hilbert-space tensor product* — for Hilbert spaces A and B, $A \otimes B$ is defined as a completion of the *algebraic tensor product* $A \otimes_{\mathrm{alg}} B$ with respect to the inner product induced on $A \otimes_{\mathrm{alg}} B$ by those on each of A and B (for full details see [23], for instance). This identification lets us consider an everywhere-dense subset of $\mathscr{B}_2(\mathcal{H}_{\mathrm{c}})$ as linear combinations of *ket-bra*s:

$$\mathscr{B}_2(\mathcal{H}_{\mathrm{c}}) = \overline{\operatorname{span}\{|m_1,m_2\rangle\langle n_1,n_2| \mid n_i, m_i \in \mathbb{N}\}}, \tag{2.1.14}$$

where the overbar denotes the completion. For brevity (and because for our physics it suffices to work on a dense subset), we will hereafter suppress writing (and remarking on) the completion.

The restriction of having to commute with $\hat{r}^2$ forces operators in $\mathcal{H}_{\mathrm{q}}$ to restrict to each of the subspaces $\mathcal{F}_n$ in (2.1.7). Explicitly this means

$$\mathcal{H}_{\mathrm{q}} = \bigoplus_{n\in\mathbb{N}} \mathscr{B}_2(\mathcal{F}_n) \subset \mathscr{B}_2\left(\bigoplus_{n\in\mathbb{N}} \mathcal{F}_n\right) = \mathscr{B}_2(\mathcal{H}_{\mathrm{c}}), \tag{2.1.15}$$

which we can write in the simpler notation of (2.1.14) as

$$\mathcal{H}_{\mathrm{q}} = \operatorname{span}\{|m_1,m_2\rangle\langle n_1,n_2| \mid n_i, m_i \in \mathbb{N}, n_1+n_2 = m_1+m_2\}, \tag{2.1.16}$$

[1] This particular inner product is chosen so that the resulting norm of the projection operator, $\hat{P}_N$, onto the subspace $\mathcal{F}_0 \oplus \cdots \oplus \mathcal{F}_N \subseteq \mathcal{H}_{\mathrm{c}}$ tends to the volume, $4\pi r^3$, of the sphere of radius $r = \lambda(N+1)$, as $N \to \infty$ [20].

recalling from (2.1.7) the constraint defining each $\mathcal{F}_n$. This is a fairly simple picture of our quantum states. Of course, each ket $|n_1, n_2\rangle \in \mathcal{H}_c$ is also a simultaneous eigenket of $\hat{r}^2 = \hat{x}_\mu \hat{x}_\mu$ and $\hat{x}_3$:

$$\begin{aligned} \hat{r}^2 \,|n_1, n_2\rangle &= 4\lambda^2\, j(j+1)\,|n_1, n_2\rangle\,, \quad \text{where} \quad j = \frac{n_1+n_2}{2} \\ \hat{x}_3\,|n_1, n_2\rangle &= 2\lambda\, m\,|n_1, n_2\rangle\,, \qquad\quad \text{where} \quad m = \frac{n_1-n_2}{2}, \end{aligned} \tag{2.1.17}$$

allowing us to alternately label using quantum numbers j and m, which, wherever they appear, (implicitly) range over $j \in \mathbb{N}/2$ and $m \in \mathbb{Z}/2 \cap [-j, j]$. In this notation, we can write each $\mathfrak{su}(2)$-irrep $\mathcal{F}_n$ appearing in the decomposition of (2.1.7) as $\mathcal{F}_n = \text{span}\,\{|j = n/2, m\rangle\}$, and (2.1.16) is simply

$$\mathcal{H}_q = \text{span}\left\{ \left| j = n/2, m \right\rangle\!\!\left\langle j = n/2, m' \right| \;\middle|\; n \in \mathbb{N} \right\}. \tag{2.1.18}$$

2.1.3 Quantum observables in fuzzy space

With our configuration- and state spaces defined, we must now define quantum observables. As in the commutative case, these will be Hermitian operators on $\mathcal{H}_q$, and we similarly begin by seeking the operators corresponding to position and angular momentum. For this we must identify a unitary representation of the algebra

$$\begin{aligned} [X_i, X_j] &= 2i\lambda\, \epsilon_{ijk} X_k, \\ [L_i, X_j] &= i\hbar\, \epsilon_{ijk} X_k, \\ [L_i, L_j] &= i\hbar\, \epsilon_{ijk} L_k, \end{aligned} \tag{2.1.19}$$

in terms of operators, $\hat{X}_i$ and $\hat{L}_j$ respectively, acting on $\mathcal{H}_q$ (we use capital letters to distinguish observables from operators on $\mathcal{H}_c$). Note that this algebra is a straightforward modification of the usual algebra of coordinate and angular momentum components from commutative quantum mechanics; the only change is that we now demand the same coordinate commutation relations as in (2.1.5), rather than the typical $[X_i, X_j] = 0$.

Representing the position operators $\hat{X}_i$ is straightforward, as they share commutation relations with the coordinates x_i:

$$\hat{X}_i\,|\psi) \coloneqq |\hat{x}_i \psi)\,. \tag{2.1.20}$$

This is what was meant in section 2.1.1 by "lifting" the algebra of the operators $\hat{x}_i$ to the observables — the multiplicative action trivially ensures identical commutation relations. This action mirrors the usual left-multiplicative action of position operators in the Schrödinger representation of commutative quantum mechanics, $\hat{x}_i\,\psi(\mathbf{x}) \coloneqq x_i\,\psi(\mathbf{x})$. We also lift the radius operator $\hat{r}$ to an observable by the same multiplicative action

$$\hat{R}\,|\psi) \coloneqq |\hat{r}\psi)\,. \tag{2.1.21}$$

Angular momentum operators have the adjoint action,

$$\hat{L}_i\,|\psi) \coloneqq \left| \frac{\hbar}{2\lambda}\,[\hat{x}_i, \psi] \right), \tag{2.1.22}$$

which is easily shown to yield the normal angular momentum commutation relations.

Some other observables are straightforward generalisations of their commutative counterparts. For instance, the Hamiltonian takes a familiar form

$$\hat{H} = -\frac{\hbar^2}{2m}\hat{\Delta} + V(\hat{R}), \tag{2.1.23}$$

only now the Laplacian is defined

$$\hat{\Delta}\left|\psi\right) \coloneqq -\left|\frac{1}{\lambda\hat{r}}[a_\alpha^\dagger,[a_\alpha,\psi]]\right). \tag{2.1.24}$$

This form of the Laplacian is motivated in [20]; in particular, it is chosen to commute with each of the angular momentum operators. Notably, since they commute with $\hat{\Delta}$, the angular momentum operators also commute with $\hat{H}$, ensuring angular momentum conservation.[2]

Another conserved observable, defined on the entirety of $\mathscr{B}_2(\mathcal{H}_\mathrm{c})$, is

$$\hat{\Gamma}\left|\psi\right) \coloneqq \left|[\hat{n},\psi]\right). \tag{2.1.25}$$

This is indeed an observable (that is, a Hermitian operator), since

$$\begin{aligned}\left(\phi\middle|\hat{\Gamma}\psi\right) &= 4\pi\lambda^2\,\mathrm{Tr}_\mathrm{c}\left(\phi^\dagger\hat{r}\,[\hat{n},\psi]\right)\\ &= 4\pi\lambda^2\,\mathrm{Tr}_\mathrm{c}\left(\left[\phi^\dagger,\hat{n}\right]\hat{r}\psi\right)\\ &= 4\pi\lambda^2\,\mathrm{Tr}_\mathrm{c}\left([\hat{n},\phi]^\dagger\,\hat{r}\psi\right)\\ &= \left(\hat{\Gamma}\phi\middle|\psi\right),\end{aligned}$$

where we have used the fact that $[\hat{r},\hat{n}]=0$, together with properties of the trace. Therefore we can write a basis for $\mathscr{B}_2(\mathcal{H}_\mathrm{c})$ consisting of eigenvectors for $\hat{\Gamma}$. Indeed, the eigenstates of $\hat{\Gamma}$ are simply those of the form $|m_1,m_2\rangle\langle n_1,n_2|$, since

$$\hat{\Gamma}\left|m_1,m_2\right\rangle\!\left\langle n_1,n_2\right| = (m_1+m_2-n_1-n_2)\left|m_1,m_2\right\rangle\!\left\langle n_1,n_2\right|,$$

and these states manifestly span (a dense subset of) $\mathscr{B}_2(\mathcal{H}_\mathrm{c})$, since $\mathscr{B}_2(\mathcal{H}_\mathrm{c})\cong\mathcal{H}_\mathrm{c}\otimes\mathcal{H}_\mathrm{c}^*$, as noted above. Then (2.1.16) implies that the physical subspace, $\mathcal{H}_\mathrm{q}$, of $\mathscr{B}_2(\mathcal{H}_\mathrm{c})$ is simply the zero eigenspace (or kernel) of $\hat{\Gamma}$. The fact that $\hat{\Gamma}$ is conserved then simply reassures us that the physical subspace $\mathcal{H}_\mathrm{q}$ is preserved under time-evolution.

Finally, the linear operator

$$\hat{Q} \coloneqq \frac{1}{2\pi}\int_0^{2\pi} e^{i\phi\hat{\Gamma}}\,d\phi, \tag{2.1.26}$$

is easily seen by the spectral theorem to just be the projection operator from $\mathscr{B}_2(\mathcal{H}_\mathrm{c})$ onto $\ker\hat{\Gamma}\cong\mathcal{H}_\mathrm{q}$. This projection operator will prove useful in section 2.2 for defining position measurement.

2.2 Position measurement and related matters

At this stage, we have a completely valid starting point for doing quantum mechanics. Our quantum states are elements of some Hilbert space, $\mathcal{H}_\mathrm{q}$, and our observables are Hermitian operators on that Hilbert space. This is the typical structure — the internal details of the Hilbert space $\mathcal{H}_\mathrm{q}$ are essentially irrelevant to the abstract formulation (as in, say, [7]) of quantum mechanics. So at this stage, one might wonder why we have gone to great lengths to explicitly construct $\mathcal{H}_\mathrm{c}$ and $\mathcal{H}_\mathrm{q}$, and, for that matter, how NCQM differs at all from the ordinary formalism of quantum mechanics on an abstract Hilbert space of states.

[2] This is because the time evolution operator takes the usual form, $\hat{U}(t)\coloneqq e^{-i\hat{H}t/\hbar}$, so that, as in commutative quantum mechanics, an observable $\hat{O}$ commuting with $\hat{H}$ implies its conservation. Indeed, using the Heisenberg picture of time evolution, we have $\hat{O}(t)=\hat{U}^\dagger(t)\hat{O}\hat{U}(t)=\cancel{\hat{U}^\dagger(t)\hat{U}(t)}\hat{O}=\hat{O}(t=0)$.

To the latter question, we might point out that, from an abstract mathematical perspective, NCQM ultimately *is* ordinary quantum mechanics; it differs from the usual framework only in how it handles position, position measurements, and wavefunctions — those matters that rely normally on the existence of commuting coordinates. These are more differences in our physical interpretation of the underlying mathematical structure (which observables we call "position", how we measure them, and so on) than in said structure itself. This also serves to answer the former question: we explicitly construct the spaces $\mathcal{H}_\mathrm{c}$ and $\mathcal{H}_\mathrm{q}$ for added convenience in performing calculations, and physically interpreting the results of those calculations, especially when said calculations pertain to position.

In this section, we turn our attention to the remaining subtleties (in a sense, the defining subtleties) of NCQM, namely the matters of position — specifically we formulate position measurement, and coordinate representations of states (the analogues of wavefunctions). The main obstacle to the usual formulation is the following: since our position operators $\hat{X}_i$ do not commute, they have no simultaneous eigenbasis, meaning there are no fully-localised position eigenstates of the form $|\boldsymbol{x}\rangle$. In the absence of fully-localised states, we strive instead for *maximally-localised* — alternately, *minimal-uncertainty* — states.

Since our position observables $\hat{X}_i$ share commutation relations with the operators $\hat{x}_i$, we will start by formulating the minimal-uncertainty states of the $\hat{x}_i$. It is well known [25] that the Glauber coherent states $|\boldsymbol{z}\rangle$ suit this purpose, so we will start by reviewing their pertinent properties, all of which can be found in [25]. In subsequent sections we will outline position measurement, and finally lift the coherent states $|\boldsymbol{z}\rangle \in \mathcal{H}_\mathrm{c}$ to analogous states $|\boldsymbol{z}) \in \mathcal{H}_\mathrm{q}$ that will be used to define the coordinate representations of states.

2.2.1 Coherent states

The Glauber coherent states, written

$$|\boldsymbol{z}\rangle \equiv |z_1, z_2\rangle\,, \quad \text{for } \boldsymbol{z} = \begin{bmatrix} z_1 \\ z_2 \end{bmatrix} \in \mathbb{C}^2,$$

are defined to be eigenstates of the annihilation operators, $a_\alpha |\boldsymbol{z}\rangle = z_\alpha |\boldsymbol{z}\rangle$. Such eigenstates can be constructed by application of the displacement operator, defined

$$\hat{D}(\boldsymbol{z}) := e^{z_\alpha a_\alpha^\dagger - \bar{z}_\alpha a_\alpha}, \tag{2.2.1}$$

on the vacuum state, $|\boldsymbol{z}\rangle = \hat{D}(\boldsymbol{z})\,|0\rangle$. For our purposes, we prefer the alternative form

$$\begin{aligned} |\boldsymbol{z}\rangle &= \hat{D}(\boldsymbol{z})\,|0\rangle \\ &= e^{-\frac{1}{2}\left[z_\alpha a_\alpha^\dagger, -\bar{z}_\beta a_\beta\right]} e^{z_\alpha a_\alpha^\dagger} \cancel{e^{-\bar{z}_\alpha a_\alpha}} |0\rangle \\ &= e^{-\frac{1}{2}\bar{z}_\alpha z_\alpha} e^{z_\alpha a_\alpha^\dagger} |0\rangle\,, \end{aligned} \tag{2.2.2}$$

in which the operator acting on the vacuum state contains no explicit annihilation operators. It is easy to confirm directly that this construction satisfies the definition:

$$\begin{aligned} a_\beta \left(e^{-\frac{1}{2}\bar{z}_\alpha z_\alpha} e^{z_\alpha a_\alpha^\dagger}\right) |0\rangle &= e^{-\frac{1}{2}\bar{z}_\alpha z_\alpha} \left[a_\beta, e^{z_\alpha a_\alpha^\dagger}\right] |0\rangle \\ &= z_\beta \left(e^{-\frac{1}{2}\bar{z}_\alpha z_\alpha} e^{z_\alpha a_\alpha^\dagger}\right) |0\rangle\,. \end{aligned}$$

The commutator above is easily computed from (2.1.9), together with the fact that $[\hat{J}, \hat{K}] = c\mathbf{1}$ implies $[\hat{J}, f(\hat{K})] = cf'(\hat{K})$ (easily proven by induction using the Leibniz rule).

The coherent states are normalised (as constructed above), but not orthogonal (since the a_i are not self-adjoint, their eigenstates need not be orthogonal), with their overlap given by

$$\langle \boldsymbol{z} | \boldsymbol{z}' \rangle = e^{-\frac{1}{2}(\bar{z}_\alpha z_\alpha + \bar{z}'_\alpha z'_\alpha - 2\bar{z}_\alpha z'_\alpha)} = e^{-\frac{1}{2}\left(\|\boldsymbol{z}\|^2 + \|\boldsymbol{z}'\|^2\right) + \boldsymbol{z}^\dagger \boldsymbol{z}'}. \tag{2.2.3}$$

Finally, the coherent states form an overcomplete basis for $\mathcal{H}_\mathrm{c}$, which is expressed by the resolution of the identity operator, $\mathbf{1}_\mathrm{c}$, on $\mathcal{H}_\mathrm{c}$ as

$$\int \frac{d^4 z}{\pi^2} \, |\boldsymbol{z}\rangle\langle \boldsymbol{z}| = \mathbf{1}_\mathrm{c}, \tag{2.2.4}$$

where the integral measure $d^4 z$, sometimes also written $d\bar{z}_1 dz_1 d\bar{z}_2 dz_2$ in the literature, is shorthand for $d\,\mathrm{Re}(z_1) d\,\mathrm{Im}(z_1) d\,\mathrm{Re}(z_2) d\,\mathrm{Im}(z_2)$.

2.2.2 Position measurement POVM

We will now turn our attention to defining position measurement. To this end, we will use the framework of Positive-Operator-Valued Measure (POVM) measurement (see section 2.2.6 of [30], for a good introduction to this framework). At this stage, we should note that our choice of $\mathfrak{su}(2)$ coherent states, as defined in the previous section, differs slightly from that in [27], wherein states of the form $|n, z\rangle$ are used, with the radius fixed by the choice of n. Instead, our coherent states coincide with those used in [37], but this latter source does explicitly not use its coherent states for the sake of furnishing a POVM for position measurement. The construction we describe in this section therefore mimics that of [27], but also differs superficially in places due to the different choices of convention. This disparity is compounded by the fact that the POVM definition in [27] (given in equation 17) makes use of a star product, while our definition (given in (2.2.7) below) does not. To help bridge this notational gap, we will also derive a form of our POVM operators involving a star product, although we only do so in section 2.2.3 (specifically, see (2.2.17)).

Our construction starts with the use of coherent states to represent points in space: the two complex values, z_1 and z_2, needed to specify a coherent state together provide sufficient degrees of freedom to encode a point in three-dimensional space. More precisely, for the sake of describing a position measurement occurring at a point, $\boldsymbol{D} \in \mathbb{R}^3$, we will encode the spherical coordinates (r, θ, ϕ) of $\boldsymbol{D}$ in the values

$$z_1 = \sqrt{\frac{r}{\lambda}} \cos\left(\frac{\theta}{2}\right) e^{-i\frac{\phi}{2}} e^{i\gamma}, \quad \text{and} \quad z_2 = \sqrt{\frac{r}{\lambda}} \sin\left(\frac{\theta}{2}\right) e^{i\frac{\phi}{2}} e^{i\gamma}. \tag{2.2.5}$$

of a coherent state $|\boldsymbol{z}\rangle$. Hereafter we adopt the notation $R \coloneqq \frac{r}{\lambda}$, for the dimensionless radius. The encoding is such that the expectation values,

$$\begin{aligned} \langle \boldsymbol{z} | \hat{x}_i | \boldsymbol{z} \rangle &= \lambda \, \langle \boldsymbol{z} | a^\dagger_\mu \sigma^i_{\mu\nu} a_\nu | \boldsymbol{z} \rangle \\ &= \lambda \, z^\dagger_\mu \sigma^i_{\mu\nu} z_\nu \\ &= \lambda \, \boldsymbol{z}^\dagger \sigma^i \boldsymbol{z}, \end{aligned}$$

reproduce the (Cartesian) coordinates of $\boldsymbol{D}$:

$$\begin{aligned} x_1 \equiv \langle \boldsymbol{z} | \hat{x}_1 | \boldsymbol{z} \rangle &= r \sin\theta \cos\phi \\ x_2 \equiv \langle \boldsymbol{z} | \hat{x}_2 | \boldsymbol{z} \rangle &= r \sin\theta \sin\phi \\ x_3 \equiv \langle \boldsymbol{z} | \hat{x}_3 | \boldsymbol{z} \rangle &= r \cos\theta. \end{aligned}$$

Notably, the global phase γ drops out of each of the above (as it must), and so constitutes an additional degree of freedom when choosing the z_i.

Of course, this notion of position exists on the level of the configuration space, $\mathcal{H}_{\mathrm{c}}$; we seek to lift it to a corresponding notion of position on the level of the quantum Hilbert space, $\mathcal{H}_{\mathrm{q}}$. To this end, first introduce corresponding states $|z_1, z_2, n_1, n_2) \in \mathscr{B}_2(\mathcal{H}_{\mathrm{c}})$, defined

$$|z_1, z_2, n_1, n_2) \coloneqq \frac{1}{\sqrt{4\pi\lambda^2\hat{r}}}\,|\boldsymbol{z}\rangle\langle n_1, n_2|\,,$$

where the inverse square-root is included for the sake of normalisation:

$$(z_1, z_1, n_1, n_2|z_1, z_1, n_1, n_2) = 4\pi\lambda^2\,\mathrm{Tr}_{\mathrm{c}}\left(|n_1, n_2\rangle\langle\boldsymbol{z}|\,\frac{1}{4\pi\lambda^2\hat{r}}\hat{r}\,|\boldsymbol{z}\rangle\langle n_1, n_2|\right) = 1.$$

Clearly these states do not commute with $\hat{n}$, and so are not physical (meaning they do not lie in the quantum state space, $\mathcal{H}_{\mathrm{q}} \equiv \ker\Gamma$, for Γ as in (2.1.25)). In order to obtain physical states in $\mathcal{H}_{\mathrm{q}}$, we can apply the projection operator $\hat{Q}$, as defined in (2.1.26),

$$\begin{aligned}|z_1, z_2, n_1, n_2)_{\mathrm{ph}} &\coloneqq \hat{Q}\,|z_1, z_2, n_1, n_2)\\ &= \hat{Q}\frac{1}{\sqrt{4\pi\lambda^2\hat{r}}}\,|\boldsymbol{z}\rangle\langle n_1, n_2|\,.\end{aligned} \tag{2.2.6}$$

Of course, due to the application of the projection operator, $\hat{Q}$, the states $|z_1, z_2, n_1, n_2)_{\mathrm{ph}}$ are no longer normalised in general. For our purposes, this is thankfully not a problem, but to explain why, we must first formulate the definition of our POVM operators.

Using the physical states of (2.2.6), we are finally able to define position measurements. As stated above, we use the framework of POVM measurement, whereby we specify a set of positive operators on $\mathcal{H}_{\mathrm{q}}$,

$$\hat{\Pi}_{\boldsymbol{z}} \coloneqq \sum_{n_1,n_2} |z_1, z_2, n_1, n_2)_{\mathrm{ph}}\,{}_{\mathrm{ph}}(z_1, z_2, n_1, n_2|. \tag{2.2.7}$$

These are clearly Hermitian and positive semi-definite (but not orthogonal), as required for a POVM. The other requirement for a POVM is that the $\hat{\Pi}_{\boldsymbol{z}}$ operators satisfy a completeness relation on $\mathcal{H}_{\mathrm{q}}$, of the form

$$\int \frac{d^4z}{\pi^2}\hat{\Pi}_{\boldsymbol{z}} = \hat{Q} = \mathbf{1}_{\mathrm{q}}. \tag{2.2.8}$$

At this point, we can appreciate why the normalisation of the states in (2.2.6) is non-essential. The additional application of $\hat{Q}$ in (2.2.6) simply causes the integral $\int \frac{d^4z}{\pi^2}\hat{\Pi}_{\boldsymbol{z}}$ to equal $\hat{Q}$ instead of the identity operator. But this is fine, since $\hat{Q} = \mathbf{1}_{\mathrm{q}}$ (the identity on the physical subspace $\mathcal{H}_{\mathrm{q}}$), and we are ultimately only interested in the behaviour on $\mathcal{H}_{\mathrm{q}}$. Proving (2.2.8) and other equations like it is straightforward, but potentially error-prone. In particular, we must be careful to remember that the bra ${}_{\mathrm{ph}}(z_1, z_2, n_1, n_2|$ represents a more subtle object than the Hermitian conjugate (on the level of $\mathcal{H}_{\mathrm{c}}$),

$$|n_1, n_2\rangle\langle\boldsymbol{z}|\,\frac{1}{\sqrt{4\pi\lambda^2\hat{r}}}\hat{Q},$$

of the right-hand-side of (2.2.6); indeed, this bra instead represents the linear functional,

$${}_{\mathrm{ph}}(z_1, z_2, n_1, n_2|\colon \mathcal{H}_{\mathrm{q}} \to \mathbb{C}\colon\ |\psi) \to 4\pi\lambda^2\,\mathrm{Tr}_{\mathrm{c}}\left(|n_1, n_2\rangle\langle\boldsymbol{z}|\,\frac{1}{\sqrt{4\pi\lambda^2\hat{r}}}\hat{Q}\,\hat{r}\,\psi\right)$$

as per the inner product, (2.1.11). The easiest way to check (2.2.8) (and other such equations where bras on $\mathcal{H}_\mathrm{q}$ appear outside of an inner product) without confusion is therefore by acting the left-hand-side on an arbitrary physical state $|\psi)$,

$$\left(\int \frac{d^4z}{\pi^2}\hat{\Pi}_{\boldsymbol{z}}\right)|\psi) = \int \frac{d^4z}{\pi^2}\sum_{n_1,n_2}|z_1,z_2,n_1,n_2)_{\mathrm{ph\ ph}}(z_1,z_2,n_1,n_2|\psi).$$

Next, simplify the inner product using (2.2.6) and (2.1.11),

$$\begin{aligned}{}_{\mathrm{ph}}(z_1,z_2,n_1,n_2|\psi) &= (z_1,z_2,n_1,n_2|\hat{Q}^\dagger|\psi)\\ &= (z_1,z_2,n_1,n_2|\psi)\\ &= 4\pi\lambda^2\,\mathrm{Tr}_\mathrm{c}\left(\frac{1}{\sqrt{4\pi\lambda^2\hat{r}}}\,|n_1,n_2\rangle\langle\boldsymbol{z}|\,\hat{r}\psi\right)\\ &= 4\pi\lambda^2\,\langle\boldsymbol{z}|\frac{1}{\sqrt{4\pi\lambda^2\hat{r}}}\hat{r}\psi|n_1,n_2\rangle\,,\end{aligned} \tag{2.2.9}$$

whence

$$\begin{aligned}\left(\int \frac{d^4z}{\pi^2}\hat{\Pi}_{\boldsymbol{z}}\right)|\psi) &= 4\pi\lambda^2\int\frac{d^4z}{\pi^2}\sum_{n_1,n_2}\hat{Q}\frac{1}{\sqrt{4\pi\lambda^2\hat{r}}}\,|\boldsymbol{z}\rangle\langle n_1,n_2|\cdot\,\langle\boldsymbol{z}|\frac{1}{\sqrt{4\pi\lambda^2\hat{r}}}\hat{r}\psi|n_1,n_2\rangle\\ &= 4\pi\lambda^2\hat{Q}\frac{1}{\sqrt{4\pi\lambda^2\hat{r}}}\left(\int\frac{d^4z}{\pi^2}\,|\boldsymbol{z}\rangle\langle\boldsymbol{z}|\right)\frac{1}{\sqrt{4\pi\lambda^2\hat{r}}}\hat{r}\psi\left(\sum_{n_1,n_2}|n_1,n_2\rangle\langle n_1,n_2|\right)\\ &= \hat{Q}\psi = \psi,\end{aligned} \tag{2.2.10}$$

where we have inserted (2.2.6) and (2.2.9), then rearranged, and finally applied completeness relations (2.2.4) and $\sum_{n_1,n_2}|n_1,n_2\rangle\langle n_1,n_2| = \mathbf{1}_\mathrm{c}$. This completes the proof that the operators $\hat{\Pi}_{\boldsymbol{z}}$ indeed form a POVM.

Given the POVM operators, the probability density function (PDF) associated with measuring a particle having initial density matrix ρ at the point $\boldsymbol{D}$ is given by the usual Born rule,

$$P(\boldsymbol{D}) = \mathrm{Tr}_\mathrm{q}\left(\hat{\Pi}_{\boldsymbol{z}}\rho\right), \tag{2.2.11}$$

which is nothing but the usual Born rule for POVM measurement [30]. The subscript on Tr_q indicates that the trace is taken over $\mathcal{H}_\mathrm{q}$. Of particular interest to us is the special case of (2.2.11) where the pre-measurement density matrix is a pure state, $\rho = |\psi)(\psi|$. In this case, the Born rule reduces to

$$\begin{aligned}P(\boldsymbol{D}) &= (\psi|\hat{\Pi}_{\boldsymbol{z}}|\psi)\\ &= \sum_{n_1,n_2}(\psi|z_1,z_2,n_1,n_2)_{\mathrm{ph\ ph}}(z_1,z_2,n_1,n_2|\psi)\\ &= (4\pi\lambda^2)^2\sum_{n_1,n_2}\langle\boldsymbol{z}|\frac{1}{\sqrt{4\pi\lambda^2\hat{r}}}\hat{r}\psi|n_1,n_2\rangle\,\langle n_1,n_2|\psi^\dagger\hat{r}\frac{1}{\sqrt{4\pi\lambda^2\hat{r}}}|\boldsymbol{z}\rangle\\ &= 4\pi\lambda^2\,\langle\boldsymbol{z}|\psi\hat{r}\psi^\dagger|\boldsymbol{z}\rangle\,,\end{aligned} \tag{2.2.12}$$

where we have substituted the inner products computed in (2.2.9),and used the fact that ψ commutes with $\hat{r}$, since $|\psi) \in \mathcal{H}_\mathrm{q}$. As expected, $P(\boldsymbol{D})$ is independent of the global phase γ in (2.2.5), and furthermore the normalisation of $|\psi)$ implies the normalisation of

the probability distribution:

$$\begin{aligned} 1 = (\psi|\psi) &= 4\pi\lambda^2 \operatorname{Tr}_{\mathrm{c}}\left(\psi^\dagger \hat{r} \psi\right) \\ &= 4\pi\lambda^2 \int \frac{d^4 z}{\pi^2} \langle \boldsymbol{z}|\psi \hat{r} \psi^\dagger|\boldsymbol{z}\rangle \,, \end{aligned}$$

where we identify the integral as running over the probability distribution, as per (2.2.12).

Of course, the normalised pure state ψ has dimension length$^{-3/2}$, implying that $P(\boldsymbol{D})$ is dimensionless. We may therefore wonder how it relates to a *spatial* probability density with dimension length^{-3}. For this we rewrite the integration measure in terms of explicit coordinates $(r, \theta, \phi, \gamma)$, computing the relevant Jacobian from (2.2.5),

$$\frac{d^4 z}{\pi^2} \equiv \frac{d\operatorname{Re}(z_1) d\operatorname{Im}(z_1) d\operatorname{Re}(z_2) d\operatorname{Im}(z_2)}{\pi^2} = \frac{r \sin\theta}{8\pi^2\lambda^2} dr d\theta d\phi d\gamma. \tag{2.2.13}$$

Therefore,

$$\begin{aligned} \int \frac{d^4 z}{\pi^2} P(\boldsymbol{D}) &= 4\pi\lambda^2 \int \frac{d^4 z}{\pi^2} \langle \boldsymbol{z}|\psi \hat{r} \psi^\dagger|\boldsymbol{z}\rangle \\ &= 4\pi\lambda^2 \int \frac{r \sin\theta}{8\pi^2\lambda^2} dr d\theta d\phi d\gamma \; \langle \boldsymbol{z}|\psi \hat{r} \psi^\dagger|\boldsymbol{z}\rangle \\ &= \int r^2 \sin\theta \, dr d\theta d\phi \, \frac{\langle \boldsymbol{z}|\psi \hat{r} \psi^\dagger|\boldsymbol{z}\rangle}{r}, \end{aligned}$$

which leads to the interpretation of

$$\frac{1}{4\pi r \lambda^2} P(\boldsymbol{D}) \equiv \frac{\langle \boldsymbol{z}|\psi \hat{r} \psi^\dagger|\boldsymbol{z}\rangle}{r}$$

as the spatial probability density function that we sought. This distinction is actually very important, for instance when comparing the measurement PDF derived in NCQM with that derived in ordinary commutative quantum mechanics (the latter being a spatial density). In our investigation, this will become relevant in section 4.4.1, where we check that the commutative limit of the fuzzy space interference pattern derived in section 4.2 coincides with the commutative result from section 4.1. We must take such a commutative limit on the level of the spatial density, $\frac{1}{4\pi r\lambda^2} P(\boldsymbol{D})$, to have the correct units (and thus any hope of agreement).

2.2.3 Coordinate representation

We have yet to formulate the analogues of wavefunctions — that is, coordinate representations of states. We saw in section 2.2.2 how coherent states can encode positions (see (2.2.5)) and define position measurements (see (2.2.7) and (2.2.11)). If we could lift this position encoding from coherent states $|\boldsymbol{z}\rangle \in \mathcal{H}_{\mathrm{c}}$ to corresponding states $|\boldsymbol{z}) \in \mathcal{H}_{\mathrm{q}}$, we could then define the coordinate representation of a state $|\psi) \in \mathcal{H}_{\mathrm{q}}$ by $\psi(\boldsymbol{z}) \coloneqq (\boldsymbol{z}|\psi)$, resembling the approach of commutative quantum mechanics, as per (2.1.1). Furthermore, as long as our position-encoding states $|\boldsymbol{z})$ satisfy a completeness relation analogous to (2.1.2), we immediately get that a coordinate representation $\psi(\boldsymbol{z})$ is square-integrable by an identical argument to (2.1.3).

Now, in writing down our POVM in (2.2.7), we have already encountered one possible way of "lifting" coherent states to states in $\mathcal{H}_{\mathrm{q}}$, namely the states $|z_1, z_2, n_1, n_2)_{\mathrm{ph}}$ of (2.2.6). Indeed, these states possess many of the same desiderata we now seek to fulfil — they lift

the coordinate encoding to $\mathcal{H}_{\mathrm{q}}$, and satisfy completeness relation (2.2.8) — but they carry an undesired additional dependence on n_1 and n_2. Eliminating these labels will force us to adopt a non-trivial product between coordinate-represented states (which of course must be non-commutative). We set about eliminating this n_1 and n_2 dependence.

As a first step we rewrite the trace in (2.2.7) instead as an integral running over coherent states. Specifically, start by rearranging $\hat{\Pi}_{\boldsymbol{z}} |\psi)$ (for arbitrary $|\psi) \in \mathcal{H}_{\mathrm{q}}$) exactly as in (2.2.10),

$$\hat{\Pi}_{\boldsymbol{z}} |\psi) = 4\pi\lambda^2 \hat{Q} \frac{1}{\sqrt{4\pi\lambda^2 \hat{r}}} |\boldsymbol{z}\rangle\langle\boldsymbol{z}| \frac{1}{\sqrt{4\pi\lambda^2 \hat{r}}} \hat{r}\psi \left(\sum_{n_1,n_2} |n_1, n_2\rangle\langle n_1, n_2| \right),$$

then invoke (2.2.4) to replace the parenthesised expression by an integral,

$$\sum_{n_1,n_2} |n_1, n_2\rangle\langle n_1, n_2| = \mathbf{1}_{\mathrm{c}} = \int \frac{d^4 w}{\pi^2} |\boldsymbol{w}\rangle\langle\boldsymbol{w}|,$$

over new coherent states $|\boldsymbol{w}\rangle$, and finally reorder once more to obtain

$$\hat{\Pi}_{\boldsymbol{z}} = \int \frac{d^4 w}{\pi^2} |\boldsymbol{z}, \boldsymbol{w})_{\mathrm{ph}\ \mathrm{ph}}(\boldsymbol{z}, \boldsymbol{w}|. \tag{2.2.14}$$

Here, the states $|\boldsymbol{z}, \boldsymbol{w})_{\mathrm{ph}}$ are defined in the expected way,

$$|\boldsymbol{z}, \boldsymbol{w})_{\mathrm{ph}} \coloneqq \hat{Q} \frac{1}{\sqrt{4\pi\lambda^2 \hat{r}}} |\boldsymbol{z}\rangle\langle\boldsymbol{w}|. \tag{2.2.15}$$

Of course, at this stage we have not accomplished much — we have removed the n_i dependence from the states appearing in $\hat{\Pi}_{\boldsymbol{z}}$, but at the cost of introducing a w_i dependence. The motivation for our rewriting is that it enables use of calculus techniques, by which we are in fact able to completely perform the integral in (2.2.14), thus removing all w_i dependence. The trick is to shift the integral with the substitution $\boldsymbol{v} \coloneqq \boldsymbol{w} - \boldsymbol{z}$,

$$\hat{\Pi}_{\boldsymbol{z}} = \int \frac{d^4 v}{\pi^2} |\boldsymbol{z}, \boldsymbol{z} + \boldsymbol{v})_{\mathrm{ph}\ \mathrm{ph}}(\boldsymbol{z}, \boldsymbol{z} + \boldsymbol{v}|, \tag{2.2.16}$$

and rewrite the result in terms of translation operators acting on $|\boldsymbol{z}, \boldsymbol{z})_{\mathrm{ph}}$. The relevant operators are found by noting that

$$\partial_{z_\alpha} |\boldsymbol{z}\rangle\langle\boldsymbol{z}| = \partial_{z_\alpha} \left[e^{-\bar{z}_\beta z_\beta} e^{z_\beta a_\beta^\dagger} |0\rangle\langle 0| e^{\bar{z}_\beta a_\beta} \right] = (-\bar{z}_\alpha + a_\alpha^\dagger) |\boldsymbol{z}\rangle\langle\boldsymbol{z}|,$$

by (2.2.2), and so

$$\begin{aligned} e^{v_\alpha \partial_{z_\alpha}} |\boldsymbol{z}\rangle\langle\boldsymbol{z}| &= e^{v_\alpha a_\alpha^\dagger - v_\alpha \bar{z}_\alpha} |\boldsymbol{z}\rangle\langle\boldsymbol{z}| \\ &= e^{-v_\alpha \bar{z}_\alpha} e^{-\frac{1}{2}\bar{z}_\alpha z_\alpha} e^{v_\alpha a_\alpha^\dagger} e^{z_\alpha a_\alpha^\dagger} |0\rangle\langle\boldsymbol{z}| \\ &= e^{\frac{1}{2}(\bar{v}_\alpha v_\alpha + \bar{v}_\alpha z_\alpha - v_\alpha \bar{z}_\alpha)} |\boldsymbol{z} + \boldsymbol{v}\rangle\langle\boldsymbol{z}|. \end{aligned}$$

Inserting such translation operators into (2.2.16) simplifies it to

$$\begin{aligned} \hat{\Pi}_{\boldsymbol{z}} &= \int \frac{d^4 v}{\pi^2} e^{-\frac{1}{2}(\bar{v}_\alpha v_\alpha + \cancel{\bar{v}_\alpha z_\alpha} - \cancel{v_\alpha \bar{z}_\alpha})} e^{-\frac{1}{2}(\bar{v}_\alpha v_\alpha + \cancel{v_\alpha \bar{z}_\alpha} - \cancel{\bar{v}_\alpha z_\alpha})} |\boldsymbol{z}, \boldsymbol{z})_{\mathrm{ph}}\ e^{\bar{v}_\alpha \overleftarrow{\partial}_{\bar{z}_\alpha}} e^{v_\alpha \overrightarrow{\partial}_{z_\alpha}}\ {}_{\mathrm{ph}}(\boldsymbol{z}, \boldsymbol{z}| \\ &\equiv |\boldsymbol{z}) \bar{\star} (\boldsymbol{z}|, \end{aligned} \tag{2.2.17}$$

where the states $|\boldsymbol{z}) \equiv |\boldsymbol{z}, \boldsymbol{z})_{\text{ph}}$ are, in fact, exactly those we set out to find. We have also introduced the "star-product",

$$\bar{\star} := \int \frac{d^4v}{\pi^2}\, e^{-\bar{v}_\alpha v_\alpha} e^{\bar{v}_\alpha \overleftarrow{\partial}_{\bar{z}_\alpha}} e^{v_\alpha \overrightarrow{\partial}_{z_\alpha}},$$

the form of which can be simplified further by explicitly performing the remaining Gaussian integrals; setting $v_i \equiv x_i + iy_i$ for $x_i, y_i \in \mathbb{R}$, we have

$$\begin{aligned}
\bar{\star} &= \prod_{i=1}^{2} \int \frac{dx_i}{\sqrt{\pi}}\, e^{-x_i^2 + x_i(\overrightarrow{\partial}_{z_i} + \overleftarrow{\partial}_{\bar{z}_i})} \int \frac{dy_i}{\sqrt{\pi}}\, e^{-y_i^2 + iy_i(\overrightarrow{\partial}_{z_i} - \overleftarrow{\partial}_{\bar{z}_i})} \\
&= \prod_{i=1}^{2} \exp\Big[\frac{1}{4}(\overrightarrow{\partial}_{z_i} + \overleftarrow{\partial}_{\bar{z}_i})^2\Big] \exp\Big[-\frac{1}{4}(\overrightarrow{\partial}_{z_i} - \overleftarrow{\partial}_{\bar{z}_i})^2\Big] \\
&= \prod_{i=1}^{2} \exp\Big[\overleftarrow{\partial}_{\bar{z}_i} \overrightarrow{\partial}_{z_i}\Big] \\
&= \exp\Big[\overleftarrow{\partial}_{\bar{z}_\alpha} \overrightarrow{\partial}_{z_\alpha}\Big],
\end{aligned} \tag{2.2.18}$$

where Einstein summation convention only applies to the repeated α-indices in the last line. In fact, this product is exactly the conjugate (treating differential operators as Wirtinger derivatives [24]) of the well-known Voros product (2.16 in [5]), $\star := \exp\Big[\overleftarrow{\partial}_{z_\alpha} \overrightarrow{\partial}_{\bar{z}_\alpha}\Big]$, as suggested by the overbar. As mentioned earlier, the form of the $\Pi_{\boldsymbol{z}}$ as given by (2.2.17) more closely resembles the definition of the POVM operators from other sources like [27]. Finally, in this notation, the completeness relation of (2.2.8) becomes

$$\int \frac{d^4z}{\pi^2}\, |\boldsymbol{z})\, \bar{\star}\, (\boldsymbol{z}| = \mathbf{1}_{\text{q}}, \tag{2.2.19}$$

giving a sort of star-product completeness of the states $|\boldsymbol{z})$, which resembles the completeness of normal coherent states $|\boldsymbol{z}\rangle$, as per (2.2.4).

In summary, we define the coordinate representation of a state $|\psi)$ by

$$\psi(\boldsymbol{z}) := (\boldsymbol{z}|\psi) = \langle \boldsymbol{z}|\sqrt{4\pi\lambda^2 \hat{r}}\, \psi|\boldsymbol{z}\rangle\,. \tag{2.2.20}$$

in complete analogy with (2.1.1). This defines $\psi(\boldsymbol{z})$ as a function of two complex variables, which can alternatively be considered a function on $\mathbb{R}^4$. However, if we parameterise z_1 and z_2 as in (2.2.5), then we observe that $\psi(\boldsymbol{z})$ is actually independent of γ (being of a similar form, when written out, to (2.2.12)), making it a function on $\mathbb{C}^2/\mathrm{U}(1) \cong \mathbb{R}^3$, as expected. As alluded to earlier, the expected square-integrability of the coordinate representation is automatically implied by the finiteness of the operator norm, $\|\psi\|$; we simply invoke (2.2.19) to insert the identity in the operator inner product (much as in (2.1.3)),

$$\begin{aligned}
(\psi|\psi) &= \int \frac{d^4z}{\pi^2}\, (\psi|\boldsymbol{z})\, \bar{\star}\, (\boldsymbol{z}|\psi) \\
&= \int \frac{d^4z}{\pi^2}\, \bar{\psi}(\boldsymbol{z})\, \bar{\star}\, \psi(\boldsymbol{z}) < \infty.
\end{aligned}$$

Whenever we care about the radial dependence of the coordinate representation, we must account for the factor of $\sqrt{\hat{r}}$ in (2.2.20) coming from our weighted inner product. In such cases, we can normalise ψ with a factor of $\frac{1}{\sqrt{4\pi\lambda^2\hat{r}}}$ before computing the coordinate

representation, which then reduces to the simple expectation value, $\psi(\boldsymbol{z}) = \langle \boldsymbol{z}|\psi|\boldsymbol{z}\rangle$, called the *symbol* of ψ. Symbols compose via the (unconjugated) Voros product [5],

$$\langle \boldsymbol{z}|\psi\phi|\boldsymbol{z}\rangle = \langle \boldsymbol{z}|\psi|\boldsymbol{z}\rangle \star \langle \boldsymbol{z}|\phi|\boldsymbol{z}\rangle . \tag{2.2.21}$$

The derivation for this is very similar to that of (2.2.17). It amounts to observing that

$$e^{v_\alpha \partial_{z_\alpha}} \langle \boldsymbol{z}|\psi|\boldsymbol{z}\rangle = e^{\frac{1}{2}(\bar{v}_\alpha v_\alpha + \bar{v}_\alpha z_\alpha - v_\alpha \bar{z}_\alpha)} \langle \boldsymbol{z}|\psi|\boldsymbol{z}+\boldsymbol{v}\rangle ,$$

whereby (2.2.21) follows after inserting the identity (as per (2.2.4)) and shifting the resulting integral:

$$\begin{aligned}
\langle \boldsymbol{z}|\psi\phi|\boldsymbol{z}\rangle &= \int \frac{d^4w}{\pi^2} \langle \boldsymbol{z}|\psi|\boldsymbol{w}\rangle \langle \boldsymbol{w}|\phi|\boldsymbol{z}\rangle \\
&= \int \frac{d^4v}{\pi^2} \langle \boldsymbol{z}|\psi|\boldsymbol{z}+\boldsymbol{v}\rangle \langle \boldsymbol{z}+\boldsymbol{v}|\phi|\boldsymbol{z}\rangle \\
&= \int \frac{d^4v}{\pi^2} \langle \boldsymbol{z}|\psi|\boldsymbol{z}\rangle e^{-\bar{v}_\alpha v_\alpha} e^{v_\alpha \overleftarrow{\partial}_{z_\alpha}} e^{\bar{v}_\alpha \overrightarrow{\partial}_{\bar{z}_\alpha}} \langle \boldsymbol{z}|\phi|\boldsymbol{z}\rangle \\
&= \langle \boldsymbol{z}|\psi|\boldsymbol{z}\rangle \star \langle \boldsymbol{z}|\phi|\boldsymbol{z}\rangle .
\end{aligned}$$

Knowing this composition law, we can draw one further parallel with commutative wave mechanics. In wave mechanics, given a particle with wavefunction $\psi(\boldsymbol{x})$, the Born rule determines the probability density function for measuring the particle at a point $\boldsymbol{D}$ to be $P(\boldsymbol{D}) = |\psi(\boldsymbol{D})|^2 = \psi(\boldsymbol{D}) \cdot \bar{\psi}(\boldsymbol{D})$. Combining (2.2.20) with (2.2.21) and (2.2.12) gives an analogous form of the position measurement PDF in our context,

$$P(\boldsymbol{D}) = \psi(\boldsymbol{z}) \star \bar{\psi}(\boldsymbol{z}),$$

where, as usual, $\boldsymbol{z} \in \mathbb{C}^2$ encodes the point $\boldsymbol{D}$ via (2.2.5).

Altogether, the transition from states to their coordinate representations is entirely analogous to the procedure in commutative quantum mechanics, as described at the start of section 2.1, only with position eigenstates replaced by the "lifted" coherent states, $|\boldsymbol{z}\rangle$, and the usual pointwise product of functions replaced with the Voros product (or its conjugate).

We are actually able to formulate a slightly different geometric picture of the quantum states. At the time of writing, it is not entirely clear to the author how this alternate formulation relates to that outlined above, or indeed whether the alternate picture is useful at all. Still, we briefly outline the alternate construction, and leave it as an open problem to establish a connection with the material above. We begin with the Peter-Weyl theorem (theorem D.8 in [22]), which in our context reads

$$L^2(\mathrm{SU}(2)) \cong \bigoplus_{n\in\mathbb{N}} \mathcal{F}_n \otimes \mathcal{F}_n^*, \tag{2.2.22}$$

where $L^2(\mathrm{SU}(2))$ is the usual space of square-integrable functions:

$$L^2(\mathrm{SU}(2)) := \left\{ f\colon \mathrm{SU}(2) \to \mathbb{C} \;\middle|\; \int_{\mathrm{SU}(2)} dg\ |f(g)|^2 < \infty \right\}, \tag{2.2.23}$$

where the integral is with respect to the Haar measure dg on SU(2). For the parameterisation,

$$g \equiv g(\boldsymbol{k}) = e^{i\boldsymbol{k}\cdot\hat{\boldsymbol{x}}}, \quad \text{where} \quad \boldsymbol{k} \equiv k\hat{\boldsymbol{k}} = k \begin{bmatrix} \sin\theta_k \cos\phi_k \\ \sin\theta_k \sin\phi_k \\ \cos\theta_k \end{bmatrix},$$

of (represented) SU(2) group elements (as per appendix A), the integral with respect to the Haar measure can be explicitly expanded as

$$\begin{aligned}\int_{\mathrm{SU}(2)} dg\ \square &\equiv \int \frac{d\Omega_k}{4\pi} \int_0^{\pi/\lambda} \frac{2\lambda dk}{\pi} \sin^2(\lambda k)\ \square \\ &= \frac{\lambda}{2\pi^2} \int d\Omega_k \int_0^{\pi/\lambda} dk\ \sin^2(\lambda k)\ \square,\end{aligned}$$

where $\square$ stands in for a generic integrand, and where we integrate over the usual angle measure, $d\Omega_k = \sin\theta_k\, d\theta_k\, d\phi_k$. Technically, $L^2(\mathrm{SU}(2))$ is the space of *equivalence classes* of such functions under the identification of functions that agree *almost everywhere* (with respect to the Haar measure). Much as in (2.1.13), we have $\mathscr{B}_2(\mathcal{F}_n) \cong \mathcal{F}_n \otimes \mathcal{F}_n^*$, which combines with (2.1.15) and (2.2.22) to give

$$\mathcal{H}_{\mathrm{q}} = \bigoplus_{n\in\mathbb{N}} \mathscr{B}_2(\mathcal{F}_n) \cong L^2(\mathrm{SU}(2)). \tag{2.2.24}$$

Note that the Peter-Weyl isomorphism is one at the level of *algebras*, not just vector spaces. Specifically, we upgrade $L^2(\mathrm{SU}(2))$ to an algebra, called the *group algebra*, by equipping it with the convolution product [33],

$$f_1 * f_2 \coloneqq \int_{\mathrm{SU}(2)} dh\ f_1(gh^{-1}) f_2(h),$$

and the algebra on $\mathscr{B}_2(\mathcal{F}_n)$ (likewise on $\mathcal{H}_{\mathrm{q}}$) is defined with the product being operator composition (correspondingly, "contraction on the middle two tensors" if we think of $\mathscr{B}_2(\mathcal{F}_n)$ instead as $\mathcal{F}_n \otimes \mathcal{F}_n^*$). We can write an explicit basis-free form of the algebra homomorphism

$$\pi\colon L^2(\mathrm{SU}(2)) \to \mathcal{H}_{\mathrm{q}}$$

in terms of our representation of SU(2). Notationally, we will suppress the explicit representation, opting to simply consider the group element $g \in \mathrm{SU}(2)$ to also be an element of $\bigoplus_{n\in\mathbb{N}} \mathscr{B}_2(\mathcal{F}_n) = \mathcal{H}_{\mathrm{q}}$ (of course, this is well-defined because the representation respects the group multiplication). Then define

$$\pi(f) \coloneqq \int_{\mathrm{SU}(2)} dg\ f(g) g.$$

It is straightforward enough to check that this is indeed an algebra homomorphism with respect to the products defined above:

$$\begin{aligned}\pi(f_1 * f_2) &= \int_{\mathrm{SU}(2)} dg\ (f_1 * f_2)(g) g \\ &= \int_{\mathrm{SU}(2)} dg \int_{\mathrm{SU}(2)} dh\ f_1(gh^{-1}) f_2(h) g \\ &= \int_{\mathrm{SU}(2)} dg \int_{\mathrm{SU}(2)} dh\ f_1(g) f_2(h) gh \\ &= \int_{\mathrm{SU}(2)} dg\ f_1(g) g \int_{\mathrm{SU}(2)} dh\ f_2(h) h \\ &= \pi(f_1)\pi(f_2),\end{aligned}$$

where we applied the right-invariance of the Haar measure.

Finally, it is well-known [22] that, as a manifold, SU(2) is homeomorphic to S^3, so the picture due to the Peter-Weyl theorem gives us an interpretation of quantum states as "wavefunctions" on S^3, which we can think of as being embedded in $\mathbb{R}^4$, where instead of the Voros product (or its conjugate), the algebra is given by the normal convolution product. It is possible (though currently not certain) that this alternative formulation of quantum states may be useful in some contexts.

2.2.4 Position measurement as weak measurement

An interpretation of this POVM framework for position measurement in the language of *weak measurement* is presented in [32], in the case of the 2D Moyal plane. However, the situation is very similar in our formalism, so we discuss the connection here briefly. It is worth briefly mentioning here (deferring to the reference for details), mainly because it preempts the quantum-to-classical transition presented in section 4 (by drawing parallels with similar suppression of quantum effects that emerges in the decoherence program), but also because it highlights how position measurement is distinguished from other kinds of measurement within our formalism.

Recall (2.1.15), which decomposed our state space as

$$\mathcal{H}_{\mathrm{q}} = \bigoplus_{n\in\mathbb{N}} \mathcal{F}_n \otimes \mathcal{F}_n^* \subset \mathcal{H}_{\mathrm{c}} \otimes \mathcal{H}_{\mathrm{c}}^*.$$

Now the key observation is that the position observables $\hat{X}_i$ act via left-multiplication (as per (2.1.20)), and thereby only act on one sector, $\mathcal{H}_{\mathrm{c}}$, of $\mathcal{H}_{\mathrm{q}}$. For this reason, position measurements are in fact *local* measurements, only capable of providing information on this sector. The other sector, $\mathcal{H}_{\mathrm{c}}^*$, acts as an *environment* (in the sense of decoherence; see [36], for instance), providing states with additional degrees of freedom that remain unprobed by position measurements.

That is to say, upon performing a local measurement such as a position measurement, a state's environmental degrees of freedom can be traced out via a partial trace over the unobserved subsystem, in this case $\mathcal{H}_{\mathrm{c}}^*$, yielding a post-measurement reduced density matrix. This reduced density matrix is generally a mixed state, usually called an *improper* mixed state, since it derives not from the usual statistical ensemble of pure states, but rather from restriction of a pure state on the full (tensor-product) Hilbert space to a subsystem.

The above process is precisely the underlying mechanism of decoherence. The interpretation of our position-measurement formalism within the framework of decoherence is noteworthy because decoherence is well-understood to generally give rise to suppression of interference terms and thereby to emergent classical behaviour [36].

Chapter 3

Free Particle Solutions

Analogous to the commutative case, the free particle time independent Schrödinger equation (TISE) reads

$$\hat{H}\,|\psi) = -\frac{\hbar^2}{2m}\hat{\Delta}\,|\psi) = E\,|\psi)\,. \tag{3.0.1}$$

As in the commutative case, we can obtain both plane wave and radial (spherical wave) solutions. Both forms will be useful in our investigation, so in this chapter we will treat both forms of solution. In the case of spherical waves, we also revise the commutative form for comparison.

This chapter can be seen as a continuation of the literature review portion of the thesis, as the key results can readily be found in existing literature (most notably in [20], with alternate derivations in [12], and a nice summary of the results in [27]), though we have added details to the derivations. In particular, our discussion of plane wave normalisation in section 3.1.2 is absent from existing literature.

3.1 Non-commutative plane waves

A natural candidate for the form of a wave solution is

$$|\boldsymbol{p}) \equiv |\boldsymbol{k}) \coloneqq \exp\left[\frac{i}{\hbar}\,\boldsymbol{p}\cdot\hat{\boldsymbol{x}}\right] = e^{i\boldsymbol{k}\cdot\hat{\boldsymbol{x}}}, \tag{3.1.1}$$

up to appropriate normalisation (of which we defer discussion to subsection 3.1.2), and where $\boldsymbol{k} = \boldsymbol{p}/\hbar$ is the de Broglie wave-vector. We will confirm that this form does indeed solve the free-particle TISE by explicitly computing its energy eigenvalue E in section 3.1.1 below; until then, we simply take for granted that it does.

Since each $\hat{x}_i$ represents an $\mathfrak{su}(2)$ element (and since SU(2) is simply connected [22]), the plane waves are representations of SU(2) group elements. Moreover, the exponential map $\exp\colon \mathfrak{su}(2) \to \mathrm{SU}(2)$ is surjective, (because SU(2) is connected and compact — see, for instance, corollary 11.10 in [22]), so that *every* (represented) SU(2) element assumes the form of (3.1.1). An important consequence of this is that composing two plane waves produces another plane wave:

$$e^{i\boldsymbol{k}_1\cdot\hat{\boldsymbol{x}}}e^{i\boldsymbol{k}_2\cdot\hat{\boldsymbol{x}}} = e^{i\boldsymbol{k}_3\cdot\hat{\boldsymbol{x}}}.$$

We can explicitly compute the momentum $\boldsymbol{k}_3$ of this new plane wave using the well-known Baker–Campbell–Hausdorff (BCH) expansion for $\log\left(e^X e^Y\right)$, which has a simple closed

form in the case of SU(2). For this, first rewrite the plane waves in terms of dimensionless quantities κ_i as

$$e^{i\boldsymbol{k}_i\cdot\hat{\boldsymbol{x}}} \equiv e^{i\kappa_i\,\hat{\boldsymbol{k}}_i\cdot\frac{\hat{\boldsymbol{x}}}{\lambda}}, \quad \text{where} \quad \kappa_i \coloneqq \lambda\|\boldsymbol{k}_i\|, \tag{3.1.2}$$

for unit vectors $\hat{\boldsymbol{k}}_i$. Then solve for κ_3 and $\hat{\boldsymbol{k}}_3$ using

$$\begin{aligned}\cos\kappa_3 &= \cos\kappa_1\cos\kappa_2 - \hat{\boldsymbol{k}}_1\cdot\hat{\boldsymbol{k}}_2\sin\kappa_1\sin\kappa_2,\\ \hat{\boldsymbol{k}}_3 &= \frac{1}{\sin\kappa_3}\left(\hat{\boldsymbol{k}}_1\sin\kappa_1\cos\kappa_2 + \hat{\boldsymbol{k}}_2\sin\kappa_2\cos\kappa_1 - \hat{\boldsymbol{k}}_1\times\hat{\boldsymbol{k}}_2\sin\kappa_1\sin\kappa_2\right).\end{aligned} \tag{3.1.3}$$

Since the Pauli matrices σ^i share commutation relations with the operators $\hat{x}_i/\lambda$, an entirely analogous composition rule holds for (unrepresented) SU(2) group elements written as exponentials in this way. This closed form of the BCH formula, is first attributed to Rodrigues [34], and can be derived from the spherical law of cosines.

3.1.1 Plane wave energy

We turn our attention to computing the energy eigenvalue associated with the plane waves of (3.1.1). As a first step, we derive the transformation law for the action of a rotation operator on a plane wave, both because this will simplify the subsequent energy calculation, and because similar computational techniques appear again later (for instance in appendix A).

Let $R \equiv R_\phi(\hat{\boldsymbol{u}}) \in \mathrm{SO}(3)$ be the rotation matrix encoding a rotation of angle ϕ about axis $\hat{\boldsymbol{u}}$, and let

$$\Pi(R) \coloneqq \exp\left[-\frac{i}{\hbar}\,\phi\hat{\boldsymbol{u}}\cdot\hat{\boldsymbol{L}}\right]$$

be its representation on $\mathcal{H}_\mathrm{q}$. For convenience in the calculation to follow, write $\hat{J}_i \equiv \frac{1}{2\lambda}\hat{x}_i$. Note, from the coordinate commutation relations, (2.1.5), that $[\hat{x}_i, \hat{J}_j] = i\epsilon_{ijk}\hat{x}_k = [\hat{J}_i, \hat{J}_j]$, implying that $\hat{\boldsymbol{x}}$ is a *vector operator* with respect to the $\hat{J}_i$, from which it immediately follows by the Baker-Hausdorff lemma (see section 5.1.2 of [1], for instance) that

$$e^{-i\phi\hat{\boldsymbol{u}}\cdot\hat{\boldsymbol{J}}}\,\hat{x}_i\,e^{i\phi\hat{\boldsymbol{u}}\cdot\hat{\boldsymbol{J}}} = \left[R_{-\phi}(\hat{\boldsymbol{u}})\right]_{ij}\hat{x}_j = \left[R^T\hat{\boldsymbol{x}}\right]_i.$$

Using the above definition, together with (2.1.22), as well as the linearity of the adjoint representation,

$$\mathrm{ad}\colon X \mapsto (\mathrm{ad}_X\colon Y \mapsto [X,Y])$$

in X, we compute

$$\begin{aligned}\Pi(R)\,|\boldsymbol{k}) &= \exp\left[\mathrm{ad}_{-i\phi\hat{\boldsymbol{u}}\cdot\hat{\boldsymbol{J}}}\right]e^{i\boldsymbol{k}\cdot\hat{\boldsymbol{x}}}\\ &= \mathrm{Ad}_{\exp[-i\phi\hat{\boldsymbol{u}}\cdot\hat{\boldsymbol{J}}]}\left(e^{i\boldsymbol{k}\cdot\hat{\boldsymbol{x}}}\right)\\ &= e^{-i\phi\hat{\boldsymbol{u}}\cdot\hat{\boldsymbol{J}}}\,e^{i\boldsymbol{k}\cdot\hat{\boldsymbol{x}}}\,e^{i\phi\hat{\boldsymbol{u}}\cdot\hat{\boldsymbol{J}}}\\ &= \exp\left[e^{-i\phi\hat{\boldsymbol{u}}\cdot\hat{\boldsymbol{J}}}\,i\boldsymbol{k}\cdot\hat{\boldsymbol{x}}\,e^{i\phi\hat{\boldsymbol{u}}\cdot\hat{\boldsymbol{J}}}\right]\\ &= \exp[i(R\boldsymbol{k})\cdot\hat{\boldsymbol{x}}]\\ &= |R\boldsymbol{k})\,.\end{aligned} \tag{3.1.4}$$

Here we have used the fact that $e^{\mathrm{ad}_X} = \mathrm{Ad}_{e^X}$, which is proposition 3.34 in Hall [22], but really is just a special case of the general relationship between Lie group and Lie algebra homomorphisms.

Returning to the computation of the plane wave energy, we make use of the above rotation law together with the rotational invariance of the Schrödinger equation, (3.0.1), to focus on the case $\boldsymbol{k} = k\hat{\boldsymbol{z}}$. In this case,

$$|k\hat{\boldsymbol{z}}) = e^{ik\hat{x}_3} = e^{ik\lambda\left(a_1^\dagger a_1 - a_2^\dagger a_2\right)}. \tag{3.1.5}$$

We can now derive the corresponding energy directly using the commutation relations,

$$f(\hat{n}_j)a_j = a_j f(\hat{n}_j - 1), \quad \text{and} \quad f(\hat{n}_j)a_j^\dagger = a_j^\dagger f(\hat{n}_j + 1),$$

where $\hat{n}_j \coloneqq a_j^\dagger a_j$ for some fixed j and any function f. Specifically, in the case where $f(\hat{n}_1, \hat{n}_2) \coloneqq e^{ik\lambda(\hat{n}_1 - \hat{n}_2)}$, we have

$$\begin{aligned}\left[a_\alpha^\dagger, [a_\alpha, f(\hat{n}_1, \hat{n}_2)]\right] &= \hat{n} f(\hat{n}_1, \hat{n}_2) - a_1^\dagger a_1 f(\hat{n}_1 - 1, \hat{n}_2) - a_2^\dagger a_2 f(\hat{n}_1, \hat{n}_2 - 1) \\ &\quad - a_1 a_1^\dagger f(\hat{n}_1 + 1, \hat{n}_2) - a_2 a_2^\dagger f(\hat{n}_1, \hat{n}_2 + 1) + (\hat{n} + 2) f(\hat{n}_1, \hat{n}_2) \\ &= (\hat{n} + 1)\left(2 - \left[e^{ik\lambda} + e^{-ik\lambda}\right]\right) f(\hat{n}_1, \hat{n}_2) \\ &= \frac{4\hat{r}}{\lambda} \sin^2\left(\frac{k\lambda}{2}\right) f(\hat{n}_1, \hat{n}_2),\end{aligned}$$

where we have repeatedly used the commutator $a_j a_j^\dagger = \hat{n}_j + 1$. Thus,

$$\hat{H}\,|k\hat{\boldsymbol{z}}) = \frac{2\hbar^2}{m\lambda^2} \sin^2\left(\frac{k\lambda}{2}\right) |k\hat{\boldsymbol{z}}). \tag{3.1.6}$$

The non-commutativity has clearly affected the usual dispersion relation, in particular introducing an energy upper bound $E_{\max} = \frac{2\hbar^2}{m\lambda^2}$. This is consistent with the restriction $k \in [0, \pi/\lambda)$ on k required for the states in (3.1.5) to be linearly independent.

3.1.2 Plane wave normalisation

Next, we take some time to motivate our choice of plane wave normalisation. Firstly, note that, being eigenstates of a Hermitian operator (as per (3.1.6)), plane waves with different energies are necessarily orthogonal. Equivalently, plane waves $|\boldsymbol{k}_1)$ and $|\boldsymbol{k}_2)$ with non-trivial overlap must satisfy

$$\sin^2\left(\frac{k_1\lambda}{2}\right) = \sin^2\left(\frac{k_2\lambda}{2}\right),$$

which reduces to the condition

$$k_1 = \pm k_2 + m\frac{2\pi}{\lambda}, \quad \text{for some} \quad m \in \mathbb{Z}.$$

This is at least consistent with the observation, discussed at the end of section 3.1, that a plane wave with wavenumber outside of the interval $[0, \pi/\lambda)$ may be written in terms of one having wavenumber within this interval. In any case, this suggests that we should not expect to impose a simple normalisation condition such as $(\boldsymbol{k}_1|\boldsymbol{k}_2) = \delta^3(\boldsymbol{k}_1 - \boldsymbol{k}_2)$, unless, perhaps, we also impose the restriction that $k_1, k_2 \in [0, \pi/\lambda)$. This is the observation which prompts us to present a more thorough discussion of our chosen normalisation condition.

To aid in selecting an appropriate normalisation condition, let us explicitly compute the overlap of two plane waves. By (2.1.11), together with (3.1.1), we have

$$(\boldsymbol{k}_1|\boldsymbol{k}_2) = 4\pi\lambda^3 |N|^2 \operatorname{Tr}_{\mathrm{c}}\left(e^{-i\boldsymbol{k}_1\cdot\hat{\boldsymbol{x}}}(\hat{n} + 1)\, e^{i\boldsymbol{k}_2\cdot\hat{\boldsymbol{x}}}\right). \tag{3.1.7}$$

Now the plane waves each commute with $\hat{n}$ (as each of the coordinates does), and we can compose the plane waves using (3.1.3) to obtain

$$(\boldsymbol{k}_1|\boldsymbol{k}_2) = 4\pi\lambda^3|N|^2 \sum_{j,m} \langle j,m|e^{i\boldsymbol{k}_3\cdot\hat{\boldsymbol{x}}}(\hat{n}+1)|j,m\rangle\,, \tag{3.1.8}$$

for some new wave-vector $\boldsymbol{k}_3$. Here, $|j,m\rangle$ is a simultaneous eigenket of $\hat{r}^2$ and $\hat{x}_3$, as in (2.1.17). In particular, recall that $j = (n_1+n_2)/2$, so that $\hat{n}\,|j,m\rangle = 2j\,|j,m\rangle$. From this we obtain

$$(\boldsymbol{k}_1|\boldsymbol{k}_2) = 4\pi\lambda^3|N|^2 \sum_{j,m}(2j+1)\,\langle j,m|e^{i\boldsymbol{k}_3\cdot\hat{\boldsymbol{x}}}|j,m\rangle\,. \tag{3.1.9}$$

In this expression we recognise the *character* of the jth SU(2) irrep, usually written

$$\chi^j(\boldsymbol{k}_3) \equiv \chi^j(\alpha,\beta,\gamma) \coloneqq \sum_m D^j_{mm}(\alpha,\beta,\gamma),$$

where $D^j_{m',m}(\alpha,\beta,\gamma)$ is the Wigner-D matrix element, defined

$$D^j_{m',m}(\alpha,\beta,\gamma) \coloneqq \left\langle j,m'\middle|e^{i\alpha\frac{\hat{x}_3}{\lambda}}e^{i\beta\frac{\hat{x}_2}{\lambda}}e^{i\gamma\frac{\hat{x}_3}{\lambda}}\middle|j,m\right\rangle.$$

The above definitions rely on the decomposition, $e^{i\boldsymbol{k}_3\cdot\hat{\boldsymbol{x}}} \equiv e^{i\alpha\frac{\hat{x}_3}{\lambda}}e^{i\beta\frac{\hat{x}_2}{\lambda}}e^{i\gamma\frac{\hat{x}_3}{\lambda}}$, of our plane wave into Euler angles (α,β,γ). Importantly, due to the cyclic property of the trace, group characters are invariant on conjugacy classes. Therefore, the character of a plane wave depends only on the magnitude of its wave-vector, as we may conjugate with another plane wave to arbitrarily rotate the wave-vector direction (we have seen this being done in (3.1.4)) without affecting the character. Thus, we will opt to rotate $\boldsymbol{k}_3$ to lie entirely along the $\hat{x}_2$-axis, whence we can take $\alpha=\gamma=0$ and $\beta=\kappa_3 \coloneqq \lambda k_3$. Finally, we can invoke the completeness relation for characters (equation 3.95 in [39]) to write

$$\begin{aligned}(\boldsymbol{k}_1|\boldsymbol{k}_2) &= 4\pi\lambda^3\sum_j(2j+1)\chi^j(\kappa_3)\\ &= 4\pi\lambda^3\sum_j\chi^j(0)\chi^j(\kappa_3)\\ &= 4\pi\lambda^3\,\delta(\kappa_3),\end{aligned} \tag{3.1.10}$$

since $\chi^j(0)$ is the dimension of the jth SU(2) irrep, $2j+1$.

Let us consider momentarily whether this result is sensible, by determining the conditions under which the overlap of (3.1.10) is non-zero. The overlap is clearly non-zero (indeed, singular) exactly when $\kappa_3 = 0$, whereupon the composition $\left(e^{i\boldsymbol{k}_1\cdot\hat{\boldsymbol{x}}}\right)^\dagger e^{i\boldsymbol{k}_2\cdot\hat{\boldsymbol{x}}}$ of our original plane waves gives the identity operator, $\mathbf{1}_{\mathrm{c}} \equiv e^{0\,\hat{\boldsymbol{k}}_3\cdot\frac{\hat{\boldsymbol{x}}}{\lambda}}$, on $\mathcal{H}_{\mathrm{c}}$. Because our representation of SU(2) is *faithful*, this happens precisely when the corresponding (unrepresented) SU(2) group elements compose to the identity matrix,

$$\left(e^{i\lambda\boldsymbol{k}_1\cdot\boldsymbol{\sigma}}\right)^\dagger e^{i\lambda\boldsymbol{k}_2\cdot\boldsymbol{\sigma}} = I,$$

and of course elements in SU(2) (as in any group) have unique inverses. Thus, $(\boldsymbol{k}_1|\boldsymbol{k}_2)$ is non-zero precisely when

$$e^{i\lambda\boldsymbol{k}_2\cdot\boldsymbol{\sigma}} = \left[\left(e^{i\lambda\boldsymbol{k}_1\cdot\boldsymbol{\sigma}}\right)^\dagger\right]^{-1} = e^{i\lambda\boldsymbol{k}_1\cdot\boldsymbol{\sigma}};$$

that is, when the corresponding unrepresented SU(2) group elements are equal. As mentioned earlier, this translates into a slightly non-trivial condition on $\boldsymbol{k}_1$ and $\boldsymbol{k}_2$, since the exponential map $\exp\colon \mathfrak{su}(2) \to \mathrm{SU}(2)$ is not injective [22]. To make this more precise, we first expand both exponentials (using (A.0.2) from appendix A),

$$\cos(\lambda k_1)I + i\sin(\lambda k_1)\hat{\boldsymbol{k}}_1 \cdot \boldsymbol{\sigma} = \cos(\lambda k_2)I + i\sin(\lambda k_2)\hat{\boldsymbol{k}}_2 \cdot \boldsymbol{\sigma},$$

then note that the matrices $\{I, \hat{\sigma}_1, \hat{\sigma}_2, \hat{\sigma}_3\}$ forms a basis for $\mathcal{M}_{2,2}(\mathbb{C})$, the complex vector space of 2×2 complex matrices, whereby we can equate the coefficients,

$$\begin{aligned}\cos(\lambda k_1) &= \cos(\lambda k_2),\\ \sin(\lambda k_1)\hat{\boldsymbol{k}}_1 &= \sin(\lambda k_2)\hat{\boldsymbol{k}}_2.\end{aligned}$$

It follows that $(\boldsymbol{k}_1|\boldsymbol{k}_2)$ is non-zero exactly when $k_1 \pm k_2 \in \frac{2\pi}{\lambda}\mathbb{Z}$, and either

1. $k_1 \in \frac{\pi}{\lambda}\mathbb{Z}$, or
2. $\hat{\boldsymbol{k}}_1 = \mp\hat{\boldsymbol{k}}_2$.

If we restrict $k_1, k_2 \in [0, \pi/\lambda)$ then these cases collapse into the much simpler single condition that $\boldsymbol{k}_1 = \boldsymbol{k}_2$. Therefore, the overlap we obtained is entirely expected.

The conclusion of our discussion is that we may simply choose

$$N = \frac{1}{\sqrt{4\pi\lambda^3}}, \tag{3.1.11}$$

with which to normalise our plane waves, so that the normalisation condition reads

$$(\boldsymbol{k}_1|\boldsymbol{k}_2) = \delta(\kappa_3), \tag{3.1.12}$$

where $\cos\kappa_3$ is given by (3.1.3). This normalisation condition, while unconventional, is both convenient and sensible as seen in our discussion. It also gives the state $|\boldsymbol{k})$ the correct dimensions, namely length$^{-3/2}$, as per the discussion of dimensions presented at the end of section 2.2.2.

3.2 Spherical waves

Spherical waves play an important role in the pinhole interference setup which we study in section 4. As such, before we treat the non-commutative free particle spherical wave solutions, it bears revising the standard commutative spherical waves for comparison. In both the commutative and non-commutative cases, we will primarily be interested in the large-radius asymptotic behaviour (specifically of the radial part), as this is the relevant regime for the main calculation in chapter 4.

3.2.1 Commutative spherical waves

The spherical wave free-particle solutions of commutative quantum mechanics are derived in many standard introductory texts; see for instance sections 3.3 and 3.4 of Abers [1]. They have the general form

$$\psi_{klm}(r, \theta, \phi) = R_{kl}(r)Y_l^m(\theta, \phi),$$

labelled by momentum, k, and the angular momentum quantum numbers $l \in \mathbb{N}$ and $m \in [-l, l] \cap \mathbb{N}$. The normalisation condition on the full wavefunction implies separate normalisation conditions on the angular and radial components thereof, expressed respectively as

$$\int |Y_l^m(\theta, \phi)|^2 \, d\Omega = 1, \quad \text{and} \quad \int_0^\infty |R_{kl}(r)|^2 \, r^2 dr = 1. \tag{3.2.1}$$

Inserting a solution of the above form causes the free particle Schrödinger equation to split into separate angular- and radial equations. The former admits the standard spherical harmonic solutions, which we omit. The latter admits solutions of the form

$$R_{kl}(r) = A g_{J,l}(kr) + B g_{Y,l}(kr),$$

where $g_{J,l}$ and $g_{Y,l}$ denote respectively the order-l spherical Bessel- and Neumann functions, and where the coefficients A and B are determined by the boundary conditions. The Neumann functions are only valid solutions away from the origin, but this regime is relevant for our later interference calculations. Indeed, we will use the large-r form of the radial solutions (see equation 3.132 of [1], for instance),

$$R_{kl}(r) = N \frac{1}{r} e^{\pm ikr}, \tag{3.2.2}$$

for some normalisation constant N. This asymptotic behaviour may be derived as the large-r limiting behaviour of the spherical Hankel functions of the first kind, $g_{H,l} = g_{J,l} + i g_{Y,l}$, the calculation for which is treated in section A.2.3 of [1]. This approach informs how we derive the asymptotic behaviour of the analogous *non-commutative* spherical wave solutions in section 3.2.2 below.

Concerning the normalisation of the asymptotic solutions in (3.2.2), there are two important observations to be made. Firstly, it is clear from (3.2.1) that the radial part of any wavefunction has dimensions of length$^{-3/2}$; therefore, N must be dimensionful, with dimensions of length$^{-1/2}$. Secondly, the integral as given in (3.2.1) diverges if we insert the asymptotic form of $R_{k,l}$,

$$\int_0^\infty \left| N \frac{1}{r} e^{\pm ikr} \right|^2 r^2 dr = |N|^2 \int_0^\infty dr \not< \infty.$$

We can address both of these observations by regularising the divergent integral — we imagine bounding our entire system within some large finite volume V, say a sphere, and take the radial integral only to the boundary of the sphere, $\sim V^{1/3}$. Then N is proportional to $V^{-1/6}$, which introduces the missing dimensionality. We will not bother to calculate the exact dimensionless proportionality constant, as it is neither very meaningful ((3.2.2) is merely an approximation for large r) nor necessary for the ensuing discussion.

3.2.2 Non-commutative spherical waves

Returning to our non-commutative formalism, the free particle angular momentum eigenstates are shown in [20] to have the form

$$|k, l, m) \coloneqq \sum_{(m_i, n_i) \in \Lambda} \frac{(a_1^\dagger)^{m_1} (a_2^\dagger)^{m_2}}{m_1! \, m_2!} g(\hat{n}, k) \frac{(a_1)^{n_1} (-a_2)^{n_2}}{n_1! \, n_2!}. \tag{3.2.3}$$

Here, the values $l \in \mathbb{N}$ and $m \in \mathbb{Z} \cap [-l, l]$ are fixed, and our summation runs over the set

$$\Lambda \coloneqq \left\{ (m_1, m_2, n_1, n_2) \in \mathbb{N}^4 \;\middle|\; m_1 + m_2 = n_1 + n_2 = l, \; m_1 - m_2 - n_1 + n_2 = 2m \right\}. \tag{3.2.4}$$

Inserting this form into (3.0.1) yields a difference equation for g which admits two linearly independent solutions (derived in section 7 of [12]) which have the forms

$$g_{J,l}(n,k) = \left[\frac{\sqrt{\pi}\,\sin^{l+1}\kappa}{2^{l+1}\,\Gamma\left(\frac{3}{2}+l\right)}\right]\cos^n\kappa\;{}_2F_1\left(\frac{1-n}{2},-\frac{n}{2},\frac{3}{2}+l,-\tan^2\kappa\right), \tag{3.2.5}$$

for $n \geq 0$, and

$$\begin{aligned} g_{Y,l}(n,k) = &\left[-\frac{\sqrt{\pi}(-2)^l\cos^{l+1}\kappa}{\tan^l\kappa\Gamma\left(\frac{1}{2}-l\right)}\right]\frac{n!\,\cos^n\kappa}{\Gamma(2+2l+n)} \\ &\times\;{}_2F_1\left(\frac{-1-l-n}{2},-l-\frac{n}{2},\frac{1}{2}-l,-\tan^2\kappa\right), \end{aligned} \tag{3.2.6}$$

for $n > 0$, respectively. Here the functions ${}_2F_1$ are the (Gauss) hypergeometric functions, and $\kappa \coloneqq \lambda k$ is a dimensionless quantity. These solutions are the non-commutative analogues of the spherical Bessel- and Neumann functions, respectively. Like its commutative counterpart, the latter solution, $g_{Y,l}$, is only valid away from the origin, captured by the restriction $n > 0$. When away from the origin, another valid solution is the linear combination

$$g_{H,l} \coloneqq g_{J,l} + i g_{Y,l},$$

which is the non-commutative analogue for the Hankel functions of the first kind.

We are again interested in the asymptotic behaviour of the spherical waves. Following the approach in section D of [27], we first consider the asymptotic behaviour of the radial function, g. This involves expressing $g_{Y,l}(n,k)$ and $g_{J,l}(n,k)$ in terms of Jacobi polynomials, using identities 15.3.21 and 15.4.6 from [2], then expanding these polynomials for large n (corresponding to large radius) using theorem 8.21.8 from [45]. The result, as given in [27], is that for large n,

$$g_{J,l}(n,k) \approx \frac{\sin((n-l-1)\kappa - l\pi/2)}{n^{l+1}}, \quad \text{and} \quad g_{Y,l}(n,k) \approx -\frac{\cos((n-l-1)\kappa - l\pi/2)}{n^{l+1}},$$

whence the linear combination $g_{H,l}$ behaves asymptotically like an outgoing radial wave:

$$g_{H,l}(n,k) \approx \frac{e^{i(n+l+1)\kappa}}{(in)^{l+1}}. \tag{3.2.7}$$

Compared to its commutative analogue, there is an additional factor of n^{-l} in this expression. However, this is compensated by the remaining radial dependence in (the other factors of) the spherical wave. To see this, consider the (asymptotic) symbol (see section 2.2.3),

$$\begin{aligned} \langle \boldsymbol{z}|k,l,m|\boldsymbol{z}\rangle &= \sum_{(m_i,n_i)\in\Lambda}\frac{\bar{z}_1^{m_1}\bar{z}_2^{m_2}z_1^{n_1}(-z_2)^{n_2}}{m_1!\,m_2!\,n_1!\,n_2!}\,\langle \boldsymbol{z}|g_{H,l}(\hat{n},k)|\boldsymbol{z}\rangle \\ &\approx R^l\,\langle \boldsymbol{z}|\frac{e^{i(\hat{n}+l+1)\kappa}}{(i\hat{n})^{l+1}}|\boldsymbol{z}\rangle\,e^{im\phi} \\ &\quad\times\sum_{(m_i,n_i)\in\Lambda}\frac{(-1)^{n_2}}{m_1!\,m_2!\,n_1!\,n_2!}\cos^{m_1+n_1}\left(\frac{\theta}{2}\right)\sin^{m_2+n_2}\left(\frac{\theta}{2}\right), \end{aligned}$$

of the state $|k,l,m)$. In the first line, we have just acted the creation and annihilation operators of (3.2.3) to the left and right respectively on the coherent states (which are their respective eigenstates), and in the second line we have substituted the representation of (2.2.5) (recall $R \coloneqq r/\lambda$). The radial dependence of this symbol is shared between the

first two factors, so we should compute the remaining matrix element. This calculation ends up being somewhat technical, so we delegate the details to appendix B.3.[1]There it is shown that, to leading order in the large-R expansion,

$$\langle \boldsymbol{z}| \frac{e^{i(\hat{n}+l+1)\kappa}}{(i\hat{n})^{l+1}} |\boldsymbol{z}\rangle \sim \frac{1}{(iR)^{l+1}} e^{R(\cos\kappa - 1) + iR\sin\kappa}, \tag{3.2.8}$$

cancelling the factor of R^l from the angular part of the spherical wave symbol, and leaving an overall radial dependence of $1/R$.

[1] Appendix B actually treats the more general problem of computing the matrix element of *any* function, $g(\hat{n})$, of the boson number operator, $\hat{n}$, with respect to a pair of (generally-distinct) coherent states. The particular matrix element needed here is thus merely one special case which the more general machinery of appendix B is able to handle.

Chapter 4

Pinhole Interference

Consider the configuration for three-dimensional pinhole interference shown in figure 4.1. Plane waves incident on a barrier (which is oriented normal to the direction of plane wave propagation) pass through a pair of pinholes, resulting in spherical wave fronts that interfere before being detected at the screen. We choose coordinates so that the barrier lies in the plane $x = 0$ and has pinhole apertures at $z = \pm d$.

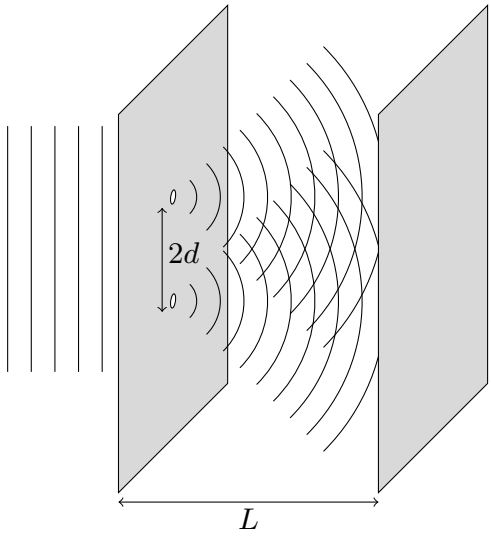

Figure 4.1: Pinhole interference configuration

For our calculations, we will fix a detection point $\boldsymbol{D} = (L, y_D, z_D)$ on the screen, separated from each of the respective pinholes by distances

$$r_\pm \coloneqq \mathrm{dist}\,(\pm d\hat{\boldsymbol{z}}, \boldsymbol{D}) \equiv \sqrt{L^2 + y_D^2 + (z_D \mp d)^2}. \tag{4.0.1}$$

Due to symmetry, the spherical waves in our setup will have equal energies, and thus equal wavenumber magnitudes, k. This is the case regardless of whether we take the standard non-relativistic dispersion relation of commutative quantum mechanics, or that of (3.1.6), the latter together with the restriction $k \in [0, \pi/\lambda)$. Of course, true spherical waves emanate radially outward in all directions. Nevertheless, it will still benefit us to define some directional wavenumber vectors, $\boldsymbol{k}_\pm$. The reason for this is that we will perform calculations within the *large-separation* approximation (also known as the *far-field* approximation), wherein L is assumed to far exceed both the slit separation, $2d$, and

the displacements, z_D and y_D, of the measurement point. Under this approximation, we will treat the spherical waves incident on the screen instead as (appropriately scaled) plane waves with momenta normal to their wavefronts. The appropriate wavenumber vectors are then

$$\boldsymbol{k}_\pm \equiv k\,\hat{\boldsymbol{k}}_\pm = \frac{k}{r_\pm}\begin{bmatrix} L \\ y_D \\ z_D \mp d \end{bmatrix}, \tag{4.0.2}$$

directed from each pinhole towards $\boldsymbol{D}$. We will see this approximation in effect in the coming sections, both for the commutative and non-commutative calculations.

Note also that, since the origin is co-linear with the pinholes, $\hat{\boldsymbol{k}}_\pm$ and $\hat{\boldsymbol{D}}$ are all co-planar. This permits us to illustrate the geometry of the setup within an appropriate planar slice; such is given by figure 4.2, whose angles we will reference in the coming calculations.

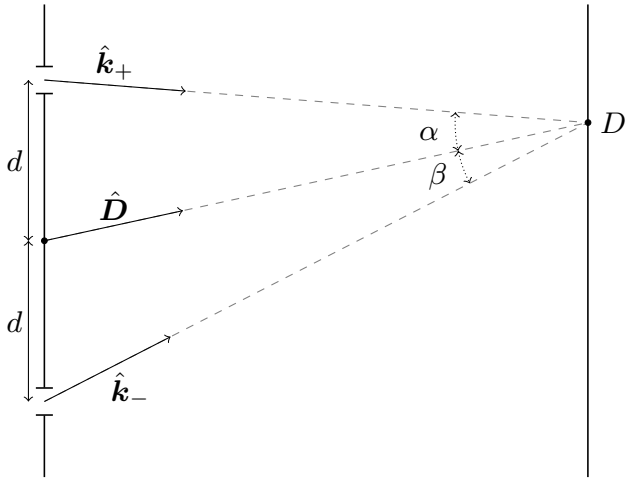

Figure 4.2: Planar slice of pinhole configuration along plane defined by pinholes and detection point

The main result of this chapter is derived in section 4.2, where we treat this pinhole configuration in the fuzzy-sphere NCQM formalism. However, in section 4.1 below, we first treat the setup using ordinary commutative quantum mechanics. This is useful for comparison with the non-commutative result — indeed, the commutative result should be viewed as a special case of the non-commutative one, and must be entirely recovered within the *commutative limit*, $\lambda \to 0$. We check this limit in section 4.4.1.

4.1 Commutative interference calculation

In our pinhole interference setup, the wavefunction incident on the screen is a superposition of spherical waves emanating from each pinhole. We invoke the large-separation assumption (in particular, that $L \gg 2d$) to use the large-r form of each spherical wave, as per (3.2.2). Then the wavefunction has the form

$$\psi(\boldsymbol{D}) = \frac{1}{\sqrt{8\pi}\,V^{1/6}}\left(\frac{1}{r_+}e^{ikr_+} + \frac{1}{r_-}e^{ikr_-}\right),$$

where V is the system's volume, as per the discussion at the end of section 3.2.1. We have chosen the simplest possible angular dependence for our spherical waves, namely the spherical harmonic $Y_0^0(\theta,\phi) = 1/\sqrt{4\pi}$. A more complicated angular dependence would only

serve to apply an additional modulation to the base interference pattern — we therefore simplify the problem by ignoring angular momentum.

Crucially, the large-separation assumption further permits us to approximate the spherical waves with (appropriately-attenuated) plane waves,

$$\psi(\boldsymbol{D}) = \frac{1}{\sqrt{8\pi}\,V^{1/6}}\left(\frac{1}{r_+}e^{i\boldsymbol{k}_+\cdot\boldsymbol{D}} + \frac{1}{r_-}e^{i\boldsymbol{k}_-\cdot\boldsymbol{D}}\right), \tag{4.1.1}$$

which is the so-called *paraxial* approximation. We should justify this step a bit more carefully by showing that the plane waves capture the correct radial dependence within our large-separation approximation. To this end, consider the triangle depicted on figure 4.2 with vertices $\mathbf{0}$, $\boldsymbol{D}$ and $d\hat{\boldsymbol{z}}$; its area can be expressed either as $\frac{1}{2}d\sqrt{L^2+y_D^2}$ or as $\frac{1}{2}r_+ r\sin\alpha$ (identity 4.3.148 in [2]), whence

$$\sin\alpha = \frac{2\cdot\frac{1}{2}d\sqrt{L^2+y_D^2}}{rr_+} = \frac{d}{L}\frac{\sqrt{1+\left(\frac{y_D}{L}\right)^2}}{\sqrt{1+\left(\frac{y_D}{L}\right)^2+\left(\frac{z_D}{L}\right)^2}\sqrt{1+\left(\frac{y_D}{L}\right)^2+\left(\frac{z_D}{L}-\frac{d}{L}\right)^2}} \approx \frac{d}{L},$$

up to first order (in all of $d/L, y_D/L, z_D/L \ll 1$). Next, applying the cosine rule, $d^2 = r_+^2 + r^2 - 2rr_+\cos\alpha$, to the same triangle and solving for r_+ gives

$$r_+ = r\cos\alpha \pm r\sqrt{\left(\frac{d}{r}\right)^2 - \sin^2\alpha} \approx r\cos\alpha, \tag{4.1.2}$$

since $d/r \approx d/L$ also, so the square root vanishes to leading order. By identical reasoning, we also have $r_- \approx r\cos\beta$, and so $\boldsymbol{k}_+\cdot\boldsymbol{D} = \|\boldsymbol{k}_+\|\|\boldsymbol{D}\|\cos\alpha = rk\cos\alpha \approx kr_+$, and similarly $\boldsymbol{k}_-\cdot\boldsymbol{D} \approx kr_-$. This justifies the paraxial approximation of (4.1.1). We should also note that only the leading-order contributions in the far-field approximation contribute to the interference pattern itself — higher-order terms serve only as modulation effects. This justifies why we only compute up to leading order in each of d/L, y_D/L, and z_D/L, both in this section and in section 4.2 below.

With the above form of the wavefunction, the spatial probability density, $P_{\text{comm}}(\boldsymbol{D})$, is (up to dimensionless normalisation prefactors)

$$\begin{aligned} P_{\text{comm}}(\boldsymbol{D}) = |\psi(\boldsymbol{D})|^2 &= \frac{1}{8\pi V^{1/3}}\left[\frac{1}{r_+^2}+\frac{1}{r_-^2}+\frac{1}{r_+r_-}\left(e^{i(\boldsymbol{k}_+-\boldsymbol{k}_-)\cdot\boldsymbol{D}}+e^{-i(\boldsymbol{k}_+-\boldsymbol{k}_-)\cdot\boldsymbol{D}}\right)\right] \\ &= \frac{1}{4\pi V^{1/3}\,r_+r_-}\left[\frac{2d^2}{r_+r_-}+\cos(\alpha+\beta)+\cos(rk(\cos\alpha-\cos\beta))\right], \end{aligned} \tag{4.1.3}$$

where we have (again) applied the cosine rule to the geometry of figure 4.2 to write

$$\begin{aligned} \frac{r_+^2+r_-^2}{2r_+r_-} &= \frac{4d^2+2r_+r_-\cos(\alpha+\beta)}{2r_+r_-} \\ &= \frac{2d^2}{r_+r_-}+\cos(\alpha+\beta). \end{aligned}$$

Qualitatively, the form of the resulting distribution is easily understood. It consists essentially of two parts: an underlying bimodal distribution superimposed with interference,

$$P_{\text{comm}}(\boldsymbol{D}) \;\propto\; \underbrace{\frac{2d^2}{r_+^2r_-^2}+\frac{1}{r_+r_-}\cos(\alpha+\beta)}_{\text{bimodal shaping function}} \;+\; \underbrace{\frac{1}{r_+r_-}\cos(rk(\cos\alpha-\cos\beta))}_{\text{interference term}}. \tag{4.1.4}$$

This is perhaps most easily seen by independently plotting each part. For the sake of illustration, we fix $y_D = 0$ and write the bimodal terms collectively as a function, $P_0(z_D)$, of z_D. Likewise, write the interference term as $P_1(z_D)$. Figure 4.3 then plots each of these functions for a range of z_D values (for arbitrarily-chosen fixed L, d and k), highlighting the behaviour we describe. The smooth bimodal distribution P_0 represents the behaviour

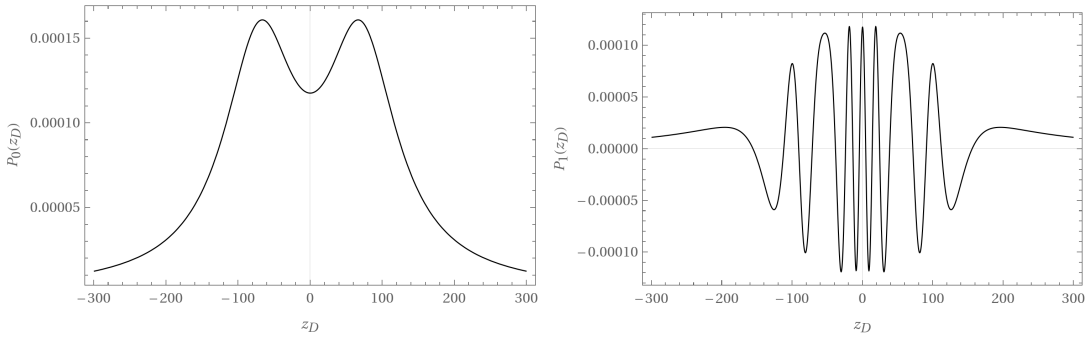

Figure 4.3: Plots of each of the "parts" of P_{comm}, as per (4.1.4), for $L = 60, d = 70, k = 0.4$. All lengths are in arbitrary units, and plots are unnormalised.

of a classical particle passing through the double-pinhole setup, while the interference, P_1, captures all of the quantum behaviour. In the next section, we will repeat the interference calculation in the NCQM formalism, and in section 4.3 we will qualitatively examine the form of the distribution resulting from the NCQM context. To foreshadow the outcome, we will obtain a form very much like the above, only with an additional exponential suppression sitting in front of the interference term. Moreover, the result of the non-commutative calculation must of course reduce to (4.1.4) in the limit $\lambda \to 0$ (we check this in section 4.4.1), so we already appreciate that the suppression will scale in intensity with increasing λ.

4.2 Non-commutative interference calculation

Much as in the commutative calculation, we want the state $|\psi)$ arriving at $\boldsymbol{D}$ to have the form of a superposition of spherical waves emanating from each pinhole. It is not immediately obvious how we would modify the form of the non-commutative spherical waves from section 3.2.2 to handle a different source location. That said, for the sake of determining the interference pattern it only matters that the two spherical waves traverse different path lengths (that is r_+ and r_-) between their respective sources and $\boldsymbol{D}$. With this in mind, it is straightforward to write down the *symbol* of the state $|\psi)$ arriving at $\boldsymbol{D}$,

$$\langle \boldsymbol{z}|\psi|\boldsymbol{z}\rangle = M\left[\left\langle \boldsymbol{z}^+\middle|k,0,0\middle|\boldsymbol{z}^+\right\rangle + \left\langle \boldsymbol{z}^-\middle|k,0,0\middle|\boldsymbol{z}^-\right\rangle\right].$$

In the above, all of the vectors $\boldsymbol{z}, \boldsymbol{z}_\pm \in \mathbb{C}^2$ encode the coordinates of $\boldsymbol{D}$, as per (2.2.5), only $\boldsymbol{z}$ measures these coordinates relative to the origin, while each of the $\boldsymbol{z}_\pm$ measures them relative to the respective pinhole. The constant, M, is an overall normalisation, which we discuss shortly. We have clearly again chosen $l = m = 0$ for simplicity (for the same reasons as in the commutative calculation), and we will again focus on the large-separation asymptotic behaviour,

$$\langle \boldsymbol{z}|\psi|\boldsymbol{z}\rangle \sim \frac{M}{i}\left[\frac{1}{R_+}e^{R_+(\cos\kappa-1)+iR_+\sin\kappa} + \frac{1}{R_-}e^{R_-(\cos\kappa-1)+iR_-\sin\kappa}\right], \tag{4.2.1}$$

as per (3.2.8). We refer here to dimensionless constants $R_\pm := \frac{r_\pm}{\lambda} = \bar{z}^\pm_\alpha z^\pm_\alpha$, as well as $\kappa := \lambda k$, the latter defined as in section 3.2.2.

We want to approximate the spherical waves with (scaled) plane waves in analogy with the paraxial approximation of (4.1.1). To this end, we should start by considering the symbol, $\langle \boldsymbol{z}|e^{i\boldsymbol{k}_\pm\cdot\hat{\boldsymbol{x}}}|\boldsymbol{z}\rangle$, of a plane wave (measured with respect to the origin). The idea is that by comparison of this symbol with (4.2.1), we will identify the appropriate scaling for the plane waves in our context. There is a simple transformation law for the action of a plane wave on a coherent state, the derivation of which we defer to appendix A. To be precise, a plane wave acting on a coherent state simply produces a different coherent state, which is captured by (A.0.6). As such, we can write our plane wave symbol as

$$\begin{aligned}\langle \boldsymbol{z}|e^{i\boldsymbol{k}_\pm\cdot\hat{\boldsymbol{x}}}|\boldsymbol{z}\rangle &= \langle \boldsymbol{z}|g(\boldsymbol{k}_\pm)\boldsymbol{z}\rangle \\ &= \exp\left[-\frac{1}{2}\left(\|\boldsymbol{z}\|^2+\|g(\boldsymbol{k}_\pm)\boldsymbol{z}\|^2\right)+\boldsymbol{z}^\dagger g(\boldsymbol{k}_\pm)\boldsymbol{z}\right] \\ &= \exp\left[-\frac{1}{2}\left(\|\boldsymbol{z}\|^2+\|g(\boldsymbol{k}_\pm)\boldsymbol{z}\|^2\right)+\boldsymbol{z}^\dagger(\cos\kappa+i\sin\kappa\,\hat{\boldsymbol{k}}_\pm\cdot\boldsymbol{\sigma})\boldsymbol{z}\right],\end{aligned} \tag{4.2.2}$$

where $g(\boldsymbol{k})\in \mathrm{SU}(2)$ is defined as in (A.0.6), and we have invoked the coherent state overlap, (2.2.3), as well as (A.0.2) to expand the form of $g(\boldsymbol{k}_\pm)$. Of course, being an SU(2)-element, $g(\boldsymbol{k}_\pm)$ is an isometry, so $\|g(\boldsymbol{k}_\pm)\boldsymbol{z}\|^2=\|\boldsymbol{z}\|^2=R$, as per (2.2.5). Moreover (by (2.2.5) and the immediately proceeding discussion),

$$\boldsymbol{z}^\dagger(\hat{\boldsymbol{k}}_\pm\cdot\boldsymbol{\sigma})\boldsymbol{z}=\left(\boldsymbol{z}^\dagger\sigma^i\boldsymbol{z}\right)[\hat{\boldsymbol{k}}_3]_i=\hat{\boldsymbol{k}}_\pm\cdot\boldsymbol{D}/\lambda,$$

and $\hat{\boldsymbol{k}}_\pm\cdot\boldsymbol{D}\approx r_\pm$, as derived in section 4.1 above, so

$$\langle \boldsymbol{z}|e^{i\boldsymbol{k}_\pm\cdot\hat{\boldsymbol{x}}}|\boldsymbol{z}\rangle\approx e^{R(\cos\kappa-1)+iR_\pm\sin\kappa}. \tag{4.2.3}$$

This closely resembles one of the terms in (4.2.1), and by inspection we can see that the following state will have the desired symbol,

$$|\psi)=\frac{M}{i}\left[\eta_+|\boldsymbol{k}_+)+\eta_-|\boldsymbol{k}_-)\right], \tag{4.2.4}$$

for real dimensionless constants

$$\eta_\pm\coloneqq\frac{1}{R_\pm}\exp[(R_\pm-R)(\cos\kappa-1)].$$

While (4.2.4) and (4.1.1) appear superficially to differ in form, we should note that $\eta_\pm\approx 1/R_\pm$ for large L (or small κ). This is easily seen from the geometry of figure 4.2 using similar arguments to those of section 4.1. Under this approximation, there is little difference in the form of the state at the screen between the commutative and non-commutative cases.

Lastly, we should discuss the normalisation. The plane waves $|\boldsymbol{k}_\pm)$ each come with normalisation factors $N=\frac{1}{\sqrt{4\pi\lambda^3}}$, as per (3.1.11). As in the commutative calculation, we are not much concerned with overall dimensionless normalisation factors. That said, we should include a factor of $\sqrt{\frac{\lambda}{V^{1/3}}}$ for comparison with the commutative result, given that these values define the length scales of the problem. For this reason we choose the simplest sensible overall normalisation, $M\coloneqq i\sqrt{\frac{\lambda}{2V^{1/3}}}$, for the sum.

Now the probability of observing our state at $\boldsymbol{D}$ is calculated using (2.2.12) as

$$\begin{aligned}P(\boldsymbol{D}) &= 4\pi\lambda^2\langle \boldsymbol{z}|\psi\hat{r}\psi^\dagger|\boldsymbol{z}\rangle \\ &= 4\pi\lambda^2\frac{\lambda}{2V^{1/3}}\frac{1}{4\pi\lambda^3}\langle \boldsymbol{z}|\left(\eta_+e^{i\boldsymbol{k}_+\cdot\hat{\boldsymbol{x}}}+\eta_-e^{i\boldsymbol{k}_-\cdot\hat{\boldsymbol{x}}}\right)\hat{r}\left(\eta_+e^{-i\boldsymbol{k}_+\cdot\hat{\boldsymbol{x}}}+\eta_-e^{-i\boldsymbol{k}_-\cdot\hat{\boldsymbol{x}}}\right)|\boldsymbol{z}\rangle \\ &= \frac{\lambda}{V^{1/3}}\left[\frac{\eta_+^2+\eta_-^2}{2}\langle \boldsymbol{z}|\hat{n}+1|\boldsymbol{z}\rangle+\eta_+\eta_-\,\mathrm{Re}\,\langle \boldsymbol{z}|e^{i\boldsymbol{k}_+\cdot\hat{\boldsymbol{x}}}(\hat{n}+1)e^{-i\boldsymbol{k}_-\cdot\hat{\boldsymbol{x}}}|\boldsymbol{z}\rangle\right],\end{aligned} \tag{4.2.5}$$

where we have used the fact that each plane wave commutes with $\hat{r}$ (since each $\hat{x}_i$ does). We are left with the task of computing a pair of matrix elements involving the number operator $\hat{n}$. There is a completely general approach to computing the matrix element of some function, $g(\hat{n})$, of the number operator, $\hat{n}$, with respect to a pair of (generally distinct) coherent states. This method is outlined in appendix B, where section B.2 treats the special case of a polynomial function g as we have here. As such, the first remaining matrix element, $\langle \boldsymbol{z}|\hat{r}|\boldsymbol{z}\rangle$, is readily computed using (B.2.1), whereby

$$\langle \boldsymbol{z}|\hat{n}+1|\boldsymbol{z}\rangle = R+1.$$

Let us then turn our attention to the remaining matrix element, namely

$$E \coloneqq \langle \boldsymbol{z}|e^{i\boldsymbol{k}_+\cdot\hat{\boldsymbol{x}}}(\hat{n}+1)e^{-i\boldsymbol{k}_-\cdot\hat{\boldsymbol{x}}}|\boldsymbol{z}\rangle\,.$$

The first step is to act each of the plane waves on the adjacent coherent state. As mentioned above, it is shown in appendix A that this simply yields a pair of new coherent states. That is,

$$E = \langle g(-\boldsymbol{k}_+)\boldsymbol{z}|\hat{n}+1|g(-\boldsymbol{k}_-)\boldsymbol{z}\rangle\,,$$

according to (A.0.6). We are now once more in a position to invoke (B.2.1), whereby

$$\begin{aligned} E &= \exp\left[-\frac{1}{2}\left(\|g(-\boldsymbol{k}_+)\boldsymbol{z}\|^2 + \|g(-\boldsymbol{k}_-)\boldsymbol{z}\|^2\right) + K\right](K+1) \\ &= e^{K-R}(K+1), \end{aligned}$$

where, as above, we have noted that $\|g(-\boldsymbol{k}_\pm)\boldsymbol{z}\|^2 = \|\boldsymbol{z}\|^2 = R$. Here, the complex constant

$$K \coloneqq (g(-\boldsymbol{k}_+)\boldsymbol{z})^\dagger\,(g(-\boldsymbol{k}_-)\boldsymbol{z})$$

is defined in accordance with its appearance in appendix B.2.

It now only remains to compute the constant K explicitly. Expanding its definition,

$$\begin{aligned} K &= \boldsymbol{z}^\dagger g(\boldsymbol{k}_+)g(-\boldsymbol{k}_-)\boldsymbol{z} \\ &= \boldsymbol{z}^\dagger e^{i\lambda\boldsymbol{k}_+\cdot\boldsymbol{\sigma}}e^{-i\lambda\boldsymbol{k}_-\cdot\boldsymbol{\sigma}}\boldsymbol{z}. \end{aligned} \tag{4.2.6}$$

Now express the product $e^{i\lambda\boldsymbol{k}_+\cdot\boldsymbol{\sigma}}e^{-i\lambda\boldsymbol{k}_-\cdot\boldsymbol{\sigma}}$ of SU(2) group elements as a single group element, $e^{i\kappa_3\hat{\boldsymbol{k}}_3\cdot\boldsymbol{\sigma}}$, of the same form. This is always possible, as explained in section 3.1, because SU(2) is compact and connected. Next, expand this composite exponential as $e^{i\kappa_3\hat{\boldsymbol{k}}_3\cdot\boldsymbol{\sigma}} = \cos\kappa_3 + i\,\hat{\boldsymbol{k}}_3\cdot\boldsymbol{\sigma}\,\sin\kappa_3$, as per appendix A, leaving $\boldsymbol{k}_3$ and κ_3 undetermined for the moment. Substituting this form into (4.2.6) gives

$$\begin{aligned} K &= \boldsymbol{z}^\dagger\boldsymbol{z}\cos\kappa_3 + i\sin\kappa_3\left(\boldsymbol{z}^\dagger\sigma^i\boldsymbol{z}\right)[\hat{\boldsymbol{k}}_3]_i \\ &= R\left(\cos\kappa_3 + i\,\hat{\boldsymbol{D}}\cdot\hat{\boldsymbol{k}}_3\,\sin\kappa_3\right), \end{aligned} \tag{4.2.7}$$

simplifying as we did for (4.2.2). Finally, the BCH formula — rather, the special case thereof for SU(2), (3.1.3) — gives explicit forms for $\cos\kappa_3$ and $\hat{\boldsymbol{k}}_3\sin\kappa_3$, into which we substitute

$$\begin{aligned} &\kappa_1 = \kappa_2 \equiv \kappa = \lambda k, \\ &\hat{\boldsymbol{k}}_1 \equiv \hat{\boldsymbol{k}}_+ = \frac{1}{\sqrt{L^2+y_D^2+(z_D-d)^2}}\begin{bmatrix} L \\ y_D \\ z_D-d \end{bmatrix}, \\ &\hat{\boldsymbol{k}}_2 \equiv -\hat{\boldsymbol{k}}_- = \frac{-1}{\sqrt{L^2+y_D^2+(z_D+d)^2}}\begin{bmatrix} L \\ y_D \\ z_D+d \end{bmatrix}. \end{aligned}$$

Upon substituting the above, one of the terms resulting from (3.1.3) contains the triple product $\hat{\boldsymbol{D}} \cdot (\hat{\boldsymbol{k}}_+ \times \hat{\boldsymbol{k}}_-)$, but this is easily seen to vanish, since the three vectors in question are all co-planar, as depicted in figure 4.2. We are left with

$$K = R\cos^2\kappa + R\sin^2\kappa\cos(\alpha+\beta) + iR\sin\kappa\cos\kappa(\cos\alpha - \cos\beta), \tag{4.2.8}$$

where we have written each scalar product appearing in (3.1.3) in terms of the angles α and β from figure 4.2. For brevity, let us introduce two more constants,

$$\begin{aligned} A &\coloneqq \operatorname{Re} K = R\left(\cos^2\kappa + \cos(\alpha+\beta)\sin^2\kappa\right), \\ B &\coloneqq \operatorname{Im} K = R\sin\kappa\cos\kappa(\cos\alpha - \cos\beta), \end{aligned} \tag{4.2.9}$$

in terms of which

$$\begin{aligned} \operatorname{Re} E &= e^{A-R}\operatorname{Re}[(\cos B + i\sin B)((A+1)+iB)] \\ &= e^{A-R}((A+1)\cos B - B\sin B) \end{aligned}$$

Finally, inserting everything into (4.2.5), we obtain the final form of our probability distribution,

$$P(\boldsymbol{D}) = \frac{\lambda}{V^{1/3}}\left[\frac{\eta_+^2+\eta_-^2}{2}(R+1) + \eta_+\eta_- e^{A-R}((A+1)\cos B - B\sin B)\right]. \tag{4.2.10}$$

For the remainder of this chapter we discuss our main result, (4.2.10), and consider various limiting cases. In particular, we confirm that in the commutative limit, $\lambda \to 0$, (4.2.10) reduces to the commutative result, (4.1.3). Following that, we consider the classical limit, deriving the specific conditions under which we observe a quantum-to-classical transition, and finally we derive how (4.2.10) is affected by allowing and entire collection of N particles to pass through the pinhole setup at once.

4.3 Qualitative discussion of interference pattern

We start our discussion with a few cursory remarks about the key qualitative features of our non-commutative distribution, (4.2.10), in a similar vein to the discussion closing section 4.1. The form of (4.2.10) is undeniably still somewhat complicated, especially when all of the sub-expressions are fully substituted. Much of this complexity will vanish in the limiting cases we consider in upcoming sections. Nevertheless, as foreshadowed in section 4.1, we can already at this stage divide (4.2.10) according to the qualitative functions of the various sub-expressions, much like in (4.1.4),

$$P(\boldsymbol{D}) \propto \underbrace{\frac{\eta_+^2+\eta_-^2}{2}(R+1)}_{\substack{\text{bimodal shaping} \\ \text{function}}} + \underbrace{\eta_+\eta_- e^{A-R}}_{\substack{\text{exponential} \\ \text{suppression}}} \times \underbrace{((A+1)\cos B - B\sin B)}_{\text{interference terms}}. \tag{4.3.1}$$

We could once again plot each component separately, as we did for (4.1.4), in order to confirm their respective functions, though we avoid doing as much due to the similarity with the commutative case. Instead, we focus for now on the key difference, namely the exponential factor. Notably, this exponential can easily be seen to indeed always act to *suppress* the interference, given that the exponent is manifestly always nonpostive,

$$A - R = R\sin^2\kappa\,(\cos(\alpha+\beta) - 1) \leq 0,$$

since $\kappa \in [0, \pi)$, and $\alpha + \beta \in (0, \pi)$.

For understanding the overall qualitative behaviour of the entirety of (4.2.10), it is still helpful to examine a plot. Figure 4.4 shows surface plots of (4.2.10) for some arbitrarily-chosen parameter values, along with the $y_D = 0$ traces. Actually, instead of $P(\boldsymbol{D})$, we plot $\frac{1}{4\pi\lambda^2 r} P(\boldsymbol{D})$, which is the spatial probability density corresponding to $P(\boldsymbol{D})$, as explained in section 2.2. This helps us later to meaningfully compare these plots qualitatively with those of the commutative limit. The plots in figure 4.4 indeed clearly exhibit the expected bi-modal distribution superimposed with interference. Moreover, the interference is evidently stronger for one set of parameters than for the other, and the increase in suppression at the higher of the two momenta is correlated with increased localisation of the distribution — that is, as the interference gets suppressed, we see the distribution separating into two distinct localised peaks. All of these behaviours are entirely characteristic, as we shall see in the upcoming sections.

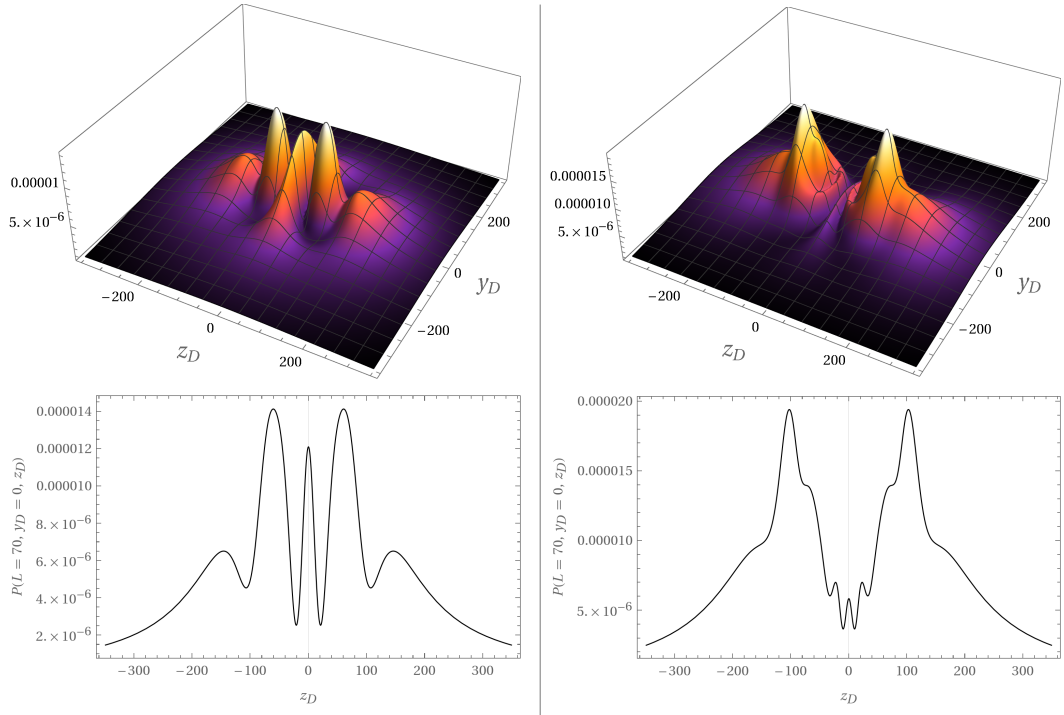

(a) $k = 0.22$ (b) $k = 0.44$

Figure 4.4: Surface plots of $\frac{1}{4\pi\lambda^2 r} P(\boldsymbol{D})$, with $y_D = 0$ traces, for different values of k. Other parameters are $L = d = 70, \lambda = 0.1$. All lengths are in arbitrary units.

More importantly, the plots also suggest that the distribution is reflection-symmetric. Indeed, we can easily algebraically verify its symmetry under $z_D \longleftrightarrow -z_D$ — each of the following quantities are manifestly invariant under this replacement: R; $\cos(\alpha + \beta)$, and hence e^{A-R}; $\cos B$ and $B \sin B$ (as B accrues a minus sign under the reflection); and finally $\eta_+\eta_-$ and $\eta_\pm^2$. This would hardly be remarkable, were it not for the fact that the double-slit interference pattern in the 2D Moyal plane is *asymmetric* under reflection [32]. The restoration of reflection symmetry in our analogous setup in 3D fuzzy space confirms the expectations of [32] that the reflection-asymmetry in the Moyal plane interference pattern arises only because the Heisenberg-Moyal commutation relations break *rotational* symmetry (as explained in section 2.1). The distribution is likewise (unsurprisingly) symmetric under the reflection $y_D \longleftrightarrow -y_D$, and thus also under 180° rotation about the x-axis (the composition of these two reflections).

4.4 Limiting cases

In this section we consider how the probability distribution of (4.2.10) simplifies in various limiting cases. Specifically, we first check that in the *commutative limit*, $\lambda \to 0$, it coincides with (4.1.3), the interference pattern from commutative quantum mechanics. Following that, we consider the *classical limit* of the interference pattern, and derive the conditions under which we can expect to observe a quantum-to-classical transition.

4.4.1 Commutative limit

Let us finally take the commutative limit $\lambda \to 0^+$, and show that (4.2.10) indeed reproduces (4.1.3), as it must. There is actually a small subtlety which we have already foreshadowed at the end of section 2.2.2. That is, since $P_{\text{comm}}(\boldsymbol{D})$ represents a *spatial* density (with dimensions of length^{-3}), and $P(\boldsymbol{D})$ does not (being dimensionless), we should instead expect to obtain $P_{\text{comm}}(\boldsymbol{D})$ as the limit

$$\lim_{\lambda\to 0^+} \frac{1}{4\pi r\lambda^2} P(\boldsymbol{D}),$$

rather than simply $\lim_{\lambda\to 0^+} P(\boldsymbol{D})$. This is because, as shown in section 2.2.2, $\frac{1}{4\pi r\lambda^2} P(\boldsymbol{D})$ is precisely the spatial density corresponding to $P(\boldsymbol{D})$.

Now, as we send $\lambda \to 0^+$, B clearly obtains a finite (generally non-zero) limit, which we call B_0,

$$\begin{aligned}\lim_{\lambda\to 0^+} B &= \lim_{\lambda\to 0^+} \frac{r}{\lambda}\left(k\lambda + \mathcal{O}(\lambda^3)\right)(\cos\alpha - \cos\beta)\\ &= rk(\cos\alpha - \cos\beta)\\ &\equiv B_0,\end{aligned}$$

whereas A diverges like $R \equiv r/\lambda$,

$$\begin{aligned}\lim_{\lambda\to 0^+} A &= \lim_{\lambda\to 0^+} \frac{r}{\lambda}\left(1 + (\cos(\alpha+\beta) - 1)k^2\lambda^2 + \mathcal{O}(\lambda^3)\right)\\ &= \lim_{\lambda\to 0^+} \frac{r}{\lambda} \not< \infty.\end{aligned}$$

But the divergence of A is cancelled in the expression $A - R$, which altogether vanishes,

$$\begin{aligned}\lim_{\lambda\to 0^+} A - R &= \lim_{\lambda\to 0^+} \frac{r}{\lambda}\left(1 + (\cos(\alpha+\beta) - 1)k^2\lambda^2 + \mathcal{O}(\lambda^4)\right) - \frac{r}{\lambda}\\ &= 0,\end{aligned}$$

meaning the interference suppression vanishes in this limit, $e^{A-R} \to 1$. Finally, the numerator, $R_\pm\eta_\pm$, of $\eta_\pm$ tends to 1,

$$\begin{aligned}\lim_{\lambda\to 0^+} R_\pm\eta_\pm &= \exp\left[\lim_{\lambda\to 0^+} \frac{r_\pm - r}{\lambda}\left(1 + k^2\lambda^2 + \mathcal{O}(\lambda^4) - 1\right)\right]\\ &= e^0 = 1,\end{aligned}$$

so that $\eta_\pm \to \lambda/r_\pm$.

Using the above limits (invoking continuity wherever applicable) together with the form of (4.2.10), we compute the commutative limit,

$$\begin{aligned}
&\lim_{\lambda\to 0^+} \frac{1}{4\pi r\lambda^2} P(\boldsymbol{D}) \\
&= \lim_{\lambda\to 0^+} \frac{1}{4\pi\lambda V^{1/3} r} \left[\frac{\eta_+^2+\eta_-^2}{2}(R+1) + \eta_+\eta_- e^{A-R}((A+1)\cos B - B\sin B)\right] \\
&= \lim_{\lambda\to 0^+} \frac{1}{4\pi V^{1/3} \cancel{r}} \left[\frac{1}{2}\left(\frac{1}{r_+^2}+\frac{1}{r_-^2}\right)\cancel{(r+\lambda)} + \frac{1}{r_+ r_-}\cancel{(r+\lambda)}\cos B_0\right] \\
&= \frac{1}{4\pi V^{1/3} r_+ r_-}\left[\frac{r_+^2+r_-^2}{2r_+r_-} + \cos(rk(\cos\alpha - \cos\beta))\right] \\
&= P_{\text{comm}}(\boldsymbol{D}).
\end{aligned}$$

Reassuringly, this is exactly the required result.

Having established that we have the correct commutative limit, we pause to compare its behaviour qualitatively with that of $P(\boldsymbol{D})$. To this end, we plot $P_{\text{comm}}(\boldsymbol{D})$ in figure 4.5 for the same parameter values (except for λ, of course) as in figure 4.4. Comparing figures 4.5

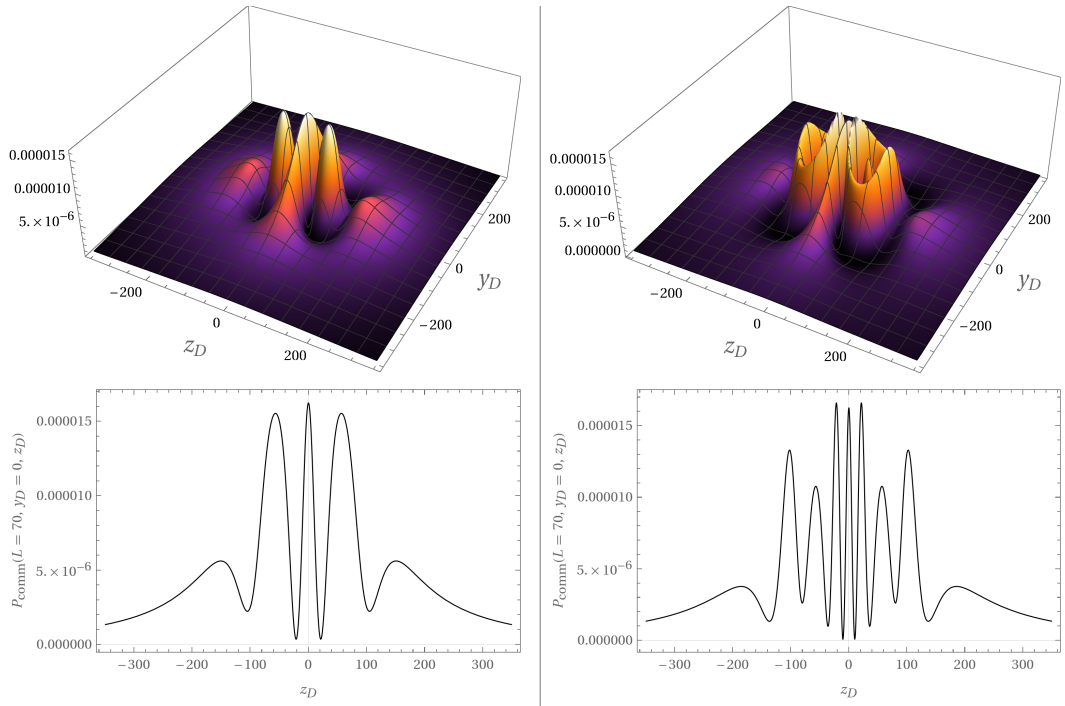

(a) $k = 0.22$ (b) $k = 0.44$

Figure 4.5: Surface plots of $P_{\text{comm}}(\boldsymbol{D})$, with $y_D = 0$ traces, for the same values of k, L, and d as in figure 4.4.

and 4.4, the low-momentum ($k = 0.22$) distributions are unsurprisingly similar, but where in the non-commutative distribution of figure 4.4 we observe a *suppression* of interference for higher momentum ($k = 0.44$), the commutative distribution of figure 4.5 actually exhibits completely the opposite behaviour, showing more pronounced interference at this higher k. This shows that the momentum-dependent quantum-to-classical transition that we observe is a uniquely non-commutative phenomenon. In the next section, we will consider this transition more carefully.

4.4.2 Classical limit and quantum-to-classical transition

We recognise the "classical-regime" of our distribution to consist of any parameter combinations that result in strong interference suppression, leaving behind the underlying bimodal distribution that one would expect to emerge classically from our pinhole setup. An example of a distribution in this regime is shown in figure 4.6. Looking at figure 4.4, or even

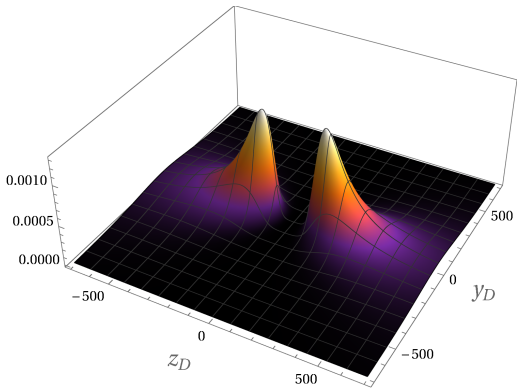

Figure 4.6: Surface plot of $\frac{1}{4\pi\lambda^2 r}P(\boldsymbol{D})$ with $k = 1$ (and L, d and λ as in figure 4.4), exhibiting classical-regime behaviour of being bimodal and localised with no visible interference.

the double slit interference in the Moyal plane [32], we might expect this regime to emerge in a large momentum limit. However, recall that, like the plane wave energy of (3.1.6), the probability distribution of (4.2.10) is periodic in k with period $2\pi/\lambda$; such periodicity does not occur in the Moyal plane [32]. The upshot is that we cannot hope to obtain a well-defined limit by sending $k \to \infty$, so it is not apparent what a large momentum limit should entail. Indeed, we will show that suppression can occur even for arbitrarily small momenta.

Recall from (4.3.1) that the factor responsible for interference suppression is

$$e^{A-R} = \exp\big[R\sin^2\kappa(\cos(\alpha+\beta)-1)\big].$$

We should therefore consider the conditions under which the exponent is significant. Firstly, we should explicitly write $\cos(\alpha+\beta)$ in terms of the length scales in the problem. Applying the cosine rule to figure 4.2, we have

$$\begin{aligned}
\cos(\alpha+\beta) &= \frac{r_+^2 + r_-^2 - 4d^2}{2r_+r_-} \\
&= \frac{r^2 - d^2}{\sqrt{(r^2+d^2)^2 - 4z_D^2 d^2}} \\
&= \frac{1-\left(\frac{d}{r}\right)^2}{\sqrt{\left(1+\left(\frac{d}{r}\right)^2\right)^2 - 4\left(\frac{z_D}{r}\right)^2\left(\frac{d}{r}\right)^2}} \\
&\approx \frac{1-\left(\frac{d}{r}\right)^2}{1+\left(\frac{d}{r}\right)^2} \\
&\approx 1 - \frac{2d^2}{r^2},
\end{aligned}$$

to first order in each of $d/r \ll 1$ and $z_D/r \ll 1$, given our large-separation approximation. Suppose for the moment that $\lambda k \ll 1$, as would be the case at low momentum. Expanding

the exponent,

$$\begin{aligned} A - R &= \lambda r k^2(\cos(\alpha+\beta) - 1) + \mathcal{O}(\lambda^3 k^3) \\ &\approx -\frac{2\lambda k^2 d^2}{r} \end{aligned}$$

to leading order, we identify the condition for strong suppression as $2\lambda k^2 d^2/r \gg 1$. It is helpful to rewrite this condition in terms of energy, and given our assumption on λk, we can expand (3.1.6) as $E \approx \frac{\hbar^2 k^2}{2m}$. The condition for interference suppression then becomes

$$\frac{4\lambda d^2 mE}{r\hbar^2} \gg 1 \quad \iff \quad r \ll \frac{4\lambda d^2 mE}{\hbar^2}, \tag{4.4.1}$$

so that, in particular, the suppression effect is only visible at sufficiently small distances. This seems in opposition with our large-separation assumption. If we combine this assumption with the above inequality, we find that the particular expression of (4.4.1) is only valid in the regime

$$1 \ll \frac{r}{d} \ll \frac{4\lambda dmE}{\hbar^2}. \tag{4.4.2}$$

Generally, the physical implications of condition (4.4.1) are entirely as expected — the strength of the suppression scales with larger values of mass, energy, and non-commutative parameter. None of these relationships come as a surprise, in light of the Moyal plane result [32]. We also note that in the commutative limit $\lambda = 0$, the upper limit on the distance of observation vanishes and interference is prevalent at all length scales of observation.

That said, there are two remarkable features of (4.4.1) that distinguish it from the analogous classicality condition for double-slit interference in the Moyal plane. Firstly, our suppression strength is affected by the distance r at which measurement is performed, whereas in the Moyal plane, it depends (for a single particle) only on the momentum and non-commutative parameter. Secondly (indeed, consequently), condition (4.4.1) can (in theory) be satisfied even for small values of k (indeed, we started by assuming $k \ll 2/\lambda$) simply by choosing r sufficiently small, meaning that, in this setting, we are theoretically capable of observing suppression at low momentum, unlike in the Moyal plane. These are important testable predictions of our three-dimensional theory.

At this point, we can perform a similar back-of-the-envelope estimate to that in [32] to get a sense of when we should expect to see suppression in practice. Supposing λ to be on the order of a Planck length, and the slit separation d on the order of 1cm, and considering the interference pattern of a single electron with an energy of 1eV, we expect to observe significant suppression when

$$\begin{aligned} r &\lesssim \frac{(10^{-35}\,\mathrm{m})(10^{-2}\,\mathrm{m})^2(10^{-31}\,\mathrm{kg})(10^{-19}\,\mathrm{kg\,m^2\,s^{-2}})}{(10^{-34}\,\mathrm{kg\,m^2\,s^{-1}})^2} \\ &= 10^{-21}\,\mathrm{m}. \end{aligned}$$

We should of course note that values which we have substituted above fall well within the bounds set by the two constraints, namely $\lambda k \ll 1$ and (4.4.2), under which (4.4.1) is valid. The resulting required value of r is obviously extremely small, so we should ultimately not expect to be able to detect any suppression at these energies. Even if we could probe such length scales (or alternatively if we tried to fix things by significantly increasing d), the constraint on r certainly is not consistent with the large-separation approximation under which (4.4.1) is valid in the first place. Conversely, to observe suppression at lengths on the order of a meter requires an electron to have energies around $10^{19}\,\mathrm{eV}$ — again, quite undetectable. Thankfully this is not concerning, since in the next section we will show how, once multiple particles are allowed to interfere, the suppression becomes much more pronounced at realistic length scales.

4.5 Macroscopic behaviour

The goal for this section is to derive how the main result of this chapter, (4.2.10), scales as a function of particle number. Specifically, we wish to modify our interference setup by considering a whole *collection* of particles passing through the pinholes and interfering together. We are interested in the collective dynamics of the particle collection, to wit the centre-of-mass dynamics. Our expectation is that the centre-of-mass dynamics will exhibit interference suppression, the strength of which should now also scale as a function of the *number of particles* in the collection (in addition to the other relevant parameters discussed in section 4.4.2 above). Having the suppression strength scale with particle number as well would offer another avenue by which we could conceivably observe the transition of our system to the classical regime, even though, as it stands, this transition is unobservable for just a single particle (as discussed at the end of section 4.4.2).

4.5.1 Many-particle definitions

We begin with a brief overview of how our core definitions and results are straightforwardly extended to the many-particle case. Consider a macroscopic object comprised of N particles of equal mass m, with total mass $M \coloneqq Nm$. Each particle has states described by some Hilbert space $\mathcal{H}_{\mathrm{q}}^{(n)}$, say. The total system is described by a Hilbert space, $\mathcal{H}_{\mathrm{q}}^{\mathrm{tot}}$, which constructed as a tensor product of the individual particle Hilbert spaces, $\mathcal{H}_{\mathrm{q}}^{(n)}$,

$$\mathcal{H}_{\mathrm{q}}^{\mathrm{tot}} \coloneqq \bigotimes_{n=1}^{N} \mathcal{H}_{\mathrm{q}}^{(n)}.$$

For simplicity, we neglect the symmetrisation (respectively, antisymmetrisation) of the tensor product states which would arise from considering a collection specifically comprised of bosons (respectively, fermions). Let the n^{th} particle coordinate operators be denoted $\hat{x}_i^{(n)}$; we assume that coordinate operators belonging to different particles commute,

$$\left[\hat{x}_i^{(l)}, \hat{x}_j^{(n)}\right] = 2i\lambda\epsilon_{ijk}\delta_{ln}\hat{x}_k^{(l)}. \tag{4.5.1}$$

The collective motion is described with *centre-of-mass* coordinates,

$$\hat{\boldsymbol{x}}^{(\mathrm{CM})} \coloneqq \frac{1}{N}\sum_{n=1}^{N}\hat{\boldsymbol{x}}^{(n)}, \tag{4.5.2}$$

satisfying the commutation relations

$$\begin{aligned}\left[\hat{x}_i^{(\mathrm{CM})}, \hat{x}_j^{(\mathrm{CM})}\right] &= \frac{1}{N^2}\sum_{l,n}\left[\hat{x}_i^{(l)}, \hat{x}_j^{(n)}\right] \\ &= 2i\frac{\lambda}{N}\epsilon_{ijk}\,\frac{1}{N}\sum_{n}\hat{x}_k^{(n)} \\ &= 2i\frac{\lambda}{N}\epsilon_{ijk}\,\hat{x}_k^{(\mathrm{CM})},\end{aligned} \tag{4.5.3}$$

which are manifestly identical to those of $\hat{x}_i$, only with $\tilde{\lambda} \equiv \frac{\lambda}{N}$ in place of λ. As usual, we also have the *relative* coordinates, defined by $\hat{\boldsymbol{\xi}}^{(n)} \coloneqq \hat{\boldsymbol{x}}^{(n)} - \hat{\boldsymbol{x}}^{(\mathrm{CM})}$, which are easily seen to have vanishing sum,

$$\sum_{n=0}^{N}\hat{\boldsymbol{\xi}}^{(n)} = \mathbf{0},$$

since collective motion is accounted for by $\hat{\boldsymbol{x}}^{(\mathrm{CM})}$.

We can also extend our free-particle solutions. The many-particle free-particle Hamiltonian reads

$$\hat{H}^{\mathrm{tot}} = \sum_{n=1}^{N} \hat{H}^{(n)}, \tag{4.5.4}$$

where each $\hat{H}^{(n)}$ is a straightforward generalisation of the free-particle Hamiltonian in (3.0.1),

$$\hat{H}^{(n)} := -\frac{\hbar^2}{2m}\hat{\Delta}^{(n)}.$$

Indeed, wherever we use a superscript (n) on a known operator, it should be assumed to act on the n^{th} Hilbert space, $\mathcal{H}_{\mathrm{q}}^{(n)}$ (or configuration space, $\mathcal{H}_{\mathrm{c}}^{(n)}$), but otherwise be defined as usual. Still, for the sake of completeness, we include below the remaining definitions for the extended observables and operators, though all the definitions closely resemble those in chapter 2, only with additional (n) superscripts:

$$\begin{aligned}
\hat{\Delta}^{(n)}\left|\psi\right) &:= -\left|\frac{1}{\lambda\hat{r}^{(n)}}[(a_\alpha^{(n)})^\dagger,[a_\alpha^{(n)},\psi]]\right), \quad \text{where} \\
\hat{r}^{(n)} &:= \lambda(\hat{n}^{(n)}+1), \quad \text{where} \\
\hat{n}^{(n)} &:= (a_\alpha^{(n)})^\dagger a_\alpha^{(n)},
\end{aligned}$$

where the $a_\alpha^{(n)}$ and $(a_\alpha^{(n)})^\dagger$ act on the n^{th} configuration space. Now the (plane wave) eigenstates of $\hat{H}^{\mathrm{tot}}$ are (up to normalisation)

$$\left|\boldsymbol{k}^{(i\cdots N)}\right) \equiv \left|\boldsymbol{k}^{(1)},\ldots,\boldsymbol{k}^{(N)}\right) := \exp\left[i\sum_{n=1}^{N}\boldsymbol{k}^{(n)}\cdot\hat{\boldsymbol{x}}^{(n)}\right], \tag{4.5.5}$$

with eigenvalues

$$\hat{H}^{\mathrm{tot}}\left|\boldsymbol{k}^{(i\cdots N)}\right) = \left[\frac{2\hbar^2}{m\lambda^2}\sum_{n=1}^{N}\sin^2\left(\frac{k^{(n)}\lambda}{2}\right)\right]\left|\boldsymbol{k}^{(i\cdots N)}\right); \tag{4.5.6}$$

this is a simple extension of the single particle plane waves, as per section 3.1. For one of these plane wave solutions, we may define the *total momentum*,

$$\boldsymbol{k}^{\mathrm{tot}} := \sum_{n=1}^{N}\boldsymbol{k}^{(n)},$$

as well as the *relative momenta*,

$$\boldsymbol{q}^{(n)} := \boldsymbol{k}^{(n)} - \frac{1}{N}\boldsymbol{k}^{\mathrm{tot}},$$

noting, as with relative coordinates, the vanishing sum

$$\sum_{n=1}^{N}\boldsymbol{q}^{(n)} = \boldsymbol{0}. \tag{4.5.7}$$

Rewriting the N-particle plane wave in terms of total and relative momenta yields

$$\begin{aligned}
\left|\boldsymbol{k}^{(i\cdots N)}\right) &= \exp\left[i\sum_{n=1}^{N}\left(\frac{1}{N}\boldsymbol{k}^{\mathrm{tot}}+\boldsymbol{q}^{(n)}\right)\cdot\hat{\boldsymbol{x}}^{(n)}\right] \\
&= \exp\left[i\boldsymbol{k}^{\mathrm{tot}}\cdot\hat{\boldsymbol{x}}^{(\mathrm{CM})} + i\sum_{n=1}^{N}\boldsymbol{q}^{(n)}\cdot\hat{\boldsymbol{x}}^{(n)}\right].
\end{aligned}$$

4.5.2 Centre-of-mass dynamics

Given the above extensions of our definitions to the many-particle case, we wish to consider now the collective dynamics of our particles. We should keep in mind that, in general, our system Hamiltonian should now contain terms accounting for interactions between the particles, and so is no-longer the simple free-particle Hamiltonian of (4.5.4). The eigenstates of (4.5.5) are therefore not the whole picture as far as the states involved in our interference setup goes.

At this stage, the typical next step (as followed in [32], for instance) would be to write the Hamiltonian (that including interactions) in terms of centre-of-mass and relative coordinates. Assuming translational invariance — *i.e.* assuming that the interactions depend only on the relative coordinates — we would then be able to decouple the centre-of-mass motion from the relative motion, leaving free-particle centre-of-mass dynamics with all of the internal dynamics captured by the evolution of the relative coordinates.

In our context, the procedure is more involved for two reasons. The first is the more complicated form of our Laplacian. Had we been able to formulate momentum observables, $\hat{\boldsymbol{P}}$, we would expect the Laplacian of a single particle to have taken the usual form, $\hat{\boldsymbol{P}}^2/2m$. In such a setting, upon extending to many particles, the centre-of-mass dynamics would simply have the kinetic term $(\hat{\boldsymbol{P}}^{(\mathrm{tot})})^2/2M$, an obvious generalisation of the single-particle kinetic term. This is the situation in [32]. In contrast, as a result of the pervasive reliance on spherical coordinates throughout the development of our formalism, we are unable to easily construct momentum operators. As such, our Laplacian, (2.1.24), is not formulated in terms of any more elementary observables, and it is unclear how the "total" Laplacian should look. The second complication in our setting comes from the fact our centre-of-mass and relative coordinates do not commute. This ultimately renders a clean decoupling of centre-of-mass and internal dynamics in the Hamiltonian impossible.

In spite of these complications, it is nevertheless still possible to isolate the centre-of-mass dynamics. For one, the centre-of-mass dynamics will still be governed, as usual, by the free-particle contribution to the total Hamiltonian, namely (4.5.4). Furthermore, in the case of non-interacting particles, we would expect the energy to comprise two contributions, namely the centre-of-mass energy and the energy of the relative (internal) motion. Let us therefore consider a plane-wave solution of the form (4.5.5), and momentarily suppose that $\boldsymbol{q}^{(n)} = \boldsymbol{0}$ for all $n \in \{1, 2, \ldots, N\}$. Under such an assumption, we expect the latter contribution to the energy to vanish, which enables us to isolate the centre-of-mass dynamics. With vanishing relative motion, the plane wave eigenstates are especially simple,

$$\left|\boldsymbol{k}^{(i\cdots N)}\right) = \exp\left[i\boldsymbol{k}^{\mathrm{tot}} \cdot \hat{\boldsymbol{x}}^{(\mathrm{CM})}\right], \tag{4.5.8}$$

as are the corresponding energy eigenvalues (4.5.6),

$$\begin{aligned} \hat{H}^{\mathrm{tot}} \left|\boldsymbol{k}^{(i\cdots N)}\right) &= \frac{2N\hbar^2}{m\lambda^2} \sin^2\left(\frac{k^{\mathrm{tot}}\lambda}{2N}\right) \left|\boldsymbol{k}^{(i\cdots N)}\right) \\ &= \frac{2\hbar^2}{M\tilde{\lambda}^2} \sin^2\left(\frac{k^{\mathrm{tot}}\tilde{\lambda}}{2}\right) \left|\boldsymbol{k}^{(i\cdots N)}\right). \end{aligned} \tag{4.5.9}$$

Without relative motion, we can even simplify the form of $\hat{H}^{\mathrm{tot}}$. To see this, first define the total boson number operator in the obvious way,

$$\hat{n}^{\mathrm{tot}} := \sum_{n=1}^{N} \hat{n}^{(n)},$$

then split the Hamiltonian as $\hat{H}^{\mathrm{tot}} \equiv \hat{H}_0 + \hat{H}_1$, where the action of each term on a state $\psi \in \mathcal{H}_{\mathrm{q}}^{\mathrm{tot}}$ (we temporarily suppress ket notation for simplicity) is defined by

$$\begin{aligned}\hat{H}^{\mathrm{tot}}\,\psi &= \frac{\hbar^2}{2m\lambda^2}\sum_{n=1}^{N}\frac{1}{\hat{n}^{(n)}+1}[a_\alpha^{(n)\dagger},[a_\alpha^{(n)},\psi]] \\ &= \underbrace{\frac{\hbar^2}{2M\tilde{\lambda}^2}\frac{1}{\hat{n}^{\mathrm{tot}}+N}\sum_{n=1}^{N}[a_\alpha^{(n)\dagger},[a_\alpha^{(n)},\psi]]}_{\hat{H}_0\,\psi} \\ &\quad + \underbrace{\frac{\hbar^2}{2m\lambda^2}\sum_{n=1}^{N}\left(\frac{1}{\hat{n}^{(n)}+1}-\frac{N}{\hat{n}^{\mathrm{tot}}+N}\right)[a_\alpha^{(n)\dagger},[a_\alpha^{(n)},\psi]]}_{\hat{H}_1\,\psi}.\end{aligned} \tag{4.5.10}$$

In doing so, we notice that it is only the first term, $\hat{H}_0$, which contributes to the energy eigenvalue associated with the plane wave $\psi_{\mathrm{CM}} \equiv \left|\boldsymbol{k}^{(i\cdots N)}\right)$. Indeed, we find that

$$\left[a_\alpha^{(n)\dagger},\left[a_\alpha^{(n)},\psi_{\mathrm{CM}}\right]\right] = \frac{4\hat{r}^{(n)}}{\lambda}\sin^2\left(\frac{k^{\mathrm{tot}}\lambda}{2N}\right)\psi_{\mathrm{CM}},$$

using the same argument as in the derivation of (3.1.6) presented in section 3.1, only with the replacement $\boldsymbol{k} \to \boldsymbol{k}^{\mathrm{tot}}/N$ and the relevant (n) superscripts. Then the full action of $\hat{H}_0$ on ψ_{CM} readily follows as

$$\begin{aligned}\hat{H}_0\left|\boldsymbol{k}^{\mathrm{tot}}\right) &= \frac{\hbar^2}{2M\tilde{\lambda}^2}\frac{1}{\hat{n}^{\mathrm{tot}}+N}\left[\sum_{n=1}^{N}4(\hat{n}^{(n)}+1)\right]\sin^2\left(\frac{k^{\mathrm{tot}}\lambda}{2N}\right)\left|\boldsymbol{k}^{\mathrm{tot}}\right) \\ &= \frac{2\hbar^2}{M\tilde{\lambda}^2}\sin^2\left(\frac{k^{\mathrm{tot}}\tilde{\lambda}}{2}\right)\left|\boldsymbol{k}^{\mathrm{tot}}\right),\end{aligned}$$

which indeed accounts for the full energy, as per (4.5.9). Consequently,

$$\hat{H}_1\left|\boldsymbol{k}^{\mathrm{tot}}\right) = 0,$$

meaning that, for plane wave solutions without relative motion, the free Hamiltonian, $\hat{H}^{\mathrm{tot}}$, reduces to just the first term, $\hat{H}_0$. The conclusion we draw from this analysis is that $\hat{H}_0$ comprises the part of $\hat{H}^{\mathrm{tot}}$ responsible for centre-of-mass dynamics, whereas $\hat{H}_1$ constitutes the part responsible for internal dynamics, together with any coupling between internal- and centre-of-mass dynamics.

For the more general case where the $\boldsymbol{q}^{(n)}$ are allowed to be non-zero, the energy acquires additional contributions. Specifically, there is a quadratic (in $\boldsymbol{q}^{(n)}$) contribution arising from the internal motion, as well as higher-order (in λ) corrections that reflect the coupling between the centre-of-mass and internal dynamics. We can verify this directly by expanding the right-hand-side of (4.5.6) in the $\boldsymbol{q}^{(n)}$,

$$\begin{aligned}\hat{H}^{\mathrm{tot}}\left|\boldsymbol{k}^{(i\cdots N)}\right) &= \left[\frac{2\hbar^2}{m\lambda^2}\sum_{n=1}^{N}\sum_{l=0}^{\infty}\frac{(-1)^l}{(2l+1)!}\left(\frac{(\boldsymbol{q}^{(n)}+\frac{1}{N}\boldsymbol{k}^{\mathrm{tot}})^2\lambda^2}{4}\right)^{2l+1}\right]\left|\boldsymbol{k}^{(i\cdots N)}\right) \\ &= \left[\frac{\hbar^2}{2m}\sum_{n=1}^{N}\left((\boldsymbol{q}^{(n)})^2+\frac{2}{N}\boldsymbol{q}^{(n)}\cdot\boldsymbol{k}^{\mathrm{tot}}+\frac{1}{N^2}(\boldsymbol{k}^{\mathrm{tot}})^2\right)+\mathcal{O}(\lambda^4)\right]\left|\boldsymbol{k}^{(i\cdots N)}\right),\end{aligned}$$

where the middle term vanishes due to (4.5.7).

For the even more general case where we introduce interactions depending only on the relative coordinates, the Hamiltonian can still be split as in (4.5.10), only now with the interactions being included in $\hat{H}_1$. In this case, the interactions will also contribute to the internal energy as a binding energy, as well as to the coupling between the centre-of-mass and internal dynamics. However this coupling is once again of higher-order in λ (since the internal and centre-of-mass dynamics decouple in the commutative limit, any coupling must be at least $\mathcal{O}(\lambda)$), so that we can decouple the centre-of-mass and internal dynamics to the lowest order in λ and include higher-order effects perturbatively. Finally, we remark that the strength of the coupling between internal and centre-of-mass coordinates will in general scale with the magnitudes of the $\boldsymbol{q}^{(n)}$, which in turn are controlled by the temperature, T, of the particle collection. This is because the internal energy is (to leading order in λ) quadratic in the $\boldsymbol{q}^{(n)}$, meaning we can apply the equipartition theorem, which states that

$$\frac{1}{2}k_B T \sim \frac{\hbar^2(\boldsymbol{q}^{(n)})^2}{2m}.$$

The upshot is that we can expect the effect of the coupling to be less significant at low temperatures.

4.5.3 Many-particle classical limit

The crucial takeaway from the previous subsection is that, comparing the eigenstates and energy eigenvalues of $\hat{H}^{\text{tot}}$ ((4.5.8) and (4.5.9)) with those of the single particle free Hamiltonian ((3.1.1) and (3.1.6)), it is clear that we can treat the centre-of-mass dynamics like those of a single particle with mass M, momentum $\boldsymbol{k}^{\text{tot}}$, and non-commutative parameter $\tilde{\lambda}$. With this in mind, we can revisit the classicality condition of (4.4.1), which for a collection of particles now requires

$$r \ll \frac{4\tilde{\lambda}\, d^2 M E_{\text{tot}}}{\hbar^2} = \frac{4\lambda d^2 m E_{\text{tot}}}{\hbar^2}. \tag{4.5.11}$$

Now the energy is extensive, since, by (4.5.9), we have that

$$\begin{aligned} E_{\text{tot}} &= N \cdot \frac{2\hbar^2}{m\lambda^2} \sin^2\left(\frac{k^{\text{tot}}/N\,\lambda}{2}\right) \\ &= N \cdot \frac{2\hbar^2}{m\lambda^2} \sin^2\left(\frac{\langle k\rangle\,\lambda}{2}\right) \\ &= N\langle E\rangle, \end{aligned}$$

where we have defined the average momentum and energy,

$$\langle k\rangle := \frac{1}{N}k^{\text{tot}}, \quad \text{and} \quad \langle E\rangle := \frac{2\hbar^2}{m\lambda^2}\sin^2\left(\frac{\langle k\rangle\,\lambda}{2}\right).$$

Finally, we can repeat the back-of-the-envelope estimate that we performed in section 4.4.2 with the new condition of (4.5.11). We again take λ to be of the order of a Planck length, d to be on the order of 1cm, and consider a collection of electrons with average energy 1eV. Supposing we have a number of electrons on the order of Avogadro's number, we can expect to see interference suppression at distances on the order of

$$\begin{aligned} r &\lesssim \frac{(10^{-35}\,\text{m})(10^{-2}\,\text{m})^2(10^{-31}\,\text{kg})(10^{23})(10^{-19}\,\text{kg}\,\text{m}^2\,\text{s}^{-2})}{(10^{-34}\,\text{kg}\,\text{m}^2\,\text{s}^{-1})^2} \\ &= 100\,\text{m}. \end{aligned}$$

This is much more realistically detectable within a laboratory. Conversely, to observe suppression at distances of the order of a meter for this number of particles requires an average energy orders of magnitude less than an electron volt, making the interference suppression entirely observable at non-relativistic energies. This represents a significant improvement over the situation in the Moyal plane, where, although a quantum-to-classical transition exists, it is only observed for particles travelling at speeds well above the speed of light, even when collections of particles are considered [32].

4.6 Prospects for experimental realisation

At this stage, we have established the plausibility of observing an isolated double-pinhole setup undergoing a classical transition at realistic length scales and energies. In particular, when we compare the discussions of sections 4.4.2 and 4.5.3, it is clear that the key ingredient for the observability of this transition, at least in the context of our double-pinhole setup, is a large number of particles. This poses a challenge when it comes to actually realising our hypothetical setup in a real laboratory, namely that one needs a means of reliably manipulating a quantum state comprised of a large number of particles. In this final section, we briefly connect our findings with existing (or feasible) experiments to evaluate the plausibility of probing the quantum suppression effect in practice.

One promising possible experiment derives from work by van Es *et al.* [49] which describes a beam-splitter setup able to dynamically split a propagating Bose-Einstein condensate (BEC) into two parts, each guided along a separate path. Repeating the beam-splitter operation, after allowing each beam to propagate some distance, yields a Mach-Zehnder interferometer. This achieves the same effect as the double-pinhole setup, where the path-length difference between each pinhole and a given measurement point is easily mimicked by adjusting the phase of the interferometer.

An issue with this proposal is that van Es *et al.* only achieve the beam-splitting operation for 3×10^4 non-interacting ^{87}Rb atoms, a far-cry from the Avogadro's number assumed for our estimates. If we repeat the estimate accounting for the smaller number of heavier particles, we get the condition $r \lesssim 10^{-11}\,\mathrm{m}$ for observable suppression. Of course, this is unreasonably small, but it is possible that the energies involved could be higher, or the non-commutative parameter larger, than we assume. We therefore conclude that an experiment of this nature, only with a slightly larger BEC sample, could conceivably probe the suppression we describe. Larger samples of BEC (with as many as 1.1×10^9 H atoms [19]) have at least successfully been prepared in the past [44, 48].

Other experimental prospects may include placing an optomechanical system into superposition, similar to the setup described by Kleckner *et al.* [26], or controlling and interfering a levitated nanosphere [15, 46, 29]. These experiments all go some way towards addressing the central difficulty with our setup, which lies in creating and manipulating a relatively massive quantum superposition.

However, such experiments all share a significant limitation, meaning we ought to exercise caution in comparing their results directly with our predictions. The issue is that real-world experiments also introduce a true environment with which the particles in the setup may interact. Such an environment would most likely lead to higher levels of decoherence and interference suppression than our theory predicts, since our predicted suppression applies to an ideally isolated system. Moreover, it is hard to imagine how one might distinguish between the two sources of decoherence in such an experiment. Still, with more control

over the environment, these types of experiments may in the future offer a way of probing this phenomenon.

Chapter 5

Summary and Conclusion

Our investigation started off premised on the idea that the non-commutative nature of space may play a role in understanding the measurement problem — more specifically, *macroscopic objectivity*, the emergence of classical behaviour in systems of sufficient scale (*i.e.* energy or number of constituent particles). We were motivated by a recent investigation which suggested that, at least in the two-dimensional Moyal plane formalism of NCQM, the non-commutative geometry itself may be responsible for giving rise to such a transition [32].

We discussed various reasons for which we feel it is worthwhile to investigate whether a similar process takes place in a higher-dimensional formalism for NCQM. As such, inspired by the approach of [32], our investigation focused on treating a two-pinhole interference setup in the three-dimensional fuzzy sphere formalism of NCQM, both for individual particles and collections of particles. In the end, we do indeed find that this combination of system and formalism exhibits another compelling example of an intrinsic quantum-to-classical transition. As in the Moyal plane, the transition we find is continuous as a function of system parameters (such as energy and number of particles), and able to take place even for a completely isolated system — that is, without the need for requiring any additional external environment such as a heat bath.

Our findings are important for several reasons. Firstly, taken in combination with [32], they reinforce the notion that it really is the small-scale structure of space which is responsible for the suppression of quantum behaviour at a macroscopic scale. Secondly, they address some key issues with the situation in the Moyal plane — most notably, they show that in three dimensional fuzzy space, unlike in the 2D Moyal plane, the quantum-to-classical transition is actually capable of being observed for realistic numbers of particles travelling at non-relativistic speeds. Thirdly, they uncover an additional system parameter which is also involved in controlling the strength of the quantum suppression in three dimensions, namely the distance away from a system at which a measurement is performed — that is to say, we find that systems appear more classical when viewed at appropriate length scales. The latter is an important testable prediction of our theory. Altogether, the results are promising and wholly support the proposed link between the microscopic structure of space and macroscopic emergence of classicality.

Of course, the model examined in this thesis is ultimately still a special case. Further research is needed to fully understand the consequences of our result and its potential implications for an understanding of the most general formulation of the measurement

problem. A starting point might be treating a general von Neumann measurement setup within the fuzzy-space formalism, similar to the treatment in the Moyal plane performed by [32]. Another direction for future research is in connecting our predictions with experimental results; we proposed some experimental setups that could form a basis for such an investigation. However, a fundamental difficulty with directly testing our theory involves isolating the system under investigation from its environment — since our predictions pertain to a perfectly-isolated system, any suitable experiment must somehow remove or account for additional decoherence effects arising from a laboratory environment.

In summary, we found that, at least in the setting of our toy model, non-commutativity of space does indeed lead to a suppression of quantum effects at realistic energy and length scales. This is a promising finding, and a incentive for future investigations to extend, generalise, or test our findings.

Appendix A

Transformation Laws of Coherent States

Several of our calculations rely on a closed form for the transformation of a Glauber coherent state $|\boldsymbol{z}\rangle$ (defined in section 2.2.1) under the action of a plane wave. In this short appendix, we derive the relevant transformation law.

As noted in section 3.1, the plane waves represent SU(2) group elements (and all SU(2) group elements are represented by the plane waves). Recall that a general $g \in \mathrm{SU}(2)$ can be written in the form

$$g \equiv g(\boldsymbol{q}) = \exp\left[\frac{i}{2}\boldsymbol{q}\cdot\boldsymbol{\sigma}\right], \tag{A.0.1}$$

for some dimensionless vector $\boldsymbol{q}$ with norm $q \in [0, 2\pi]$ and direction $\hat{\boldsymbol{q}}$. As already mentioned in section 3.1, this is because SU(2) is connected and compact, implying that the exponential map $\exp\colon \mathfrak{su}(2) \to \mathrm{SU}(2)$ is surjective. We can express (A.0.1) alternatively by Taylor expanding the relevant exponential, and using the fact that $(\hat{\boldsymbol{q}}\cdot\boldsymbol{\sigma})^2 = I$ for any unit vector $\hat{\boldsymbol{q}}$. This gives

$$g(\boldsymbol{q}) = \cos(q/2) + i\sin(q/2)\,\hat{\boldsymbol{q}}\cdot\boldsymbol{\sigma}, \tag{A.0.2}$$

Now, thanks to the Lie algebra isomorphism $\hat{x}_i \mapsto \lambda\sigma^i$, we can represent g as an operator on $\mathcal{H}_\mathrm{c}$ by

$$\hat{\Pi}(g) = \exp\left[i\boldsymbol{q}\cdot\frac{\hat{\boldsymbol{x}}}{2\lambda}\right],$$

which formally resembles a plane wave with wavenumber $\boldsymbol{q}$ (see (3.1.1)), only $\boldsymbol{q}$ is dimensionless, and so does not represent a true wavenumber. To completely write $\hat{\Pi}(g)$ in the form of a plane wave, we could introduce dimensions by replacing $\boldsymbol{q} \equiv 2\lambda\,\boldsymbol{k}$, where $\boldsymbol{k}$ is a true dimensionful wavenumber.

Note that, since $\hat{\Pi}(g)$ commutes with $\hat{r}^2$ (as each $\hat{x}_i$ does), it preserves the $\hat{r}^2$-eigenspaces (*i.e.* those with fixed j, as defined in (2.1.17)). In particular, plane waves preserve the vacuum state,

$$\hat{\Pi}(g)\,|0\rangle = |0\rangle\,,$$

and in the $j = 1/2$ irrep they act simply as ordinary SU(2) matrices,

$$\hat{\Pi}(g)\,|j = 1/2, m\rangle = g\begin{bmatrix}|j = 1/2, m = +1/2\rangle \\ |j = 1/2, m = -1/2\rangle\end{bmatrix}; \tag{A.0.3}$$

This is merely a statement of the $j = 1/2$ Wigner D-function entries (see section 4.3.4 in [1], for instance).

Now consider the action of a plane wave on a coherent state. The following computation closely mirrors that of (3.1.4) and the subsequent lines, so we likewise define $\hat{J}_i \equiv \frac{1}{2\lambda}\hat{x}_i$ in this context. Then

$$\begin{aligned}\hat{\Pi}(g)\,|\boldsymbol{z}\rangle &= e^{-\frac{1}{2}\bar{z}_\alpha z_\alpha}\,\hat{\Pi}(g)\,e^{z_\alpha a_\alpha^\dagger}\,|0\rangle \\ &= e^{-\frac{1}{2}\bar{z}_\alpha z_\alpha}\,\hat{\Pi}(g)\,e^{z_\alpha a_\alpha^\dagger}\,\hat{\Pi}(g)^\dagger\,|0\rangle \\ &= e^{-\frac{1}{2}\bar{z}_\alpha z_\alpha}\,\exp\Big[z_\alpha\left(\hat{\Pi}(g)\,a_\alpha^\dagger\,\hat{\Pi}(g)^\dagger\right)\Big]\,|0\rangle\,,\end{aligned}$$

so the problem reduces to deriving the transformation law for the boson creation operators $a_\alpha^\dagger$ under the conjugation $e^{i\boldsymbol{q}\cdot\hat{\boldsymbol{J}}}a_\alpha^\dagger e^{-i\boldsymbol{q}\cdot\hat{\boldsymbol{J}}}$. But it can be easily shown that these boson creation operators transform like rank-1/2 *spherical tensor operators* with respect to the $\hat{J}_i$. This just amounts to checking (see section 5.2.3 in [1], for instance), the set of commutation relations

$$\begin{aligned}[\hat{J}_3, a_\alpha^\dagger] &= \left(\frac{3}{2} - \alpha\right) a_\alpha^\dagger, \\ [\hat{J}_+, a_\alpha^\dagger] &= \delta_{\alpha 2}\, a_1^\dagger, \\ [\hat{J}_-, a_\alpha^\dagger] &= \delta_{\alpha 1}\, a_2^\dagger,\end{aligned} \tag{A.0.4}$$

where $\hat{J}_\pm \coloneqq \hat{J}_1 \pm i\hat{J}_2$, as usual. These commutators are entirely trivial (but tedious) to check, since we may use (2.1.6) to write each $\hat{J}_i$ entirely in terms of creation and annihilation operators. The implication is that the creation operators transform under conjugation with $\hat{\Pi}(g)$ by the $j = 1/2$ Wigner D-matrices (see section 5.2 of [1], for instance),

$$e^{i\boldsymbol{q}\cdot\hat{\boldsymbol{J}}}a_\alpha^\dagger e^{-i\boldsymbol{q}\cdot\hat{\boldsymbol{J}}} = g_{\beta\alpha}a_\beta^\dagger.$$

As such, we can finally write

$$\begin{aligned}\hat{\Pi}(g)\,|\boldsymbol{z}\rangle &= e^{-\frac{1}{2}\boldsymbol{z}^\dagger\boldsymbol{z}}\,\exp\Big[z_\alpha\left(e^{i\boldsymbol{q}\cdot\hat{\boldsymbol{J}}}a_\alpha^\dagger e^{-i\boldsymbol{q}\cdot\hat{\boldsymbol{J}}}\right)\Big]\,|0\rangle\,, \\ &= e^{-\frac{1}{2}(g\boldsymbol{z})^\dagger(g\boldsymbol{z})}\,e^{z_\alpha g_{\beta\alpha}a_\beta^\dagger}\,|0\rangle\,, \\ &= e^{-\frac{1}{2}(g\boldsymbol{z})^\dagger(g\boldsymbol{z})}\,e^{a_\beta^\dagger(g\boldsymbol{z})_\beta}\,|0\rangle\,, \\ &= |g\boldsymbol{z}\rangle\,,\end{aligned} \tag{A.0.5}$$

which is a remarkably simple transformation law, reminiscent of (3.1.4) itself. In summary, in terms of the dimensionful wavenumber $\boldsymbol{k}$ introduced above, the action of a general plane wave on a coherent state is given by

$$\begin{aligned}e^{i\boldsymbol{k}\cdot\hat{\boldsymbol{x}}}\,|\boldsymbol{z}\rangle &= |g(\boldsymbol{k})\,\boldsymbol{z}\rangle\,, \quad \text{where} \\ g(\boldsymbol{k}) &\coloneqq e^{i\lambda\boldsymbol{k}\cdot\boldsymbol{\sigma}} = \cos(\lambda k) + i\sin(\lambda k)\hat{\boldsymbol{k}}\cdot\boldsymbol{\sigma}.\end{aligned} \tag{A.0.6}$$

Appendix B

Matrix Elements with Coherent States

In this appendix we develop the necessary theory to compute the matrix element of a general function $g(\hat{n})$ of the boson number operator with respect to a set of coherent states. The key step involves introducing new creation operators, then expanding the coherent states in the Fock number basis of these new operators; this step is presented in [37]. The original work in this appendix comes from the special cases we consider — in particular, we derive a more compact form for the general case where g is a polynomial, and, more notably, we consider the case where g is the (non-commutative) spherical Hankel function $g_{H,l}$. The latter is relevant to the discussion in section 3.2.2, as well as the main calculation of chapter 4.

B.1 General functions $g(\hat{n})$

Consider a function $g(\hat{n})$ of the number operator $\hat{n} = a^\dagger_\alpha a_\alpha$. We wish to compute the matrix element $\langle \boldsymbol{z}^1 | g(\hat{n}) | \boldsymbol{z}^2 \rangle$, where the $|\boldsymbol{z}^i\rangle$ are (possibly distinct) coherent states, possibly different. As in [37], we start by introducing new creation operators,

$$A_i^\dagger := \frac{1}{\sqrt{R_i}} z^i_\alpha a^\dagger_\alpha, \quad \text{where} \quad R_i = \bar{z}^i_\alpha z^i_\alpha. \tag{B.1.1}$$

This allows us to write the coherent states in terms of displacement operators involving the new creation operators and acting on the vacuum state,

$$|\boldsymbol{z}^i\rangle = \hat{D}_i |0\rangle \equiv e^{-R_i/2 + \sqrt{R_i} A_i^\dagger} |0\rangle .$$

Now to compute the desired matrix element, we need only expand the exponential in each displacement operator, which lets us write each coherent state in the basis of Fock states (those corresponding to the new creation operators) as

$$|\boldsymbol{z}^i\rangle = e^{-R_i/2} \sum_{n=0}^{\infty} \frac{R_i^{n/2}}{\sqrt{n!}} |n\rangle_i , \tag{B.1.2}$$

where the subscript on the ket indicates the boson mode (*i.e.* distinguishes between application of each of the two $A_i^\dagger$).

We can now substitute this expansion into the desired matrix element, which gives

$$\begin{aligned}\langle \boldsymbol{z}^1 | g(\hat{n}) | \boldsymbol{z}^2 \rangle &= e^{-(R_1+R_2)/2} \sum_{n,m} \frac{R_1^{n/2} R_2^{m/2}}{\sqrt{n!m!}} {}_1\langle n | g(\hat{n}) | m \rangle_2 \\ &= e^{-(R_1+R_2)/2} \sum_{n,m} \frac{R_1^{n/2} R_2^{m/2}}{\sqrt{n!m!}} g(m) \, {}_1\langle n | m \rangle_2\end{aligned} \tag{B.1.3}$$

Now clearly ${}_1\langle n|m\rangle_2 = 0$ whenever $n \neq m$, since each $|n\rangle_i$ can be written (by binomial expansion on $(A_i^\dagger)^n$) as a linear combination of two-boson-mode number states of the form $|l_1, l_2\rangle$, where $l_1 + l_2 = n$ — to wit, $|n\rangle_i$ indeed contains n total particles. However, we must be careful to evaluate ${}_1\langle n|n\rangle_2$, since there is a non-trivial commutator,

$$\begin{aligned}\left[A_1, A_2^\dagger\right] &= \frac{1}{\sqrt{R_1 R_2}} \bar{z}_\alpha^1 z_\beta^2 \left[a_\alpha, a_\beta^\dagger\right] \\ &= \frac{1}{\sqrt{R_1 R_2}} \bar{z}_\alpha^1 z_\alpha^2.\end{aligned} \tag{B.1.4}$$

This leads directly to a non-trivial Fock state overlap, since

$$\begin{aligned}{}_1\langle n|n\rangle_2 &= \frac{1}{n!} \langle 0 | (A_1)^n (A_2^\dagger)^n | 0 \rangle \\ &= \frac{1}{n!} \langle 0 | (A_1)^{n-1} \left(\left[A_1, (A_2^\dagger)^n\right] + \cancel{(A_2^\dagger)^n A_1} \right) | 0 \rangle \\ &= \frac{n}{n!} \left[A_1, A_2^\dagger\right] \langle 0 | (A_1)^{n-1} (A_2^\dagger)^{n-1} | 0 \rangle \\ &= \frac{n(n-1)}{n!} \left[A_1, A_2^\dagger\right]^2 \langle 0 | (A_1)^{n-2} (A_2^\dagger)^{n-2} | 0 \rangle \\ &= \dots \\ &= \left[A_1, A_2^\dagger\right]^n.\end{aligned}$$

Here we have repeatedly used the fact that it follows from $[\hat{J}, \hat{K}] = c\hat{I}$ that $[\hat{J}, \hat{K}^n] = cn\hat{K}^{n-1}$ (which is easily proven by induction using the Leibniz rule).

With these expressions, (B.1.3) simplifies to

$$\begin{aligned}\langle \boldsymbol{z}^1 | g(\hat{n}) | \boldsymbol{z}^2 \rangle &= e^{-(R_1+R_2)/2} \sum_{n,m} \frac{R_1^{n/2} R_2^{m/2}}{\sqrt{n!m!}} g(m) \left[A_1, A_2^\dagger\right]^n \delta_{n,m} \\ &= e^{-(R_1+R_2)/2} \sum_n g(n) \frac{\left(\bar{z}_\alpha^1 z_\alpha^2\right)^n}{n!}.\end{aligned} \tag{B.1.5}$$

Deriving a closed form for the sum of this series is often straightforward using the umbral calculus [35]. That said, this little-known calculus is thankfully seldom needed; indeed, we proceed to explicitly compute the sum for polynomial functions g without reference to umbral calculus.

B.2 Polynomials $g(\hat{n})$

In the case where g is a polynomial, deriving a closed form for the sum of the series in (B.1.5) is a straightforward exercise. To avoid unnecessarily complicating the notation (and recognising that both sides of (B.1.5) are linear in g), suppose without loss of generality

that $g(n) = n^k$. For convenience, also define $K \coloneqq \bar{z}^1_\alpha z^2_\alpha$. Then we may rewrite $g(n)$ using the well-known relationship [35]

$$g(n) = n^k = \sum_{m=0}^{k} \left\{ {k \atop m} \right\} n^{\underline{m}},$$

where $n^{\underline{m}}$ denotes the falling factorial,

$$n^{\underline{m}} \coloneqq \prod_{k=0}^{m-1} (x-k),$$

and $\left\{ {k \atop m} \right\}$ are the Stirling numbers of the second kind. Then the sum in (B.1.5) becomes

$$\begin{aligned}
\sum_{n=0}^{\infty} g(n) \frac{K^n}{n!} &= \sum_{m=0}^{k} \left\{ {k \atop m} \right\} \sum_{n=0}^{\infty} n^{\underline{m}} \frac{K^n}{n!} \\
&= \sum_{m=0}^{k} \left\{ {k \atop m} \right\} \sum_{n=m}^{\infty} n^{\underline{m}} \frac{K^n}{n!} \\
&= \sum_{m=0}^{k} \left\{ {k \atop m} \right\} \sum_{n=0}^{\infty} (n+m)^{\underline{m}} \frac{K^{n+m}}{(n+m)!} \\
&= \sum_{m=0}^{k} \left\{ {k \atop m} \right\} K^m \cdot \sum_{n=0}^{\infty} \frac{K^n}{n!}.
\end{aligned}$$

The second line is justified by the observation that the first m terms of the n-sum are identically zero, since $n^{\underline{m}} = 0$ for all $n \in \{0, 1, \ldots, m-1\}$, so we can take the lower bound of the sum as $n = m$. Then in the third line, we shift this bound back down to start at zero. We are left with the product of two well-known power series, namely that of the exponential map,

$$e^x = \sum_{n=0}^{\infty} \frac{x^n}{n!},$$

and that of the Touchard polynomial (or sometimes Bell polynomial),

$$T_k(x) = \sum_{m=0}^{k} \left\{ {k \atop m} \right\} x^m.$$

The latter also has a closed form (unsurprisingly, that of a polynomial) which is easily looked up, say in the OEIS [42]. We tabulate the first few Touchard polynomials in table B.1 for convenience in our calculations.

$\boldsymbol{k}$	$\boldsymbol{T_k(x)}$
0	1
1	x
2	$x^2 + x$
3	$x^3 + 3x^2 + x$
4	$x^4 + 6x^3 + 7x^2 + x$

Table B.1: Touchard polynomials $T_k(x)$ up to $k = 4$

In summary, we have the special case of (B.1.5),

$$\left\langle \boldsymbol{z}^1 \middle| \hat{n}^k \middle| \boldsymbol{z}^2 \right\rangle = e^{-(R_1+R_2)/2+K} T_k(K), \tag{B.2.1}$$

for $R_i = \bar{z}^i_\alpha z^i_\alpha$ and $K = \bar{z}^1_\alpha z^2_\alpha$. This of course recovers the usual overlap of coherent states, as per (2.2.3), in the case $k = 0$.

B.3 Spherical Hankel function $g(\hat{n}) = g_{H,l}(\hat{n}, k)$

In this subsection, we consider one more special case — we compute the (leading-order behaviour of the) matrix element of the (asymptotically-expanded) non-commutative spherical Hankel function (see (3.2.7)),

$$g(\hat{n}) \equiv g_{H,l}(\hat{n}, k) = \frac{e^{i(\hat{n}+l+1)\kappa}}{(i\hat{n})^{l+1}},$$

with respect to an identical pair of coherent states, $|\boldsymbol{z}^1\rangle = |\boldsymbol{z}^2\rangle \equiv |\boldsymbol{z}\rangle$. This particular case, while highly specific, is of great importance to the discussion in section 3.2 and the subsequent calculation in chapter 4, so it warrants discussion.

Now, we can of course apply the result of section B.1 in the present context, but some care is needed — the coherent state $|\boldsymbol{z}\rangle$ is a superposition of all boson number states, including the vacuum state, so the singular $1/\hat{n}$ causes divergence in a naïve calculation. This is not really a problem: not only is the overlap $|\langle 0|\boldsymbol{z}\rangle|^2 = e^{-R/2}$ vanishingly small for $R \equiv \bar{z}_\alpha z_\alpha \gg 1$ (which is assumed for the asymptotic form of $g_{H,l}$ as given above), but we can entirely remove the divergence by defining g piecewise as the regular solution $g_{J,l}$ within some region around the origin and the irregular solution $g_{H,l}$ outside of this region (see section 3.2.2 for a detailed discussion of the solutions in question). Equivalently, we may as well use only the irregular form, but exclude the point $n = 0$ from our computations. As such, we invoke (B.1.5), but begin the sum at $n = 1$, whereby

$$\begin{aligned} H_{l,\kappa}(R) &\equiv \langle \boldsymbol{z}| \frac{e^{i(\hat{n}+l+1)\kappa}}{(i\hat{n})^{l+1}} |\boldsymbol{z}\rangle \\ &= e^{-R} \sum_{n=1}^{\infty} \frac{e^{i(n+l+1)\kappa}}{n!\,(in)^{l+1}} R^n \\ &= \frac{e^{i(l+1)\kappa}}{i^{l+1}} e^{-R} (e^{i\kappa} R) \sum_{n=0}^{\infty} \frac{(e^{i\kappa} R)^n}{(n+1)!\,(n+1)^{l+1}}, \end{aligned}$$

using the shorthand notation $H_{l,\kappa}(R)$ for the desired matrix element. Now the remaining sum can be written as a generalised hypergeometric function,

$${}_pF_q \left[\begin{matrix} a_1, a_2, \cdots a_p \\ b_1, b_2, \cdots b_q \end{matrix}; e^{i\kappa} R \right].$$

Indeed, if β_n denotes the nth coefficient,

$$\beta_n := \frac{1}{(n+1)!(n+1)^{l+1}},$$

then we have $\beta_0 = 1$ (as required by convention of the coefficients in the series of a hypergeometric function), and the ratio

$$\frac{\beta_{n+1}}{\beta_n} = \frac{(n+1)^{l+2}}{(n+2)^{l+2}(n+1)},$$

is clearly a rational function of n, from which we can read off the values $p = q = l + 2$, $a_1 = a_2 = \cdots = a_p = 1$, and $b_1 = b_2 = \cdots = b_q = 2$, giving

$$H_{l,\kappa}(R) = \frac{e^{i(l+2)\kappa}}{i^{l+1}} R e^{-R}\, {}_{l+2}F_{l+2} \left[\begin{matrix} 1, 1, \cdots 1 \\ 2, 2, \cdots 2 \end{matrix}; e^{i\kappa} R \right]. \tag{B.3.1}$$

It is worth noting that (by the ratio test) the series representing this hypergeometric function is both convergent on all of $\mathbb{C}$ and entire, since $p = l + 2 = q$ [50].

There is unfortunately no algebraic representation of ${}_{l+2}F_{l+2}$, so (B.3.1) is the best we can do without further approximation. However, since we are already using an asymptotic form of $g_{H,l}$, we should similarly seek only the leading-order large-R asymptotic behaviour of $H_{l,k}$. Thankfully, the relevant hypergeometric function has a well-known asymptotic expansion, given in equations 1.2 and 1.3 of [50], which in our context simplifies to

$$ {}_{l+2}F_{l+2}\left[\begin{matrix}1, 1, \cdots 1 \\ 2, 2, \cdots 2\end{matrix}; z\right] \sim e^z z^{-(l+2)} \sum_{k=0}^{\infty} c_k \, z^{-k}, $$

for $z \to \infty$. The coefficients c_k are defined recursively; for our purposes it suffices to merely note that $c_0 = 1$, since it is clearly the $k = 0$ term that defines the leading-order behaviour in this asymptotic limit. As such, we simply truncate the series after the first term. Substituting the appropriate argument and simplifying, we arrive at the leading-order large-R behaviour of our matrix element,

$$ H_{l,\kappa}(R) \sim \frac{e^{R(\cos\kappa - 1) + iR\sin\kappa}}{(iR)^{l+1}}. $$

Bibliography

[1] E. Abers. *Quantum mechanics*. Benjamin Cummings, 2003.

[2] M. Abramowitz and I. A. Stegun. *Handbook of mathematical functions with formulas, graphs, and mathematical tables*, volume 55. US Government printing office, 10 edition, 1964.

[3] T. Adorno, M. Baldiotti, M. Chaichian, D. Gitman, and A. Tureanu. Dirac equation in noncommutative space for hydrogen atom. *Physics Letters B*, 682(2):235–239, 2009. doi:10.1016/j.physletb.2009.11.003.

[4] A. Y. Alekseev, A. Recknagel, and V. Schomerus. Brane dynamics in background fluxes and non-commutative geometry. *Journal of High Energy Physics*, 2000(05):010, 2000. doi:10.1088/1126-6708/2000/05/010.

[5] G. Alexanian, A. Pinzul, and A. Stern. Generalized coherent state approach to star products and applications to the fuzzy sphere. *Nuclear Physics B*, 600(3):531–547, 2001. doi:10.1016/S0550-3213\%2800\%2900743-4.

[6] A. P. Balachandran, T. R. Govindarajan, C. M. Mendes, and P. Teotonio-Sobrinho. Unitary quantum physics with time-space noncommutativity. *Journal of High Energy Physics*, 2004(10):072, 2004. doi:10.1088/1126-6708/2004/10/072.

[7] L. E. Ballentine. *Quantum mechanics: a modern development*. World Scientific Publishing Company, 2 edition, 2014. doi:10.1142/9038.

[8] M. Chaichian, M. Långvik, S. Sasaki, and A. Tureanu. Gauge covariance of the aharonov–bohm phase in noncommutative quantum mechanics. *Physics Letters B*, 666(2):199–204, 2008. doi:10.1016/j.physletb.2008.06.050.

[9] M. Chaichian, P. Prešnajder, M. Sheikh-Jabbari, and A. Tureanu. Aharonov–bohm effect in noncommutative spaces. *Physics Letters B*, 527(1-2):149–154, 2002. doi:10.1016/S0370-2693\%2802\%2901176-0.

[10] M. Chaichian, M. Sheikh-Jabbari, and A. Tureanu. Hydrogen atom spectrum and the lamb shift in noncommutative QED. *Physical Review Letters*, 86(13):2716, 2001. doi:10.1103/PhysRevLett.86.2716.

[11] M. Chaichian, M. Sheikh-Jabbari, and A. Tureanu. Non-commutativity of space-time and the hydrogen atom spectrum. *The European Physical Journal C-Particles and Fields*, 36(2):251–252, 2004. doi:10.1140/epjc/s2004-01886-1.

[12] N. Chandra, H. Groenewald, J. Kriel, F. Scholtz, and S. Vaidya. Spectrum of the three-dimensional fuzzy well. *Journal of Physics A: Mathematical and Theoretical*, 47(44):445203, 2014. doi:10.1088/1751-8113/47/44/445203.

[13] A. Connes. *Noncommutative geometry*. Academic Press, 1994.

[14] J. B. Conway. *A course in functional analysis*. Springer, 2 edition, 2019. doi:10.1007/978-1-4757-4383-8.

[15] U. Delić, M. Reisenbauer, K. Dare, D. Grass, V. Vuletić, N. Kiesel, and M. Aspelmeyer. Cooling of a levitated nanoparticle to the motional quantum ground state. *Science*, 367(6480):892–895, 2020. doi:10.1126/science.aba3993.

[16] Y. C. Devi, S. Prajapat, A. K. Mukhopadhyay, B. Chakraborty, and F. G. Scholtz. Connes distance function on fuzzy sphere and the connection between geometry and statistics. *Journal of Mathematical Physics*, 56(4):041707, 2015. doi:10.1063/1.4918648.

[17] S. Doplicher, K. Fredenhagen, and J. E. Roberts. The quantum structure of spacetime at the planck scale and quantum fields. *Communications in Mathematical Physics*, 172(1):187–220, 1995. doi:10.1007/BF02104515.

[18] M. R. Douglas and N. A. Nekrasov. Noncommutative field theory. *Reviews of Modern Physics*, 73(4):977, 2001. doi:10.1103/RevModPhys.73.977.

[19] D. G. Fried, T. C. Killian, L. Willmann, D. Landhuis, S. C. Moss, D. Kleppner, and T. J. Greytak. Bose-einstein condensation of atomic hydrogen. *Phys. Rev. Lett.*, 81:3811–3814, Nov 1998. doi:10.1103/PhysRevLett.81.3811.

[20] V. Gáliková and P. Prešnajder. Coulomb problem in non-commutative quantum mechanics. *Journal of Mathematical Physics*, 54(5):052102, 2013. doi:10.1063/1.4803457.

[21] B. C. Hall. *Quantum theory for mathematicians*, volume 267. Springer, 2013. doi:10.1007/978-1-4614-7116-5.

[22] B. C. Hall et al. *Lie groups, Lie algebras, and representations: an elementary introduction*. Springer, 2 edition, 2003. doi:10.1007/978-3-319-13467-3.

[23] R. V. Kadison and J. R. Ringrose. *Fundamentals of the theory of operator algebras*, volume 1. Academic press New York, 1986.

[24] L. Kaup and B. Kaup. *Holomorphic functions of several variables: an introduction to the fundamental theory*, volume 3. Walter de Gruyter, 2011.

[25] J. R. Klauder and B.-S. Skagerstam. *Coherent states: applications in physics and mathematical physics*. World scientific, 1985. doi:10.1142/0096.

[26] D. Kleckner, I. Pikovski, E. Jeffrey, L. Ament, E. Eliel, J. van den Brink, and D. Bouwmeester. Creating and verifying a quantum superposition in a micro-optomechanical system. *New Journal of Physics*, 10(9):095020, sep 2008. URL: https://dx.doi.org/10.1088/1367-2630/10/9/095020, doi:10.1088/1367-2630/10/9/095020.

[27] J. Kriel, H. Groenewald, and F. Scholtz. Scattering in a three-dimensional fuzzy space. *Physical Review D*, 95(2):025003, 2017. doi:10.1103/PhysRevD.95.025003.

[28] J. N. Kriel and F. G. Scholtz. The entropy of dense non-commutative fermion gases. *Journal of Physics A: Mathematical and Theoretical*, 45(9):095301, 2012. doi:10.1088/1751-8113/45/9/095301.

[29] J. Millen, P. Z. G. Fonseca, T. Mavrogordatos, T. S. Monteiro, and P. F. Barker. Cavity cooling a single charged levitated nanosphere. *Phys. Rev. Lett.*, 114:123602, Mar 2015. doi:10.1103/PhysRevLett.114.123602.

[30] M. A. Nielsen and I. L. Chuang. *Quantum Computation and Quantum Information*. Cambridge University Press, 2010. doi:10.1017/CBO9780511976667.

[31] R. Penrose. On gravity's role in quantum state reduction. *General relativity and gravitation*, 28(5):581–600, 1996. doi:10.1007/BF02105068.

[32] I. Pittaway and F. Scholtz. Quantum interference on the non-commutative plane and the quantum-to-classical transition. *arXiv e-prints*, pages arXiv–2101, 2021. doi:10.48550/arXiv.2101.06108.

[33] C. Procesi. *Lie groups: an approach through invariants and representations*. Springer Science & Business Media, 2006. doi:10.1007/978-0-387-28929-8.

[34] O. Rodrigues. Des lois géométriques qui régissent les déplacements d'un système solide dans l'espace, et de la variation des coordonnées provenant de ces déplacements considérés indépendamment des causes qui peuvent les produire. *J. Math. Pures Appl*, 5(380-400):5, 1840.

[35] S. Roman. *The umbral calculus*, page 61. Springer, 2005. doi:10.1007/0-387-27474-X_19.

[36] M. Schlosshauer. Quantum decoherence. *Physics Reports*, 831:1–57, 2019. doi:10.1016/j.physrep.2019.10.001.

[37] F. G. Scholtz. Classical dynamics on three-dimensional fuzzy space. *Physical Review D*, 98(10):104058, 2018. doi:10.1103/PhysRevD.98.104058.

[38] F. G. Scholtz, L. Gouba, A. Hafver, and C. Rohwer. Formulation, interpretation and application of non-commutative quantum mechanics. *Journal of Physics A: Mathematical and Theoretical*, 42(17):175303, 2009. doi:10.1088/1751-8113/42/17/175303.

[39] J. Schwinger. On angular momentum. Technical report, Harvard Univ., Cambridge, MA (United States); Nuclear Development Associates, Inc., 1952.

[40] N. Seiberg and E. Witten. String theory and noncommutative geometry. *Journal of High Energy Physics*, 1999(09):032, 1999. doi:10.1088/1126-6708/1999/09/032.

[41] R. Shankar. *Principles of quantum mechanics*. Springer Science & Business Media, 2012. doi:10.1007/978-1-4757-0576-8.

[42] N. J. A. Sloan and OEIS Foundation Inc. The On-Line Encyclopedia of Integer Sequences. https://oeis.org/A106800, 2019.

[43] H. S. Snyder. Quantized space-time. *Physical Review*, 71(1):38, 1947. doi:10.1103/PhysRev.71.38.

[44] E. W. Streed, A. P. Chikkatur, T. L. Gustavson, M. Boyd, Y. Torii, D. Schneble, G. K. Campbell, D. E. Pritchard, and W. Ketterle. Large atom number bose-einstein condensate machines. *Review of Scientific Instruments*, 77(2):023106, 2006. doi:10.1063/1.2163977.

[45] G. Szegö. *Orthogonal polynomials*, volume 23. American Mathematical Soc., 1939. doi:10.1090/coll/023.

[46] F. Tebbenjohanns, M. L. Mattana, M. Rossi, M. Frimmer, and L. Novotny. Quantum control of a nanoparticle optically levitated in cryogenic free space. *Nature*, 595(7867):378–382, 2021. doi:10.1038/s41586-021-03617-w.

[47] D. Trinchero and F. G. Scholtz. Pinhole interference in three-dimensional fuzzy space, 2022. doi:10.48550/ARXIV.2212.01449.

[48] K. Van der Stam, E. Van Ooijen, R. Meppelink, J. Vogels, and P. Van der Straten. Large atom number bose-einstein condensate of sodium. *Review of Scientific Instruments*, 78(1):013102, 2007. doi:10.1063/1.2424439.

[49] J. Van Es, S. Whitlock, T. Fernholz, A. Van Amerongen, and N. Van Druten. Longitudinal character of atom-chip-based rf-dressed potentials. *Physical Review A*, 77(6):063623, 2008. doi:10.1103/PhysRevA.77.063623.

[50] H. Volkmer and J. J. Wood. A note on the asymptotic expansion of generalized hypergeometric functions. *Analysis and Applications*, 12(01):107–115, 2014. doi:10.1142/S0219530513500346.